

University of New Hampshire

University of New Hampshire Scholars' Repository

Doctoral Dissertations

Student Scholarship

Winter 1991

A statistical study of narrow bandwidth, high-latitude geomagnetic pulsations

Mark Andrew Popecki
University of New Hampshire, Durham

Follow this and additional works at: <https://scholars.unh.edu/dissertation>

Recommended Citation

Popecki, Mark Andrew, "A statistical study of narrow bandwidth, high-latitude geomagnetic pulsations" (1991). *Doctoral Dissertations*. 1669.
<https://scholars.unh.edu/dissertation/1669>

This Dissertation is brought to you for free and open access by the Student Scholarship at University of New Hampshire Scholars' Repository. It has been accepted for inclusion in Doctoral Dissertations by an authorized administrator of University of New Hampshire Scholars' Repository. For more information, please contact Scholarly.Communication@unh.edu.

INFORMATION TO USERS

This manuscript has been reproduced from the microfilm master. UMI films the text directly from the original or copy submitted. Thus, some thesis and dissertation copies are in typewriter face, while others may be from any type of computer printer.

The quality of this reproduction is dependent upon the quality of the copy submitted. Broken or indistinct print, colored or poor quality illustrations and photographs, print bleedthrough, substandard margins, and improper alignment can adversely affect reproduction.

In the unlikely event that the author did not send UMI a complete manuscript and there are missing pages, these will be noted. Also, if unauthorized copyright material had to be removed, a note will indicate the deletion.

Oversize materials (e.g., maps, drawings, charts) are reproduced by sectioning the original, beginning at the upper left-hand corner and continuing from left to right in equal sections with small overlaps. Each original is also photographed in one exposure and is included in reduced form at the back of the book.

Photographs included in the original manuscript have been reproduced xerographically in this copy. Higher quality 6" x 9" black and white photographic prints are available for any photographs or illustrations appearing in this copy for an additional charge. Contact UMI directly to order.

U·M·I

University Microfilms International
A Bell & Howell Information Company
300 North Zeeb Road, Ann Arbor, MI 48106-1346 USA
313/761-4700 800/521-0600



Order Number 9209586

**A statistical study of narrow bandwidth, high-latitude
geomagnetic pulsations**

Popecki, Mark Andrew, Ph.D.

University of New Hampshire, 1991

U·M·I
300 N. Zeeb Rd.
Ann Arbor, MI 48106



**A STATISTICAL STUDY OF NARROW BANDWIDTH, HIGH LATITUDE
GEOMAGNETIC PULSATIONS**

BY

MARK A. POPECKI

BA, Saint Michael's College, 1982

DISSERTATION

**Submitted to the University of New Hampshire
in Partial Fulfillment of
the Requirements for the Degree of**


Doctor of Philosophy

in

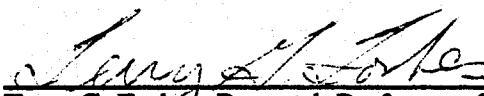
Physics

December, 1991

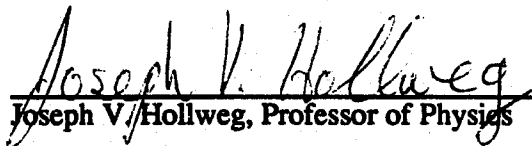
This dissertation has been examined and approved.



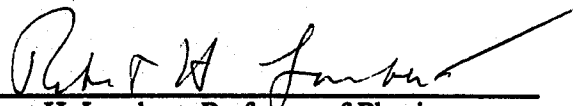
Dissertation Director, Roger L. Arnoldy
Professor of Physics



Terry G. Forbes, Research Professor of Physics



Joseph V. Hollweg, Professor of Physics



Robert H. Lambert, Professor of Physics



John J. Wright, Professor of Physics

11/26/91
Date

Acknowledgements

My three years with the Magnetospheric Research Group have been the most rewarding of my graduate career. The people I have met have awakened me to the excitement and satisfaction of doing research for the sake of curiosity.

I would like to thank Roger Arnoldy, who gave me a chance to do research and write a dissertation. His willingness to take two or three hours at a time to reorient a confused graduate student built self-esteem, and renewed faith that progress would be made.

I was fortunate to find myself working among three patient teachers: Hank Dolben, Marc Lessard and Mark Widholm. Their work in the establishment of the micropulsation stations and the data analysis software made this study possible. Thanks also go to Christopher Arnoldy, who spent part of a summer helping to select and test database programs, and subsequently helping to enter data into one of them.

I would like to thank Debadarshi Bhattacharya for his advice and conversation, particularly during times in my graduate career when the outlook was not so optimistic. Kristina Lynch very kindly read this dissertation and listened to countless presentation dry runs. Her perceptive comments and questions greatly improved the clarity and physical reasoning in both.

My parents, and my brothers and sister have encouraged me steadily. They had confidence even in the first semesters, when it seemed unlikely to me that I would complete one year, let alone a degree. My wife Carolyn has patiently tolerated long periods of time when my attention was diverted to homework or research, without complaint. Her encouragement to finish has expedited the conclusion of this study.

TABLE OF CONTENTS

Acknowledgments	iii
List of Tables	vii
List of Figures	viii
Abstract	ix
Chapter	Page
I. The Magnetosphere	1
Introduction	1
The Solar Wind	2
Formation of the Magnetospheric Boundaries	3
Boundary Layers and Convection Within the Magnetosphere	4
The Component Drifts of Convection	8
The Corotation Electric Field and Formation of the Plasmasphere	9
The Ring Current	11
II. Pc Micropulsations and Previous Work on Pc1/2	13
Introduction	13
Micropulsation Classification Scheme	13
Some Sources of Micropulsations	14
Previous Work on Micropulsations	15
III. Station Location, Instrumentation and Data Analysis	20
Station Location	20
Instrumentation	21
Data Analysis	23
Examples of Micropulsation Events in This Study	25
IV. Alfven Waves	39
Introduction	39
Derivation of the General Dispersion Relation	40
A Physical Picture of the Alfven Wave	44
Fast and Alfven Modes in a Cold Plasma; Low Frequency Limit; $k_{\perp} > 0$	46
Fast and Alfven Modes in a Cold Plasma; No Frequency Limit; $k \parallel B_0$	49
Fast, Alfven and Slow Modes in a Warm Plasma	51
Group Velocity	54
Polarization of the Fast and Alfven Modes in a Cold Plasma	55
Circular Polarization in a Cold Plasma	56
Propagation in the Presence of Multiple Ion Species in a Cold Plasma	57
Special Frequencies Due to the Presence of Heavy Ions	58
Implications of Multiple Ion Species for Micropulsations	60

V. Ionospheric Modification of Alfvén Waves	61
Introduction	64
The Incident Wave	65
Pedersen and Hall Conductivities and Currents	65
The Incident Wave as It Approaches the Ionosphere from Above	68
Wave-Mode Coupling in the Ionosphere	70
Reflectivity of the Ionosphere	71
The Rotation of the Magnetic Field as Seen on the Ground	72
Ducting Introduction	76
Evanescence of the Ducted Wave Above and Below the Duct	77
Propagation in the Duct	80
Losses in the Duct	81
Off-Meridian Propagation	82
The Contribution to Ground Observations from Field-Aligned Currents	83
Polarization Patterns on the Ground	84
VI. Wave Growth	90
Introduction	90
Ion-cyclotron Resonance	90
Probable Resonance Mechanism for Pc1 Micropulsations	91
Wavegrowth in the Presence of a Distribution of Ion Velocities	92
The Dependence of Wavegrowth on Anisotropy	96
Marginally Unstable Wave Frequency	97
The Effects of an Increased Doppler Shift	98
The Frequency Bands of Maximum Growth	98
The Effect of Cold Ion Density on the Growth Rate	99
The Effect of Magnetic Field on the Growth Rate	100
The Implications for Pc1/2 Micropulsations	101
VII. Results of Data Analysis	102
Introduction	102
Diurnal Occurrence Patterns	103
The Importance of Structured Events Relative to the Source Region	107
Diurnal Patterns for Waves Above 0.4 Hz	108
Event Length and Bandwidth	109
Comparison of Event Length for Waves Above and Below 0.4 Hz	111
Pc1/2 Global Onset	113
Seasonal Occurrence	114
Latitude Dependence of Pc1/2 and Pc1 Occurrence	115
Possible Significance of the 0.4 Hz Frequency	117
Possible Connection of Pc1/2 with the Solar Wind and Magnetic Indices	119
Solar Wind Measurements: The IMP8 Spacecraft	122
Dynamic Solar Wind Pressure During Pc1/2	123
Solar Wind Pressure: Discussion	125
IMF Orientations During Pc1/2	127
B_x and B_y Dependence	129
B_z Dependence	130
IMF Relation to Pc1/2: Discussion	134
Possible Association of Pc1/2 with Magnetospheric Sources	135
Dst During Pc1/2	136
Possibility of Pc1/2 Occurrence During the Recovery Phase of Storms	138
AE During Pc1/2	140
Kp during Pc1/2	146
DMSP F7 Coincident Measurements of the Auroral Oval	148

Discussion	152
Conclusions	156
References	182
Appendix: The Chi-square Test	191

List of Tables

Table		Page
2-1	Micropulsation Classification Scheme	13
3-1	Station Location	20
7-1	B_z Values in the Hour Preceding Pc1/2 Events	133
7-2	DMSP F7 Measurements During Pc1/2 Events	150

List of Figures

Figure		Page
1-1	A schematic of the reconnection process	12
1-2	The boundary layer dynamo	12
1-3	Reconnection/Mantle dynamo	12
3-1	Response of the search coil	28
3-2	The gain of the preamplifier	29
3-3	The response of the coil and preamplifier together	30
3-4	The sensitivity of the 1973 Siple coils	31
3-5	A Foxbase event-type database record	32
3-6	Examples of type 1 and 4 structured events, and a Pc1/2 event	33
3-7	An example of an extremely narrow band, intense Pc1/2	34
3-8	Example of a fragmented event	35
3-9	Example of a "many segs" event	36
3-10	Example of a type 5 event	37
3-11	Example of event selection from spectrograms	38
4-1	A physical picture of an Alfvén wave	63
4-2	Plasma and magnetic field perturbations by the Alfvén wave	63
5-1	Ionospheric modification of an incident Alfvén wave	88
5-2	The magnetic field from field-aligned currents	89
7-1	Diurnal patterns at Sondre Stromfjord in UT and LMT	158
7-2	Diurnal patterns at South Pole, Siple and McMurdo	159
7-3	Monthly variation in the diurnal patterns at SP, SS and Siple	160
7-4	Diurnal patterns for subsets of the 0.1-0.4 Hz band	161
7-5	Diurnal patterns for waves above and below 0.4 Hz in LMT	162
7-6	Duration vs. Mid-event time for SP, SS and Siple Pc1/2	163
7-7	A 17 hour Pc1/2 with magnetic and solar wind values noted	164
7-8	Event length by month for Pc1/2 at SS, SP and Siple	165
7-9	Cumulative event length plots for all waves at SS, SP, and Siple	166
7-10	Differences in onset times for Pc1/2 at SS, SP and Siple	167
7-11	Monthly SP-SS Pc1 and Pc1/2 distributions by fraction	168
7-12	Monthly SP-SS Pc1 and Pc1/2 distributions by quantity	169
7-13	Monthly SP-Siple Pc1 and Pc1/2 distributions by fraction	170
7-14	Monthly SP-Siple Pc1 and Pc1/2 distributions by quantity	171
7-15	He ⁺ equatorial gyrofrequency vs. radial distance	172
7-16	IMP8 IMF measurement count by month	172
7-17	Solar wind pressure averaged over Pc1/2 events	173
7-18	Pressure during the first full hour of Pc1/2 events	173
7-19	Cone Half-angles between the IMF and the Y _{gsm} and X _{gsm} axis	174
7-20	IMF B _z for Pc1/2 hours	175
7-21	Cone angles between the IMF and X and Y axes for SS Pc1/2	175
7-22	Example of AE response to the IMF B _z component	176
7-23	Solar wind pressure and Dst measured simultaneously for Pc1/2	177
7-24	Dst for Pc1/2 during June solstice ±45 days	178
7-25	Chi-square for Dst offsets before Pc1/2	179
7-26	AE during Pc1/2	180
7-27	K _p at the start of all Pc1/2 and those at least 45 minutes. long	181

ABSTRACT

A STATISTICAL STUDY OF NARROW BANDWIDTH, HIGH LATITUDE GEOMAGNETIC PULSATIONS

by

Mark A. Popecki
University of New Hampshire, December, 1991

Micropulsations are the ground signature of plasma waves that originate in the magnetosphere. In the Pc1-Pc2 frequency band, the wave mode that is amplified by energetic ions is also the mode that is guided by a magnetic field. These waves serve as evidence of energetic, loss-cone type ion distributions in the magnetosphere. The spectral character of the waves is often characteristic of the wave growth location. If the location for a particular wave may be identified, that wave provides immediate information about ion populations whenever it is observed on the ground. The location of the wavegrowth site may be identified by observing occurrence patterns at stations at a range of latitudes. This is because the Earth's field lines connect stations at different latitudes to different parts of the magnetosphere, with respect to the field-guided waves. The problem addressed by this study is to locate the growth site of Pc1/2 waves. The benefit of this knowledge is that the appearance of Pc1/2 on the ground will indicate the presence of an energetic loss cone type population of ions, in a well-known part of the magnetosphere, without the need for in situ measurements.

This study is a survey of micropulsations at three high-latitude ground stations. It revealed a diurnal occurrence pattern for waves below 0.4 Hz, and showed that the pattern was not due to the effects of sunlight on the ionosphere, but instead indicates a postnoon magnetospheric source region. The importance of He⁺ ions in the

magnetosphere to wave growth and generation is also indicated. The waves above and below 0.4 Hz have different diurnal and seasonal occurrence patterns. The waves above 0.4 Hz come primarily from plasmopause latitudes, while those below 0.4 Hz, in the Pc1/2 band, come from farther out. The different source locations for waves above and below 0.4 Hz, combined with the typically sharp, approximately 0.4 Hz upper frequency limit of the Pc1/2 spectra, suggest strongly that He⁺ ions in the outer magnetosphere influence wavegrowth and propagation. This fits well with the observations of Anderson, et al. (1990), who showed with a spacecraft study that the region beyond L=7 dominates over the region of L<7 as a wave source above the He⁺ gyrofrequency. This ground study shows that these outer magnetosphere waves above the He⁺ gyrofrequency are not readily reaching the ground. The organization of ground observations has never been shown before in previous ground studies. Since He⁺ has the capacity to prevent waves above its gyrofrequency from reaching the ground, its presence may limit the use of plasma waves to Pc1/2 as probes of the outer magnetosphere.

An extensive search for correlations between Pc1/2 occurrence and solar wind pressure and magnetic field orientation rules out the solar wind as a direct source of Pc1/2 generation. The diurnal pattern and apparent source location for the Pc1/2 are consistent with a source of plasma sheet ions that have drifted sunward on the dusk side of the magnetosphere (Kaye & Kivelson, 1979; Anderson et al., 1991).

Chapter 1

The Magnetosphere

Introduction

The solar wind flow past the Earth's magnetic field creates a magnetosphere and establishes many distinct plasma regions within it. Energy input from the solar wind drives current systems and amplifies plasma waves throughout the magnetosphere. Micropulsation studies are conducted on the ground to explore this region of space. This is possible because the ultra low frequency plasma waves that are amplified by energetic ion populations are also guided by the Earth's magnetic field. These waves follow the Earth's field, which extends throughout the magnetosphere, down to the surface. Ground detectors observe these waves as perturbations in the local magnetic field, or micropulsations.

The magnetic field of the Earth is similar to a dipole, particularly in the dayside portion of the magnetosphere. The high latitude field lines cross the equator the furthest from the Earth, while lower latitude field lines pass through a closer region of space. Since these field lines act as waveguides, one can gain information about different parts of the magnetosphere by choosing a ground site at the appropriate latitude.

Additional information about the source of a wave comes from its spectral character. Wave-particle interactions in certain parts of the magnetosphere produce distinctive spectral signatures on the ground. If the source region of a particular wave signature is

known, that wave becomes a remote sensing tool for ground observers. It provides information about the location and type of particle populations that amplified the waves. Also, the fact that certain waves are observed at certain station locations provides insight into the propagation of the waves from their remote source to the ground. In the frequency range of this study, 0.1-5.0 Hz, the waves may be amplified by ion cyclotron resonance between ions and guided, circularly polarized waves.

Some features of the magnetosphere and solar wind that are important for wave generation will be described next, beginning with the solar wind. After that, the topology of the magnetosphere will be discussed. Emphasis will be placed on those parts particularly important for wave generation in the frequency range of interest in this study.

The Solar Wind

The magnetic field in the solar wind strongly affects the efficiency with which energy from the solar wind may enter the magnetosphere. Certain orientations relative to the Earth's field can provide direct access to the magnetosphere for solar wind plasma under a process known as reconnection. This is the source of energy for substorms and current systems in the magnetosphere, and for the aurora in the atmosphere.

As the solar wind leaves the Sun, it takes the Sun's magnetic field with it, due to the high conductivity in the plasma and to the high energy density in the plasma, compared to the energy density of the magnetic field (Hess, 1965). This has the effect of stretching the dipole lines until they become nearly antiparallel at the Earth's orbit. Since a curl in a magnetic field is associated with a current ($\nabla \times \mathbf{B} = 4\pi/c \mathbf{J}$), a current sheet exists between the antiparallel magnetic field lines in the solar wind (Kelley, 1989). The direction of this current is in a sense such that if it were carried by a sheet of many parallel wires, the field from the wires would be antiparallel above and below the sheet in the same way as the Sun's field. This current sheet is not a flat disc; it has flutes, and has

been described as a ballerina skirt (for example, Kelley, 1989). The current sheet may be above or below the Earth at any time, and it may change position quickly compared to an hour. Consequently, the magnetic field in the solar wind may have a wide range of orientations near the Earth. For example, it may point toward or away from the Sun, depending on whether the sheet is above or below the Earth.

Since the Sun is a rotating source of plasma, one might imagine the solar wind being squirted out like water from a rotating sprinkler. This creates a spiral pattern in the magnetic field embedded in the solar wind (Hess, 1965). Close to the Earth, the ecliptic component of the solar wind magnetic field is found to be typically toward the Earth and East (as viewed from the subsolar point at the surface of the Earth) or vice versa. This pattern is clear in Figure 7-21 in the data analysis section of this work, which is a scatterplot of magnetic field measurements from the IMP8 satellite, located upstream of the magnetosphere.

Formation of the Magnetospheric Boundaries

When the solar wind reaches the vicinity of the Earth, a balance is established between the dynamic pressure of the solar wind (ρv^2) and the pressure of the Earth's magnetic field, $B^2/8\pi$ (Haerendel & Paschmann, 1982). This balance takes place at approximately $10 R_E$ away from the Earth, along the Sun-Earth line (Fairfield, 1971), and the flow is deflected around the obstacle of the magnetosphere. The pressure balance surface is called the magnetopause. A shock exists just outside the magnetopause, since the solar wind speed, at approximately 400 km/s, is well above the speed of sound and other waves (such as Alfvén waves) in the interplanetary medium (about 50 km/s; Hess, 1965).

The ions and electrons in the solar wind separate somewhat at the magnetopause due to their opposite charge and mass difference under the influence of the $\mathbf{v}_{sw} \times \mathbf{B}_E$ force

(Haerendel & Paschmann, 1982). The resulting surface current is known as the Chapman-Ferraro current, and it is induced to cancel the Earth's magnetic field in the conductive solar wind plasma. By canceling the Earth's field in the solar wind, the current adds to the field inside the magnetopause, approximately doubling the field there (Nishida, 1982; Haerendel & Paschmann, 1982). Increases in solar wind dynamic pressure (nmv_{sw}^2) establish a new pressure balance surface closer to the Earth, in a region of stronger magnetic field. This calls for enhanced Chapman-Ferraro currents, which increases the magnetic field inside the magnetosphere. This is referred to as a compression of the magnetosphere.

The magnetopause is a current sheet covering the entire magnetosphere, and is on the order of 100 km thick (Haerendel & Paschmann, 1982). On the dayside, the magnetopause carries the Chapman-Ferraro currents. A direct funnel-like opening through this surface exists in each hemisphere. These are the cusp/cleft regions, and there is some direct solar wind flow into them, down toward the Earth. The funnel shape of the cusp is along a line extending up from the Earth at approximately 79 degrees latitude (Lundin, 1988). The equatorward surface of the cusp/cleft region is on magnetic field lines forming a closed loop in the dayside magnetosphere. The poleward surface is on field lines that are swept back toward the tail of the magnetosphere.

Boundary Layers and Convection within the Magnetosphere

The solar wind energy, which is the source for all the waves observed at the ground, enters the magnetosphere in two principal ways. One is directly through a magnetic reconnection process (described briefly below) that temporarily joins the magnetic field of the solar wind and the Earth, and the other is through a class of viscous processes through the boundary surfaces of the magnetosphere (Baumjohann, 1986).

Inside the magnetopause is the boundary layer. At latitudes above the cusp, the boundary layer is called the high latitude boundary layer (HLBL), or plasma mantle (Lundin, 1988). At lower latitudes and around the sides of the magnetosphere it is the low-latitude boundary layer (LLBL). These layers are thought to be important for the transfer of solar wind energy and plasma to the magnetosphere (Lundin, 1988). Also, their dynamo action strongly influences the convection pattern within the magnetosphere. The LLBL is populated by magnetospheric and magnetosheath plasma flowing tailward (Lundin, 1988, with reference to Eastman et al., 1976). The magnetosheath itself contains a flow of solar wind plasma that has encountered a shock upstream of the magnetopause (Haerendel & Paschmann, 1982).

The tailward flow in the boundary layer could be established in at least two ways. One way is through viscous interaction, in which momentum is transferred from the solar wind flow across the magnetopause to the boundary layer plasma. Another way is through a process known as reconnection (Dungey, 1961; see Kelley, 1989, Nishida, 1978, Lundin, 1988 for further discussion), where adjacent, antiparallel field lines reorient themselves to become V-shaped lines meeting at their vertices (Figure 1-1). When the interplanetary magnetic field (IMF) in the solar wind has a southward component, it is directed oppositely to the Earth's field where the solar wind first meets the magnetopause, and reconnection may occur. Field lines that led from the south to the north pole of the Earth now connect to the IMF. The result is a field line that extends from the Sun through the polar caps and interior of the Earth, back to the Sun. This line is carried tailward by the solar wind, until in the tail it re-reconnects to a state of two separate field lines again: one looping through the Earth's poles, the other through the Sun's. In the magnetic merging/reconnection model, the HLBL is on "open" field lines, or field lines extending into the solar wind. These lines provide direct access for the solar wind to the boundary layer (particularly in the tail lobe; Lundin, 1988). In the "boundary-

layer model", solar wind plasma enters the LLBL from a layer just outside the magnetopause, known as the magnetosheath, via diffusion or steady-state reconnection.

A dawn to dusk electric field is impressed on the magnetosphere by the solar wind flow. This is because of a dynamo action in the boundary layer, which is described by Lundin, (1988, with reference to Lundin & Evans, 1985), or a dynamo action in the field of the mantle (HLBL) that have been connected to the solar wind field. In the boundary layer, since the flow is tailward, there will be a $\mathbf{v} \times \mathbf{B}$ force there that separates the ions and electrons somewhat (Figure 1-2). The effect can be seen in the equatorial plane of the dawnside boundary layer, for example. The electrons will be driven toward the magnetopause, and the ions inward toward the Earth, creating a separation electric field.

Charged particles may move along the magnetic field lines easily; there is little or no dissipative loss. This makes the magnetic field lines approximately equipotential lines (Kelley, 1989). They permit the separation electric field to be applied to the ionosphere where the field enters the Earth. If one follows the outermost field lines of the boundary layer, which are negatively charged because of the $\mathbf{v} \times \mathbf{B}$ force, they will enter the ionosphere near the lowest latitude of the polar cap. The positively charged inner lines of the boundary layer will enter the ionosphere at still lower latitudes. The electric field impressed on the ionosphere by the boundary layer will then be directed from dawn to dusk. Another dawn to dusk electric field is produced by the dusk side boundary layer. This electric field drives some of the tailward convection, via $\mathbf{E} \times \mathbf{B}$ drift (discussed below), at high latitudes in the ionosphere (Lundin, 1988, with reference to Cowley, 1982).

The separation electric field in the boundary layer creates currents along the the field lines from the boundary, down to the auroral region of the ionosphere, back up to the opposite boundary layer, and back via the magnetopause currents. The field-aligned current on the

dayside, between the boundary layer and the ionosphere, is known as the region 1 current (Lundin, 1988, with reference to Bythrow et al., 1981).

When the connection of the solar wind and Earth fields exists (reconnection), however, solar wind plasma may enter the magnetosphere along the field line (Nishida, 1978). The solar wind plasma would now have direct access to the boundary layer, enhancing the tailward flow as the solar wind streams past (see Lundin, 1988). This in turn would increase the dawn-dusk electric field.

In another dynamo model, the solar wind on reconnected field lines generates a cross-polar cap electric field. This arises because there is no net Lorentz force in the conductive solar wind ($\mathbf{E} + \mathbf{v} \times \mathbf{B} = 0$). In the Northern hemisphere, the tailward \mathbf{v}_{sw} crossed with a \mathbf{B} that points from the solar wind down into the polar cap produces a charge separation that creates a dawn to dusk electric field. This electric field is imposed on the ionosphere by the equipotential field lines (Figure 1-3).

Observations have shown that the electric field magnitude increases in association with a southward turning of the IMF (Reiff & Luhmann, 1986; Doyle & Burke, 1983; from Kan, 1990). It also has a minimum value when the IMF is North, at which time much less reconnection is expected to occur. This remnant electric field might be due to viscous momentum transfer from the solar wind (Kamide, 1988, with reference to Akasofu, 1979).

A return flow is established in the magnetotail on closed field lines. This sunward flowing plasma contains the dawn to dusk electric field, consistent with its drift through the Earth's magnetic field. The closed field lines map to the auroral zones, probably below the "open" polar cap lines, but above plasmaspheric field lines (see below about the formation of the plasmasphere and the exclusion of sunward convecting plasma from it). The dawn to dusk electric field in the sunward flowing plasma is impressed on the

auroral zone along the magnetic field lines as a dusk to dawn field (Kelley, 1989), extending from the equatorward edge of the polar cap to plasmaspheric latitudes. At altitudes low enough for ion collisions with neutrals and other ions to impede ion $\mathbf{E} \times \mathbf{B}$ drift in the auroral zone, with the dusk to dawn electric field, a Hall current (see the chapter on ionospheric modification of waves) will develop in the $-\mathbf{E} \times \mathbf{B}$ direction as electrons continue to $\mathbf{E} \times \mathbf{B}$ drift. In a quiet state, these are called the Eastward and Westward electrojets in the dusk and dawn auroral zones, respectively. However, during substorm activity, the Westward electrojet extends into the dusk-midnight sector (current systems in the ionosphere during substorms are discussed in more detail by Nishida, 1978, Kamide, 1988, and Akasofu, 1989). The status of the electrojets is logged by the AE index.

The Component Drifts of Convection

The dawn to dusk electric field combines with the magnetic field of the Earth to convect plasma sunward from the tail via an $\mathbf{E}_D \cdot \mathbf{D} \times \mathbf{B}_E$ drift. In general, a force \mathbf{F} applied to a plasma in a magnetic field will produce a displacement perpendicular to the force and magnetic field :

$$\mathbf{V}_F = \frac{1}{e} \frac{\mathbf{F} \times \mathbf{B}}{B^2} \quad (\text{Chen, 1974}).$$

If the force is $e\mathbf{E}$, the $\mathbf{E} \times \mathbf{B}$ drift results :

$$\mathbf{V}_{\mathbf{E} \times \mathbf{B}} = \frac{\mathbf{E} \times \mathbf{B}}{B^2} ,$$

which is independent of charge, mass and energy. Ions and electrons $\mathbf{E} \times \mathbf{B}$ drift at the same speed, in the same direction.

Other drifts develop as a consequence of the gradients in magnetic field magnitude and its curvature. This is particularly important near the Earth, and unlike $\mathbf{E} \times \mathbf{B}$ drift, these two

drifts are energy and charge dependent. In a magnetic field where the magnitude changes spatially, the gyroradius of a charged particle will change, moving it away from its gyrocenter. This is known as gradient-B drift and is, to a first order perturbation in B:

$$V_{\nabla B} = \pm \frac{v_{\perp} R}{2} \frac{\mathbf{B}_0 \times \nabla B}{B^2} \quad (\text{Chen, 1974}),$$

where R is the approximate gyroradius (Chen, 1974). This drift depends on the sign of the charge.

In a magnetic field with curvature, such as the curvature of a dipole pattern, another drift known as curvature drift develops :

$$V_R = \frac{mv_{\parallel}^2}{eB_0^2} \frac{\mathbf{R}_c \times \mathbf{B}}{R_c^2} \quad (\text{Chen, 1974}),$$

where R_c is the radius of curvature of the field, pointing away from the center of curvature; and v_{\parallel} is the speed of the particle parallel to \mathbf{B} . The curvature drift is much less than the gradient B drift in the inner magnetosphere (Nishida, 1978).

Another Drift Component: the Corotation Electric Field and the Formation of the Plasmasphere

The convecting plasma is kept out of a region close to the Earth known as the plasmasphere. This is because, inside this region, motion is dominated by the corotation electric field, while outside, it is dominated by the dawn-dusk convection electric field (Kelley, 1989). The boundary of the plasmasphere changes with the level of magnetic activity (and magnitude of the convection electric field, but is typically at a distance of 4-6 Earth radii (from the center of the Earth) in the equatorial plane (Nishida, 1978, with reference to Chappell, 1972). One of the stations in this study, Siple station, is on a field line that passes near the surface of the plasmasphere, at about 4.3 Earth radii in the equatorial plane. The corotation electric field arises because the neutral atmosphere drags

the plasma along with it. The motion of the plasma in the magnetic field of the Earth causes a charge separation because of the force:

$$(\boldsymbol{\Omega} \times \mathbf{r}) \times \mathbf{B}_0 \quad (\text{Nishida, 1978}),$$

where $\boldsymbol{\Omega}$ is the angular velocity of the Earth's rotation and \mathbf{r} is a vector to the plasma. This moves the ions to higher altitudes and electrons to lower altitudes, creating a polarization, or corotation electric field that points toward the Earth and cause the plasma to $\mathbf{E}_{\text{cor}} \times \mathbf{B}$ drift along with the atmosphere (Kelley, 1989). This corotation electric field is transmitted up into the magnetosphere along the magnetic field (Kelley, 1989). The corotation electric field becomes smaller at higher latitudes.

All four drifts, gradient-B, curvature, corotation and $\mathbf{E} \times \mathbf{B}$, operate simultaneously and drive energetic ions around the Earth on the dusk side and colder ions around the dawn side as they convect sunward. For ions with a small $v_{\perp} R$, or small magnetic moment ($ev_{\perp} R/2$), the gradient B drift will be small compared to the corotation drift. These ions will drift around the dawn side, because of the corotation electric field, as they $\mathbf{E} \times \mathbf{B}$ drift past the Earth. For ions with a large magnetic moment, the gradient B drift will dominate the corotation, and the ions will go around the Earth on the dusk side. If they continue to drift long enough, the ions may leave the magnetosphere on the dayside. This depends in part on the strength of the dawn-dusk electric field over time (Nishida, 1978). Ions whose magnetic moments are such that the corotation and gradient-B drift cancel each other may penetrate most deeply into the plasmaspheric "forbidden" region (Nishida, 1978). Electrons convect around the dawn side only, because the gradient, curvature and corotation drift all work in the same direction for them. Sunward convection of energetic particles (tens of keV) is associated with substorms, and is thought to come from the plasma sheet (DeForest & McIlwain, 1971; Nishida 1978). This is a region in the center of the magnetotail that contains relatively energetic particles, compared to most of the

magnetospheric volume. Typical energies are 1-10 keV for electrons (Jursa, 1985), and at least that for protons (Nishida, 1978).

Convecting ions starting in the tail from a distance of $10 R_E$ take between two and 20 hours to reach the subsolar magnetopause (Ejiri, 1978), depending on initial energy and pitch angle. These ions may be responsible for amplifying the Pc1/2 waves discussed in this study.

The Ring Current

During a substorm, ions from the plasma sheet drift under an intensified dawn-dusk electric field (DeForest & McIlwain, 1971), as described above. The gradient and curvature drift dominate for the ions, and after repeated substorms, a current is established in a ring around the Earth. At the surface of the Earth, the magnetic field of this current is opposite to the steady field there. The proton energy density in the earthward regions of the plasma sheet ($< 6-7 R_E$) is higher by almost a factor of 10 than the electron energy density, so the energy in the ring current is mostly carried by the protons (Nishida, 1978, with reference to Frank, 1971).

The ring current decays mostly by charge exchange (Nishida, 1978), in which a collision of an energetic ion with a cold neutral particle results in an energetic neutral and a cold ion. However, some of the ring current energy is carried away by ion-cyclotron interaction, in which ions pass energy to left polarized Alfvén waves, typically in the 0.2-5.0 Hz frequency band (see, for example, Heacock & Kivinen, 1972).

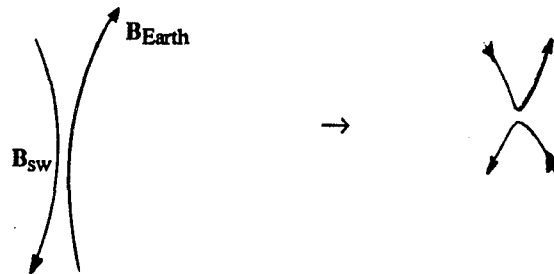


Figure 1-1 A schematic of the magnetic reconnection process is shown. This occurs on the dayside and in the magnetotail. It connects the Earth's magnetic field to the Sun's.

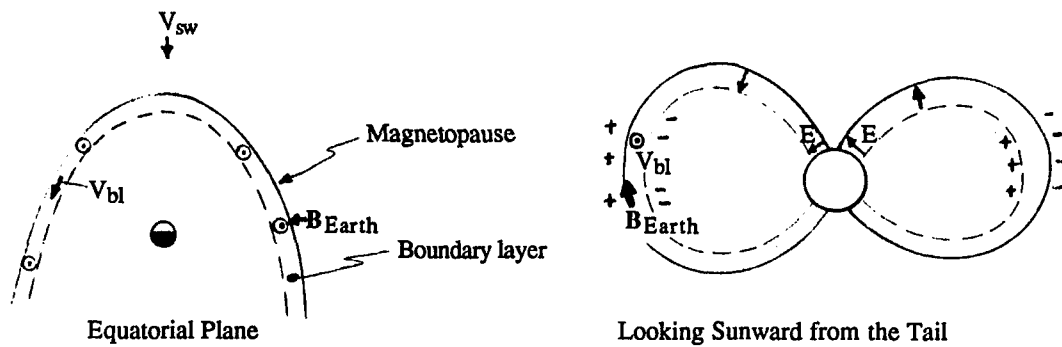


Figure 1-2 The boundary layer dynamo drives some of the tailward convection at high latitudes in the ionosphere. It can operate without reconnection.

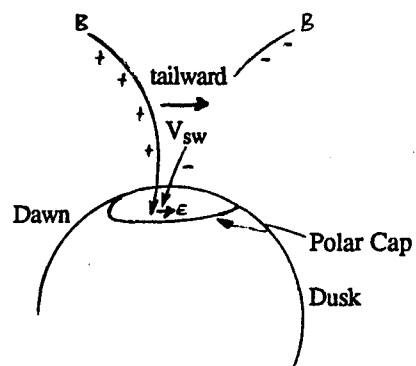


Figure 1-3 The dynamo in the mantle region operates by reconnection of the Earth and Sun's magnetic field. This accounts for most of the tailward convection in the polar cap. The dynamo is most effective for southward orientations of the IMF B_z component. (After Kelley, 1989).

Chapter 2

PC waves and previous work on Pc1/2

Introduction

In this section, the classification scheme for micropulsations and some examples of their sources will be discussed. Next, previous work on Pc1/2 pulsations, the subject of this study, will be presented.

Micropulsation Classification Scheme

Micropulsations have been organized by a classification scheme, based on the wave period and the spectral nature. The scheme, approved at the 1963 Berkeley meeting of the International Association of Geomagnetism and Aeronomy (IAGA) is as follows (Saito, 1969) :

Table 2-1 Micropulsation Classification Scheme

Type	Period (s)
Pc1	0.2 - 5.0
Pc2	5 - 10
Pc3	10 - 45
Pc4	45 - 150
Pc5	150 - 600
Pi1	1 - 40
Pi2	40 - 150

The "c" stands for "continuous", and the "i" for "irregular. The continuous emissions have a well-defined spectral peak, while the irregular are broad-band (many Fourier components are required to represent them). The "P" stands for "pulsation" (Saito, 1969).

Some Sources of Micropulsations

The following are a few examples of the geophysical processes connected to the occurrence of these waves. Pi2 pulsations are associated with the initiation of substorms, and are among the first signs of substorm commencement (for example, see Samson, 1982 and Olson & Rostoker, 1975). Some Pc5 pulsations are associated with Kelvin-Helmholtz "wind over water" instabilities at the surface of the magnetosphere, caused by the flow of solar wind (Saito, 1969; Takahashi, 1991). This is consistent with observed diurnal polarization patterns, in which the Pc5 are left polarized (ccw rotation of the electric field vector, looking along the magnetic field) in the morning and right polarized in the afternoon (Saito, 1969, Nishida, 1978). Pc5 are also associated with standing waves on field lines (Nishida, 1978), as are Pc3 and Pc4. These field line resonances could be excited when their frequencies match those of waves from Kelvin-Helmholtz instabilities at the magnetopause, or some other wave of external origin (Nishida, 1978). For example, they might also be excited by impulsive distortion of the magnetopause (Takahashi, 1991, with reference to Lee & Lysak, 1989). Pc3 and Pc4 waves are also seen upstream of the magnetopause, in the solar wind. The detection of these waves on the ground is associated with the occurrence of a nearly radial interplanetary magnetic field (Nishida, 1978; Engebretson, et al., 1991; and references therein).

Pc1 pulsations have been classified by Fukunishi (1981). A dozen separate types were noted, depending primarily on their spectral signatures. A pulsed-type emission, referred

to as "pearls" is thought to be amplified and propagate along field lines that pass near the plasmapause. Another class, called IPDP (Intervals of Pulsations of Decreasing Period) is distinguished by a generally rising frequency in events that last about an hour. These are apparently waves amplified in regions of progressively stronger magnetic field.

Quite often, these different Pc1 waves will be superimposed on a spectrogram. For example, it is common to see a pearl type signature embedded in a diffuse emission, perhaps 0.5 Hz in bandwidth, and more than 2 hours long. They may well come from different source regions and arrive simultaneously at the ground stations.

Previous Work on Pc1/2 Micropulsations

Pc1/2 waves are defined by Fukunishi (1981) as being characterized by a diffuse band mainly in the frequency range 0.1-0.4 Hz. This is a combination category from the classification scheme above. These waves have been investigated in both ground and satellite studies.

Heacock (1966) noted a broad afternoon/evening occurrence peak for pulsations in what he called the 4 second band. This band included some structured, or pulsed (pearl), events, along with some broad-band Pi events. A summer seasonal peak occurrence was found for these 'four second band' pulsations.

Rokityanskaya (1969) discussed the diurnal occurrence of micropulsations in the 4-6 second period range. A broad afternoon maximum was found, from approximately 1200-1700 LT.

Heacock (1974) noted a post-magnetic noon occurrence maximum at a 70°N (geomagnetic) station. Magnetic noon is when the magnetic meridian of a station

intersects the Earth-Sun line (Montbriand, 1970). He also found a seasonal occurrence variation, with a local summer maximum. Correlation studies between the occurrence of the Pc1/2 and the AE index, which is a crude measure of the convection electric field that will be described in more detail below. Although it was concluded that there was a weak correlation, no significant association was found. An associative study with the Dst index, a measure of ring current strength, yielded similar results. The Pc1/2 as defined by Heacock were mainly unstructured (diffuse pattern on a spectrogram), and in the frequency range 0.05 - 1.0 Hz, mostly 0.1-0.4 Hz.

Kaye and Kivelson (1979) surveyed Pc1/2 with the OGO-5 satellite, from about 7 to 14 R_E in the equatorial plane. They published 11 events, whose frequencies ranged from 0.06-0.60 Hz, and typically less than 0.2 Hz. All of the events occurred in the afternoon quadrant of the magnetosphere. In addition, all were associated with both enhanced pressure regions in the solar wind and a southward component of the interplanetary magnetic field (IMF). The threshold above which pressure was defined as "enhanced" was a value one standard deviation higher than the mean pressure from OGO-5 measurements during 1968-70. This was 2.80×10^{-8} dyn/cm². They found that "no Pc1-2 were found during extended intervals when the solar wind pressure remained less than 2.80×10^{-8} dyn/cm²". For the seven events presented in a figure, the pressure enhancements precede or follow the observation of the Pc12 by half an hour or less. The duration of the enhancement is at least one hour for five of the seven events shown, however, and approximately half an hour for the other two.

The possibility of an IMF relation was also studied, and they suggest that the IMF has a "significant southward component" two hours before the event. Hourly averages of the North-South component of the IMF, in GSM coordinates, were used. In this system, the x axis extends from the Earth to the Sun. The z axis moves as necessary to keep the

Earth's dipole axis is in the x - z plane. The z axis is positive in the same direction as the north magnetic pole. The y axis is perpendicular to these (Russell, 1971).

No close association of the Pc1/2 and storms or substorms were found. However, they suggested that during times of enhanced cross-magnetospheric electric field, both cold plasma that initially corotated with the earth, as well as energetic plasma, would convect sunward. Both types would move to the noon-dusk quadrant. The necessary pitch angle anisotropy for the energetic ions would develop from charge exchange (Kaye & Kivelson, 1979, with reference to Cornwall, 1977 and Cowley, 1977) and pitch-angle scattering from interactions with electrostatic waves (with reference to Ashour-Abdalla & Thorne, 1977). Cold ion density enhancements in the postnoon quadrant were observed by Chappell (1974) with OGO-5, however they noted that no correlations between Pc1/2 and the enhanced density regions had been made.

Bossen et al. (1976) studied waves in the 2-6 s period range (0.17-0.5 Hz) at synchronous orbit on ATS-1. They found that the afternoon quadrant was the most likely time to see these waves, particularly in the 1600-1700 local time hour. The wave frequencies of the majority of the events were 10-20% of the local ion (proton) gyrofrequency. They also noted that almost every event followed a substorm expansion onset, as determined by ground records, by less than 1.75 hours. AE values relative to the time of maximum wave amplitude were averaged over 120 wave events. This showed that the AE index rose about 40 minutes prior to the maximum wave amplitude at the spacecraft, which they said is consistent with the delay time between substorm expansion onsets and Pc 1 activity.

Fraser (1982) shows ground-satellite study between ATS-6 and Great Whale River, a ground station about 500 km east of the satellite's northern conjugate point. An afternoon

occurrence peak (12-15 LT) was observed at both, although the frequency range is not restricted to the 0.1-0.4 Hz Pc1/2 band of Fukunishi (1981). Pc1-2 is taken to be 0.1-5.0 Hz (see Fraser & McPherron, 1982). however, another occurrence peak about 10 h before is at Great Whale. The morning peak was attributed to pulsed "pearl" type emissions amplified at the plasmopause and ducted to Great Whale. This occurrence peak was not seen at ATS-6, which was at synchronous orbit, beyond the typical plasmopause radial distance.

Bolshakova et al. (1980) conducted a ground study of Pc1/2 at several latitudes. They noted the seasonal behavior, in which the Pc1/2 occur most often in local summer. A variety of diurnal patterns were presented for the stations. Some had single occurrence peaks near noon, others had small morning and large afternoon peaks. These patterns appeared to depend on latitude, and the authors associated them with the proximity of the stations to the cusp. In addition, when the magnetic activity increased, as determined by the Kp index (discussed below in the data analysis section), the Pc1/2 amplitude maximum shifted to lower latitude stations. This is consistent with the equatorward motion of the polar cap and cusp during times of increased activity in the magnetosphere.

They suggested a Pc1/2 source region near the entry layer, which is the open end of the cusp, on magnetosheath field lines. Since this source region is on solar wind field lines that have reconnected to the Earth's, instead of a closed line extending from one hemisphere to the other, not on field lines closed, they predicted very few conjugate observations would be made.

Finally, Sato & Saemunsson (1989) examined Pc1/2, according to Fukunishi's (1981) definition at stations in both northern and southern hemispheres. They also found the seasonal Pc1/2 occurrence pattern, and presented evidence to suggest conjugacy is most likely near the equinoxes. They also plotted the diurnal occurrence of events seen only in

one hemisphere at a time (non-conjugate). They found a UT time difference in the occurrence peaks in the stations. Since they have approximately the same magnetic local time, the difference was attributed to the difference in solar noon between the two. They calculated that the occurrence peak at 10 UT in the Antarctic station, and 14 UT at the Iceland conjugate station, corresponded to 1300 local solar time at both. Yamagishi (1989), studying ELF, found that waves tend to propagate along magnetic field lines in the summer hemisphere where the electron density increases along the magnetic field. Following this work, Sato & Saemunsson (1989) suggested sunlight effects as the reason for the seasonal and diurnal occurrence patterns they observed.

Chapter 3

Station Location, Instrumentation and Data Analysis

Station Location

The data for this study was acquired primarily at three high latitude arctic sites. These were:

Table 3-1 Station Location

Station	Geomagnetic Local Noon (UT)	Geomagnetic Latitude
Sondre Stromfjord, Greenland	1330	+74.1°
South Pole, Antarctica	1530	-74.9°
Siple, Antarctica	1700	-61°

The first two stations, Sondre Stromfjord and South Pole, are at approximately the same geomagnetic latitude, but in opposite hemispheres. There is also a two hour time difference in local magnetic noon, which is when the magnetic meridian of the station crosses a line extending from the Sun to the center of the earth (Montbriand, 1970). Sondre Stromfjord and South Pole are nearly conjugate stations. Both are close to the poleward edge of their respective auroral zones, which are bands in which aurora are most likely to occur, but they are at or below the latitude where low latitude boundary layer (LLBL) field lines would intersect the Earth. The LLBL comes to the surface of the Earth as a sort of buffer blanket around the funnel shape of the cusp, mainly the equatorward half of the funnel. This puts Sondre Stromfjord and South pole typically, but not always, depending on magnetic activity, on closed field lines that connect the southern and northern hemispheres (see data analysis section on DMSP data, and

Lundin, 1988 for an illustration of the cusp, cleft and LLBL relation), and pass close to the inner surface of the low latitude boundary layer. In times of increases magnetic activity, the boundary layer becomes closer to field lines connecting the South Pole and Sondre Stromfjord latitudes.

The third station is Siple, which is on a field line that crosses the equator at about $4.3 R_E$. This is close to the radial extent of the plasmasphere in the equator (the plasmopause), although the plasmaspheric radius varies by about $+1.5/-0.5 R_E$ for different levels of magnetic activity (Nishida, 1978, with reference to Chappell, 1972). The radial limit of the plasmasphere increases beyond $4 R_E$ during quiet times because the cross-magnetosphere electric field is weaker. In this case, Siple is connected to a field line that goes to the opposite hemisphere completely within the plasmasphere.

Instrumentation

The instrumentation at each station consists of two or three induction coil antennas, and a data acquisition system. These are oriented along magnetic North-South (X axis), East-West (Y axis), and in the case of Sondre Stromfjord after August 1986, along the magnetic field (Z axis). The X and Y axes are actually perpendicular to the magnetic field line. However, at these high latitude stations, the dip angle, which is the inclination of the magnetic field above the surface of the Earth, is at least 70° , so the X-Y plane is almost tangent to the surface.

In the Southern hemisphere, the signals are such that a positive dB/dt toward magnetic North corresponds to a positive X axis voltage output on a data plot. The same is true for a positive dB/dt toward magnetic East for the Y axis. In the Northern hemisphere,

positive X means a positive Northward dB/dt; positive Y means a positive Westward dB/dt, and a positive Z means an upward dB/dt.

Coil design and construction are documented in Parady (1974) and Taylor, et al. (1975). The coils consist of approximately 540,000 turns of #36 magnet wire, wrapped around a 2.5 cm mumetal (permalloy) core. The overall core length is 1.8 m. The wire is wound in sections of 30,000 turns (Lin & Plombon, 1985). A "calibration" coil of 15 turns is wound around the main coil. A current is passed through this winding with a periodic, alternating polarity, ramp signal. This produces a pulse train of alternating sign, constant magnitude dI/dt , or dB/dt , inducing a square wave output from the main coil. The calibration signal is generated automatically, approximately every four hours. Each axis signal is sampled at 10 Hz, so the maximum useable frequency is 5 Hz (the Nyquist frequency).

The signals are amplified by a preamplifier with a gain of 1000. The responses of the coil, the preamp, and the combination are shown in Figures 3-1 to 3-3 (Lin & Plombon, 1985). System sensitivities for the 1973 Siple coils are presented in Taylor, et al. (1975). The sensitivity plot is reproduced in Figure 3-4. At 0.3 Hz, the sensitivity is $9 \times 10^{-4} \gamma$ ($1 \gamma = 1$ nanoTesla), or one digitization unit in a 12 bit analog to digital converter (A/D). One digitization unit corresponded to 0.5 mV of final output voltage in the installation described in Taylor, et al. (1975).

At Sondre Stromfjord, the same type of coils and preamplifier were used, but an extra amplification was introduced just before A/D conversion. This changed the output voltage for one digitization step. Before August 28, 1986, -1 to +1 (preamplifier) volts were converted to +10 to 0 volts (a signal inversion was performed). The +10 to 0 volt range was converted by a 12 bit A/D. The same scheme was in use at McMurdo during 1986 (up through at least 1991). After that date, -2 to +2 volts were converted to +10 to 0

volts. The voltage value of a digitization step was doubled, which allowed a larger signal to be measured. All of the 1986 data was acquired with the UNH S79 controller.

South Pole and Siple data were acquired with a system operated by the University of Maryland (the "umd" controller). The amplification introduced just before the A/D conversion was such that -2 to +2 preamplifier volts were converted to +10 to -10 volts. These two stations utilized a 16 bit A/D converter. Data plots take all polarity changes and buffer amplification into account, and preamplifier output voltage is the quantity plotted.

The coil-preamplifier combination was tested by Hujanen (1987). A function generator was used with coils and a known series resistance to create a dB/dt in the micropulsation coils. The response of the system, in terms of output voltage/nT, was plotted against frequency. The output is approximately constant (± 0.025 volts), at 0.25 volts/nT, between 1 and 10 Hz. The output falls off above and below this frequency range. At 0.3 Hz, the output is 0.2-0.25 V/nT, and at 0.1 Hz, it is 0.1 (± 0.01) V/nT. The variation depends on the individual coil.

Data Analysis

The data from all three stations for all of 1986 was fast Fourier transformed, and spectrograms were printed in six hour panels. The transforms were performed using 25.6 second windows of data (128 frequencies, from 0 to 5 Hz, with data points 0.1 seconds apart) for each axis. The time steps between successive transforms was 25 seconds. This choice made it possible to clearly see "pearl" structure, which typically has two minutes between pulses. The data was stored on magnetic tape, which had between 2 and 11 days per reel, depending on the station. This variation was because other information, such as VLF antenna or riometer data from other experiments were written on the same tape. More

than 4200 six-hour spectrograms were printed. Around the clock tape processing and printing took almost seven months.

Events were visually selected from these spectral plots if they were least 10 minutes long and had a well defined spectral peak (i.e., distinctly band limited). Events separated by more than 10 minutes or 0.05 Hz were considered separate. The 10 minute standard was chosen because it is several "pearl" bounce times for an Alfvén wave packet following the field between conjugate points. For each event, the center frequency (± 0.05 Hz), maximum bandwidth, start and stop times were recorded in a database system on a Macintosh Plus computer. Other information, such as the presence of "pearl" or pulse structure, or the stations that observed the event, were noted. Some 4,500 events were collected from all three stations combined.

A sample of two database records is presented in Figure 3-5. The wave was seen at both stations, and it has the common event serial number 403.0 at each. Separate serial numbers are also given for the events at each station. In addition to the date, time, frequency information already described, other information is given. The "type" is used to distinguish any structured events (where periodic pulse strings dominate the frequency-time area in the spectrogram) from unstructured events (where such strings, if present, are a minor component). The "fragment" flag in each record indicates that the event is part of a series that correspond to an event at another station. Finally, a memo is attached, in which keywords are used to describe various features of the event. Memos might point out, for example, that some structure, or a pulse string, is present, but that the string is a minor part of the signal spectrum. The use of keywords here allows event selection on the basis of other information besides frequency or time.

Serial numbers were issued to each event at a station. Separate numbers were added for common events, which were seen at more than one station at a time. An additional

database was developed, in which all the common events were recorded, as well as the identity of the stations that observed them.

Examples of the Micropulsation Events in This Study

Structured (Pearl) and Pc1/2 Events

Examples of two structured (pearl) events are shown in Figure 3-6. One has a constant bandwidth (referred to as type 1 in the database), and the other has a widening, then narrowing bandwidth (type 4 in the database). A Pc1/2 is also present at approximately 0.4 Hz. Pc1/2 have a narrow-band structure that may persist for up to 17 hours. They are in the 0.1-0.4 Hz band, and have a diffuse character, usually with no pearl structure. Except for Figure 3-7, these figures are displayed in the 0-5 Hz frequency range and the six hour timespans of the survey plots from which the events were selected.

Another Pc1/2 is shown in Figure 3-7. Note the exceedingly sharp upper and lower frequency bounds. This feature of Pc1/2 will be discussed further in the section on results of data analysis. This event was seen in both hemispheres (South Pole and Sondre Stromfjord).

Common Station and Fragmented Events

(Hydromagnetic Chorus Example)

If several segments at one station corresponded to one monolithic event at another, the segments were identified as being seen in common with the single event. It is often the case that several events in a frequency-time plot have the same distinctive overall shape as a single event at another station, but with intermittent signal loss. This is no doubt due to the condition of the ionosphere during the observation time, which would be typically 2-6 hours in these cases. This is discussed further in the section on ionospheric modification

of micropulsation signals. An example of a fragmented event is shown in Figure 3-8. It is complete at Siple, but appears as two separate events at the two high latitude stations. This event is also referred to as a common event, since it was observed at more than one station. This is an example of a type 3 event, which is the general designation for events that are band limited, mostly diffuse emission, and are above the 0.1-0.2 Hz Pc2 frequency band.

Multiple Segment Events

Occasionally, many events overlap in such a way that it is difficult to separate them by any standard other than intensity on the spectrogram. An example of this is shown in Figure 3-9. This case was recorded as a single event, since it is impossible to say whether the component signals come from different sources, and should therefore be treated separately. A memo with the keywords "many segs" would be used in this kind of case. The selection process was intended to simply record individual occurrences on the spectrograms, without any assumptions about the association of one event with another.

Type 5 Events

An event type distinguished by nonperiodic, broadband pulses on a diffuse emission is illustrated in Figure 3-10. These were designated type 5 events for the database, but were not included in this study because they are irregular, impulsive and not band-limited. They are more common at the two high latitude stations than the plasmapause station (Siple); 120 were seen at South Pole, 128 at Sondre Stromfjord, but only 29 at Siple. Type 5 events have a postnoon peak occurrence and Kp distribution similar to that of the Pc1/2. These topics will be discussed further in the chapter on results of data analysis.

IPDP (Intervals of Pulsations of Decreasing Period) events were also noted, but not used in this study. These were far more common at the plasmapause station (Siple) than the high latitude stations (68 at Siple, vs. 9 at South Pole and 10 at Sondre Stromfjord).

Illustration of Event Selection

The selection of events is outlined in Figure 3-11. The event beginnings and ends are noted in the figure, as are the frequency limits. A calibration pulse appears as a dark vertical (broadband) line in the spectrogram at 1507 UT. Several of the wave types above are also noted in this figure.

No previous ground study has simultaneously published the length of events, their frequencies and which stations observed them. All of this information led to new insights about source regions and the presence of helium in the outer magnetosphere, which will be discussed below in the data analysis section.

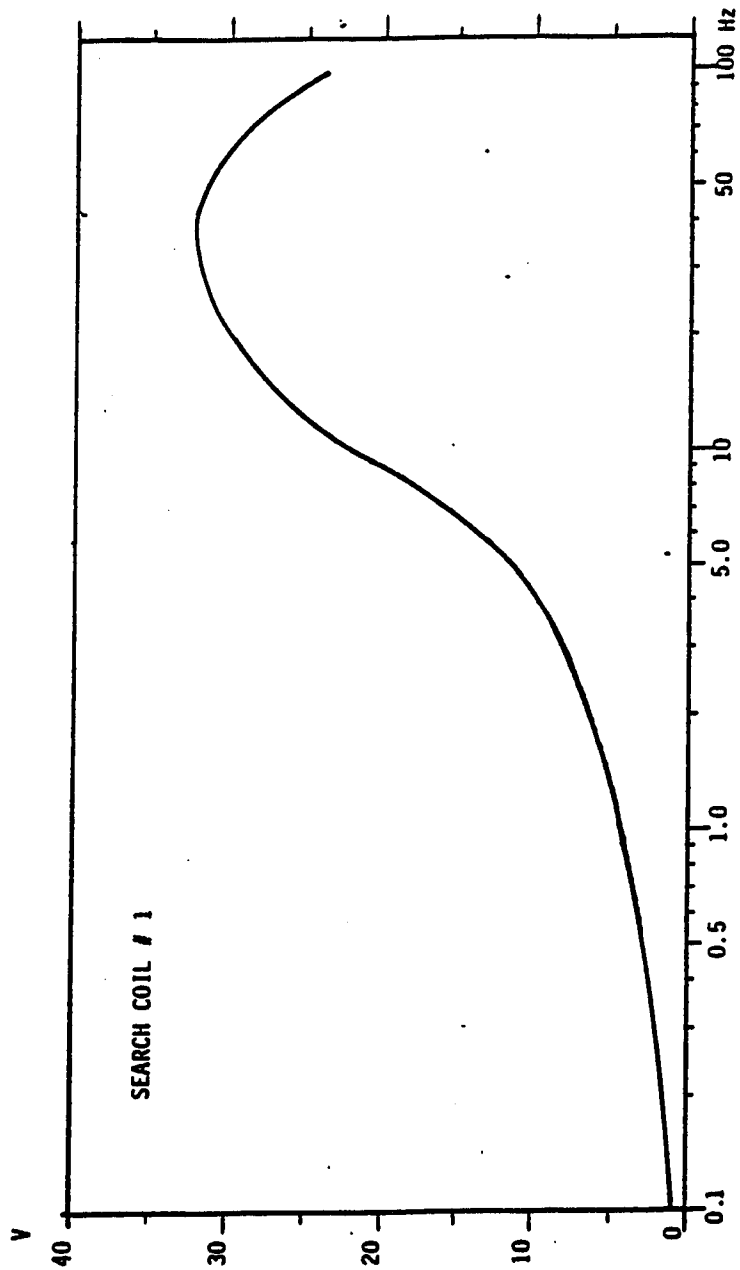


Figure 3-1 The response of the coil alone is shown as a function of frequency. The amplitude of the applied magnetic field was approximately 2.1×10^4 nT (Lin & Plombon, 1985)

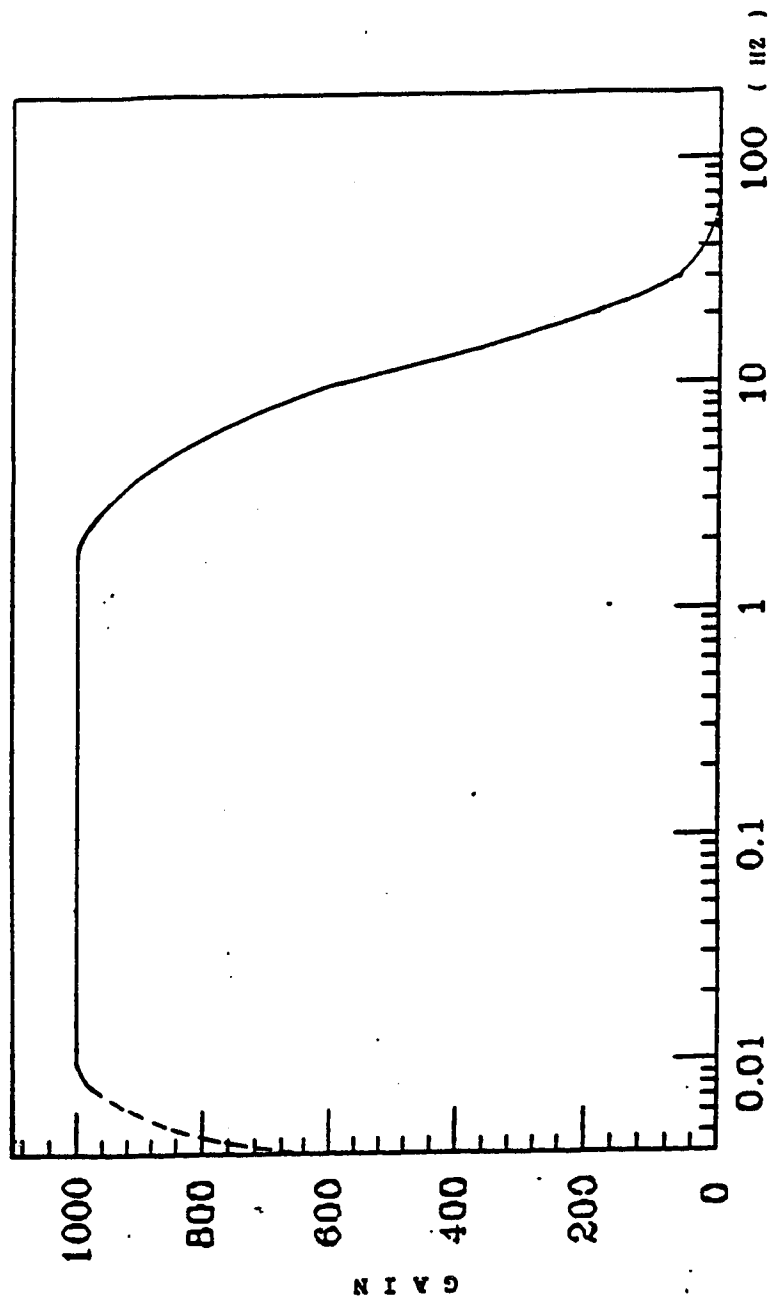


Figure 3-2 The gain of the preamplifier is shown vs. frequency (Lin & Plombon, 1985).

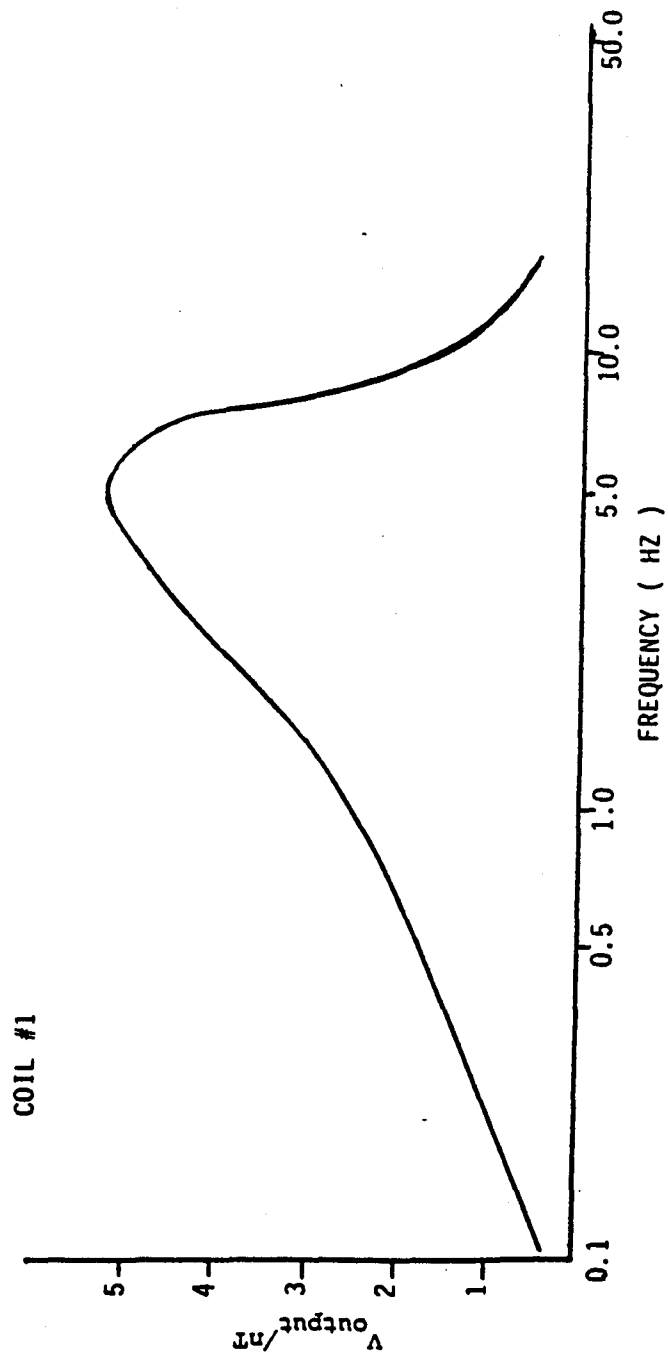


Figure 3-3 The combination of the coil and preamplifier together is shown as a function of frequency (Lin & Plombon, 1985).

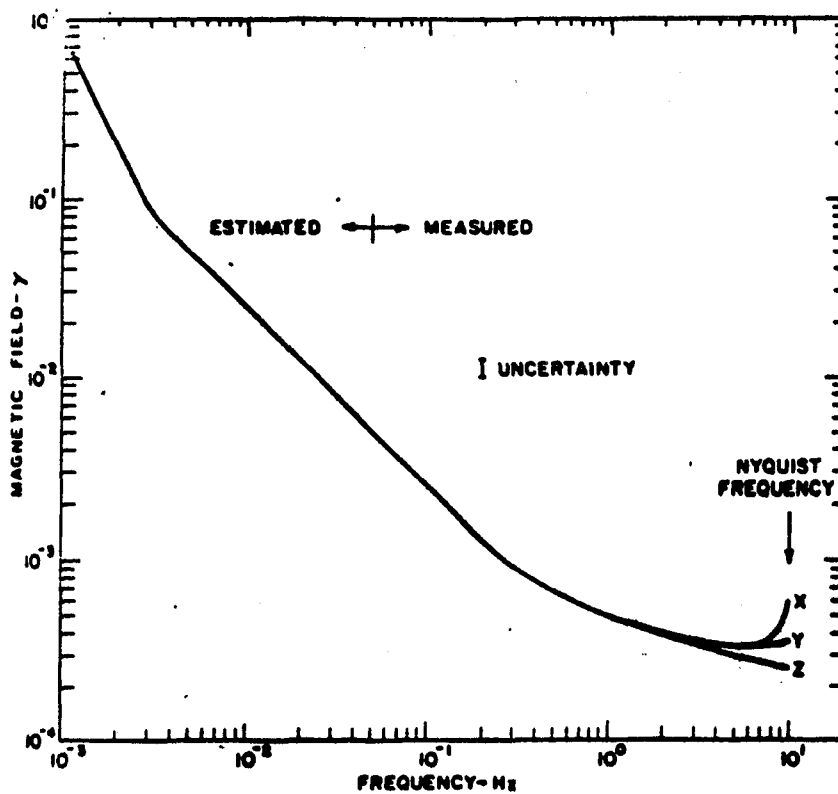


Figure 3-4 This sensitivity for the 1973 Siple coils was presented in Taylor, et al. (1975). At 0.3 Hz, in the Pc1/2 band, the sensitivity is $9 \times 10^{-4} \gamma$ ($1 \gamma = 1$ nanoTesla) for one digitization unit in a 12 bit analog to digital converter (A/D). One digitization unit corresponded to 0.5 mV of final output voltage in the installation described in Taylor, et al. (1975).

Sondre Stromfjord

Serial No.	Common Event Serial No.	Date	Start	Stop	Frequency	Bandwidth	Type
753.0	403.0	07/12/86	1220	1715	0.40	0.40	3

Fragmented .F. Memo: some str, nb seg; wb seg at beg

Siple

Serial No.	Common Event Serial No.	Date	Start	Stop	Frequency	Bandwidth	Type
1004.0	403.0	07/12/86	1225	1800	0.40	0.50	3

Fragmented .F. Memo: some str, mostly diffuse; wb gradually going to nb.

Figure 3-5. A Foxbase event database record records information about the date, the beginning and end of an event, as well as its center frequency and maximum bandwidth. The type is a simple classification of the spectral character of the event. Each event has a serial number at each station; if it was seen at more than one station, it has an additional number, in this case, 403.0, which is used in a separate database to keep track of which stations saw the event. Fragmented events are those in which several segments at one station correspond to a single, monolithic event at another station.

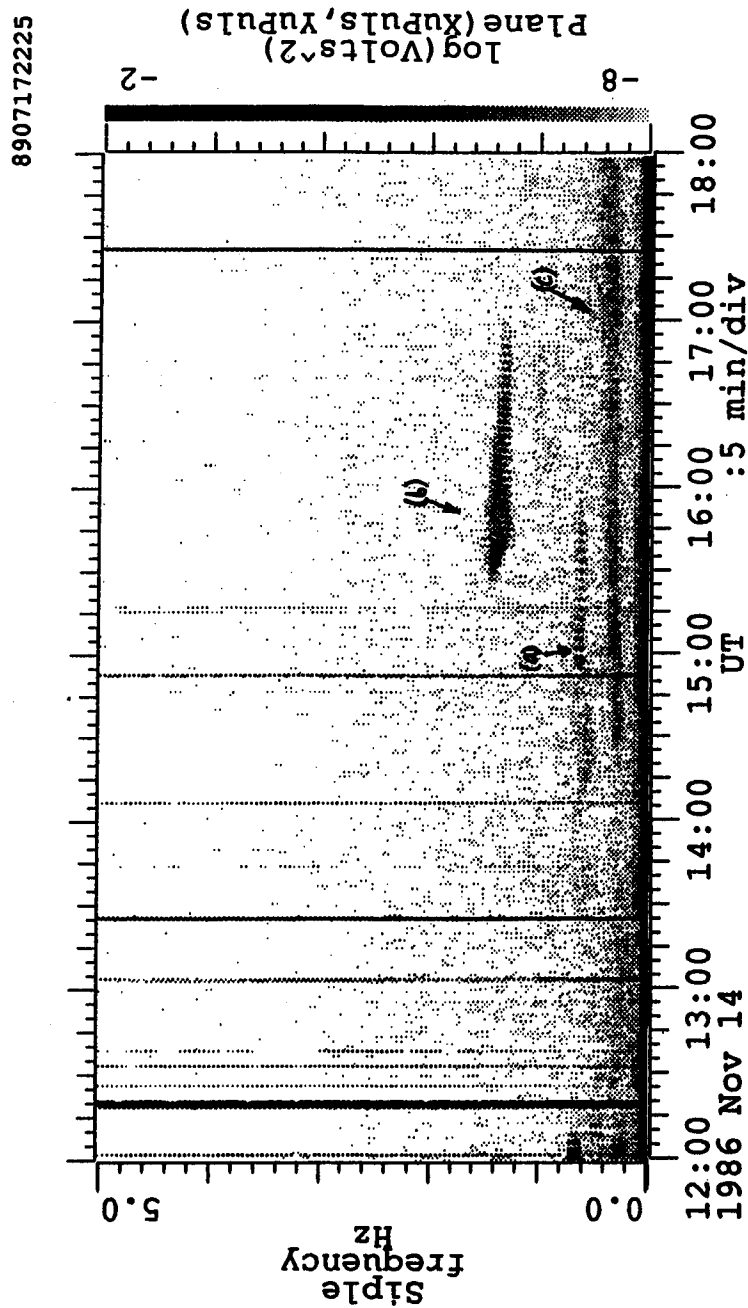


Figure 3-6 These are examples of two structured (pearl) events. One (labelled *a*) has a constant bandwidth (referred to as type 1 in the database), and the other has a widening, then narrowing bandwidth (labelled *b*, type 4 in the database). A Pc1/2 is also present at approximately 0.4 Hz (labelled *c*).

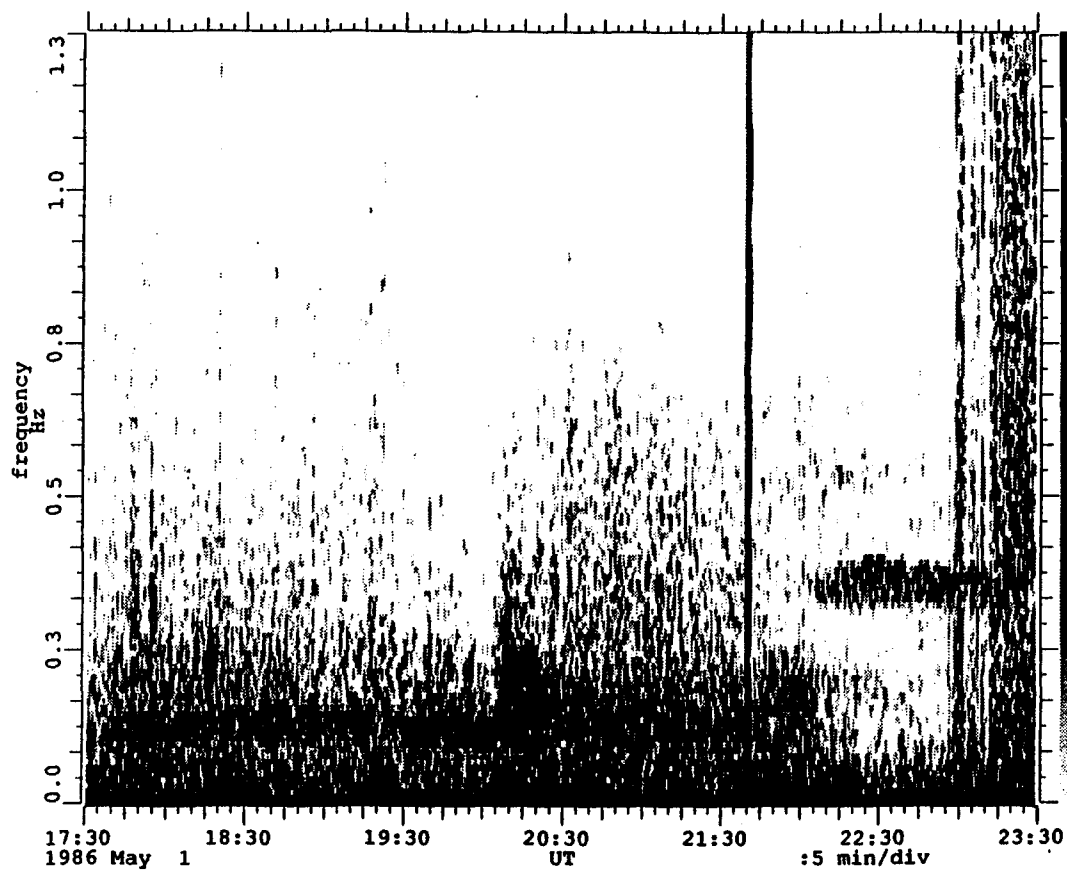


Figure 3-7 Two more Pc1/2 events are shown in this figure from South Pole. In the left hand Pc1/2 (at 0.15 Hz, 1730-2000 UT), note the exceedingly sharp upper and lower frequency bounds. The one on the right, from 2200-2300 UT, is just above 0.4 Hz. Both events were seen in both hemispheres (South Pole and Sondre Stromfjord).

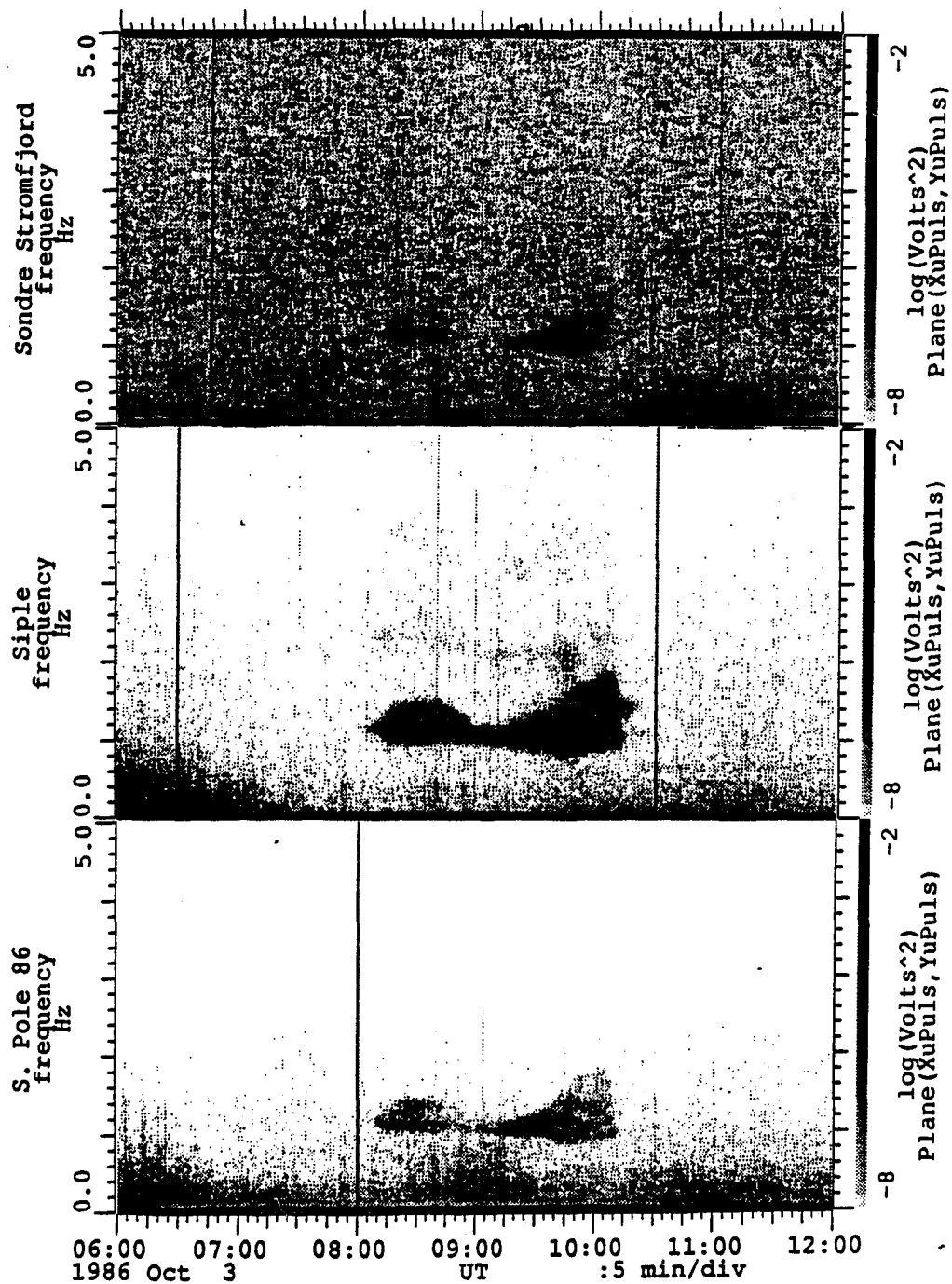


Figure 3-8 An example of a fragmented event is shown in this figure. It is complete at Siple, but appears as two separate events at the two high latitude stations. This event is also referred to as a common event, since it was observed at more than one station. This is an example of a type 3 event, which is the general designation for events that are band limited, mostly diffuse emission, and are above the 0.1-0.2 Hz Pc2 frequency band.

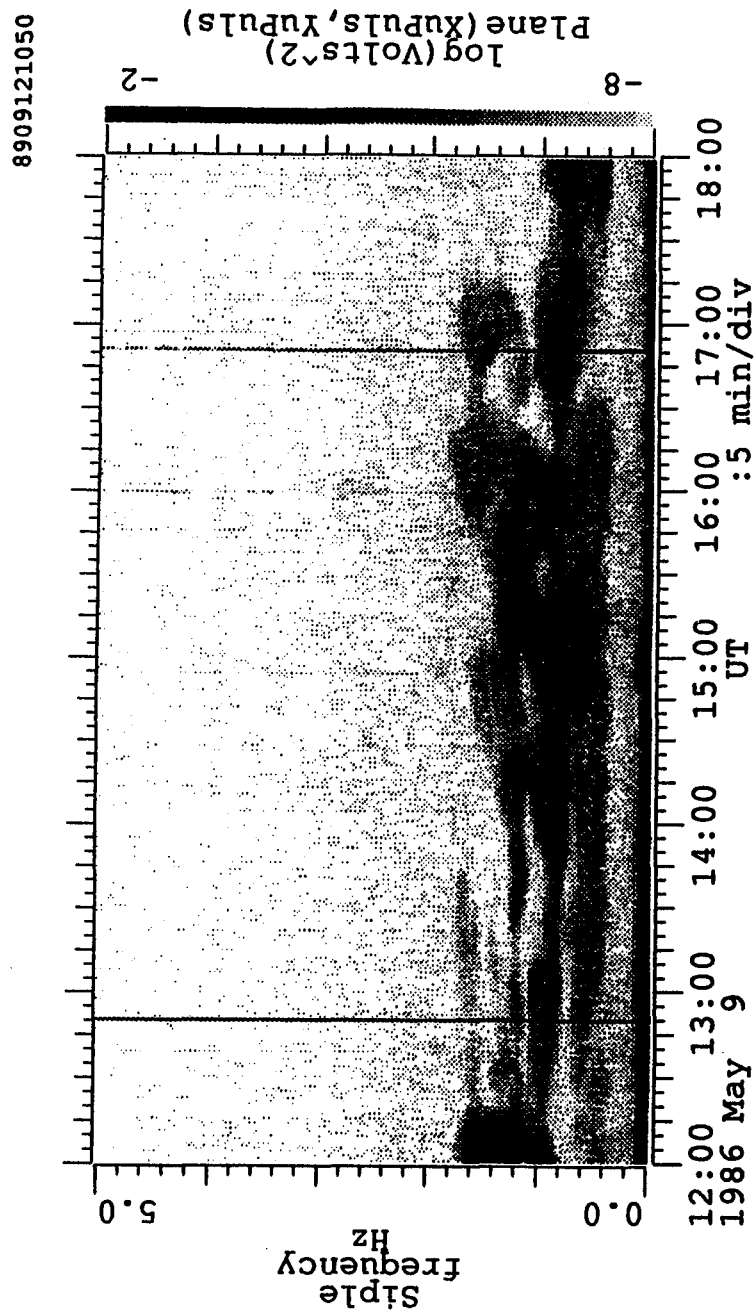


Figure 3-9 Sometimes many events overlap in such a way that it is difficult to separate them by any standard other than intensity on the spectrogram. This is an example of such an event. It was recorded as a single event, since it is impossible to say whether the component signals come from different sources, and should therefore be treated separately. A memo with the keywords "many segs" would be used in this kind of case.

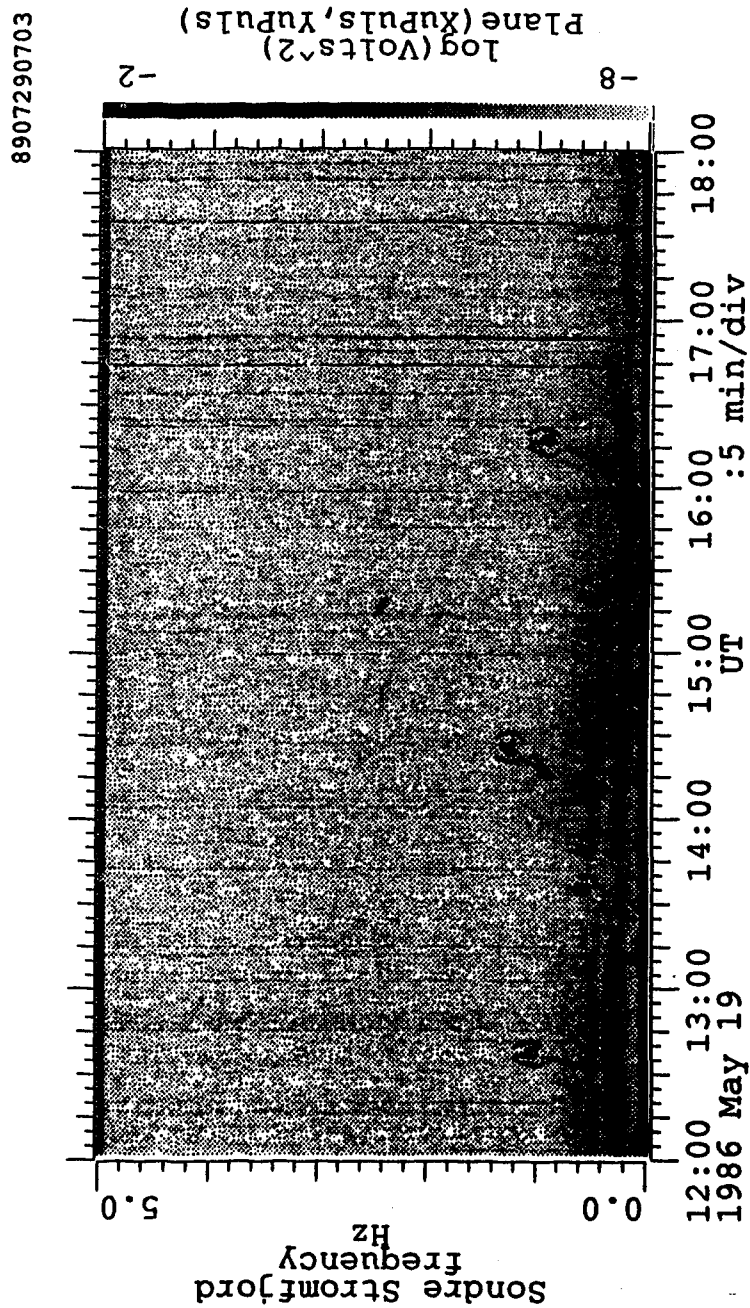


Figure 3-10 An event type distinguished by nonperiodic, broadband pulses on a diffuse emission is illustrated in this figure, labelled (a). These were designated type 5 events for the database, but were not included in this study because they are irregular, impulsive and not band-limited. They are more common at the two high latitude stations (SP, SS) than the plasmopause station (Siple). A Pc1/2 also appears at this time, labelled as (b). Type 5 events have not been studied in depth.

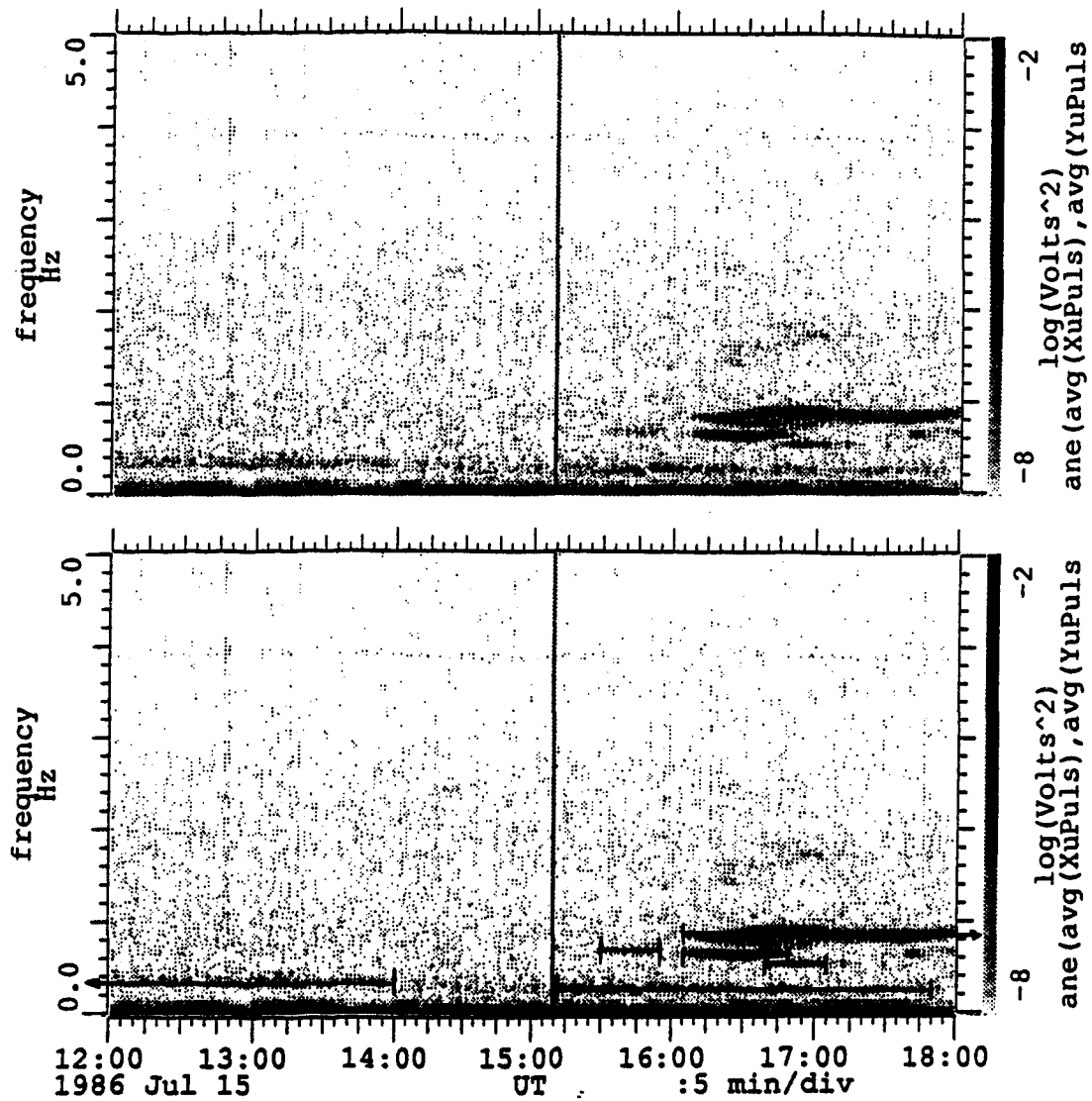


Figure 3-11 The selection of events is outlined in this figure from Siple. The same panel is shown twice. The top panel represents a typical survey plot, and the bottom indicates the events that were selected for the database. Lines have been drawn to show the center frequency, start and stop times. The maximum bandwidth was also noted, but not shown here for clarity. A calibration pulse appears as a dark vertical (broadband) line in the spectrogram at 1507 UT. Several of the wave types in previous figures also appear in this one.

Chapter 4

Alfven waves

Introduction

Micropulsations in the Pc1 range (0.2-5.0 Hz) are at such low frequencies that they resonate with and acquire energy from ions, unlike VLF and higher frequency waves which interact with ions and electrons together, or primarily with electrons. There are three solutions (wavemodes) to the dispersion relation, which is of order $(\omega/k)^6$. Each of these three is of order $(\omega/k)^2$, so two more solutions exist for each mode, representing waves traveling in opposite directions. In total, it may be said that six solutions exist. The three modes are the fast, the Alfven and slow modes. In a cold plasma, where sound speed is negligible, only the fast and Alfven modes exist. The Alfven mode is guided by the local magnetic field, while the fast mode is isotropic. These are electromagnetic waves in a medium which permits material currents \mathbf{J} . The displacement current $\partial\mathbf{E}/\partial t$ is small for these waves, in comparison to \mathbf{J} , because of the low frequencies (Dawson, 1966). The hydromagnetic modes will be derived in the following sections, assuming a single ion species plasma. After that, the effects of multiple ion species will be discussed. The presence of multiple species places certain restrictions on wave propagation, and this study will show that heavy ions in the magnetosphere strongly influence the pattern of waves observed on the ground.

Derivation of general dispersion relation

The dispersion relations for the wave modes may be derived from the equations of motion for ions and electrons, together with the wave equation, and in the case of a warm plasma, the equation of state. The necessary equations to do any case in which quasi-neutrality may be assumed will be presented in this section. In the following sections, some simple cases will be discussed for a physical description of the waves and a demonstration of the effect of various wavenormal directions, low wave frequencies, and finite plasma temperature.

Assuming harmonic, small amplitude electromagnetic perturbations and particle velocities, the equations of motion are:

$$Mn \frac{dv_i}{dt} = ne \left(\mathbf{E} + \frac{1}{c} \mathbf{v}_i \times \mathbf{B}_0 \right) - \nabla P_i \quad (\text{ions}) \quad (4-1)$$

and

$$mn \frac{dv_e}{dt} = -ne \left(\mathbf{E} + \frac{1}{c} \mathbf{v}_e \times \mathbf{B}_0 \right) - \nabla P_e \quad (\text{electrons}) \quad (4-2)$$

where n is the number density (quasi-neutrality is assumed here, so that $n_i = n_e = n$); \mathbf{v}_i and \mathbf{v}_e are first order perturbations, with zero constant velocity; \mathbf{E} is the wave electric field. P_i and P_e are the ion and electron pressures:

$$P = nk_B T ,$$

where k_B is Boltzmann's constant and T is the ion or electron temperature (Chen, 1974).

Note that since \mathbf{v}_i and \mathbf{v}_e are first order, the time derivative in the equation of motion becomes:

$$Mn \left[\frac{\partial \mathbf{v}_i}{\partial t} + \mathbf{v}_i \cdot \nabla \mathbf{v}_i \right] \rightarrow Mn \frac{\partial \mathbf{v}_i}{\partial t}$$

since $\mathbf{v}_i \cdot \nabla \mathbf{v}_i$ involves second order quantities. Also, the wave magnetic field \mathbf{b} is not in the equation of motion, since $\mathbf{v}_e \times \mathbf{b}$ would be of second order.

The wave equation is derived from the time derivative of Ampere's law and the curl of Faraday's law:

$$\frac{\partial}{\partial t} \left[\nabla \times \mathbf{B} = \frac{4\pi}{c} \mathbf{J} + \frac{1}{c} \frac{\partial \mathbf{E}}{\partial t} \right]$$

and

$$\nabla \times \left[\nabla \times \mathbf{E} = - \frac{1}{c} \frac{\partial \mathbf{B}}{\partial t} \right].$$

When added, the wave equation results:

$$\nabla \times \nabla \times \mathbf{E} = \nabla(\nabla \cdot \mathbf{E}) - \nabla^2 \mathbf{E} = - \frac{4\pi}{c^2} \frac{\partial \mathbf{J}}{\partial t} - \frac{1}{c^2} \frac{\partial^2 \mathbf{E}}{\partial t^2}, \quad (4-3)$$

where

$$\mathbf{J} = n_e e (\mathbf{v}_i - \mathbf{v}_e).$$

The displacement current may be neglected at ULF frequencies (Dawson, 1966). First order pressure amplitudes may be accounted for as follows, for either ions or electrons.

For example, for ions, we may write:

$$P_i \propto \rho_i^\gamma,$$

where $\gamma = \frac{C_p}{C_v}$, the ratio of specific heats (Chen, 1974), or equivalently $\gamma = 1 + \frac{2}{f}$,

(Halliday & Resnick, 1988) where f is the number of degrees of freedom ($f = 3$ for pure translational motion). An adiabatic state has been assumed, which is reasonable for motion perpendicular to the magnetic field (Chen, 1974). This means that

$$\nabla P_i = \gamma \rho_i \gamma^{-1} \nabla \rho_i = \gamma \frac{P_i}{\rho_i} \nabla \rho_i . \quad (4-4)$$

With the equation of continuity,

$$\frac{\partial \rho_i}{\partial t} + \nabla \cdot (\rho_i \mathbf{v}_i) = 0 ,$$

and with mass density represented by a constant, plus a first order variable:

$$\rho_i = \rho_{0i} + \rho_{1i} ,$$

pressure may be written in terms of \mathbf{k} and \mathbf{v}_i . First we have, assuming $e^{i(\mathbf{k}\cdot\mathbf{r} - \omega t)}$ harmonic dependence,

$$\nabla \cdot (\rho_i \mathbf{v}_i) = \mathbf{v}_i \cdot \nabla (\rho_{0i} + \rho_{1i}) + (\rho_{0i} + \rho_{1i}) \nabla \cdot \mathbf{v}_i \rightarrow \rho_{0i} \nabla \cdot \mathbf{v}_i \rightarrow i \rho_{0i} \mathbf{k} \cdot \mathbf{v}_i .$$

With this, mass conservation becomes

$$-i\omega \rho_{1i} + i \rho_{0i} \mathbf{k} \cdot \mathbf{v}_i = 0$$

and so

$$\nabla \rho_{1i} = i \mathbf{k} \frac{\rho_{0i}}{\omega} \mathbf{k} \cdot \mathbf{v}_i . \quad (4-5)$$

Inserting (4-5) into (4-4), we can write an expression for the pressure variation:

$$\nabla P_i = \frac{i \mathbf{k}}{\omega} \gamma P_i \mathbf{k} \cdot \mathbf{v}_i . \quad (4-6)$$

This can be written in terms of the total pressure from electrons and ions, $P = P_i + P_e$, assuming $P_i = P_e = P/2$ (Cross, 1988) :

$$\nabla P_i = \frac{i \mathbf{k}}{\omega} \gamma \frac{P}{2} \mathbf{k} \cdot \mathbf{v}_i .$$

The dispersion relation between k and ω may be derived from the ion and electron equations of motion (4-1, 4-2), the wave equation (4-3) and the pressure gradient equation (4-6). There are nine unknowns for the simple case of the electron-single ion species plasma: three components of velocity for each particle type, and three electric field components. If $\mathbf{k} = k_x \hat{x} + k_y \hat{y} + k_z \hat{z}$, and $\mathbf{B}_0 = B_0 \hat{z}$, the equations may be written in their component form (cgs units), with mass M representing the ions, and mass m representing the electrons, as :

$$\begin{aligned}
& \left[iM\omega - k_x^2 \frac{i\gamma P}{2\omega n} \right] v_{ix} + \left[\frac{e}{c} B_0 - k_x k_y \frac{i\gamma P}{2\omega n} \right] v_{iy} - k_z k_x \frac{i\gamma P}{2\omega n} v_{iz} + 0 v_{ex} + 0 v_{ey} + 0 v_{ez} \\
& + eE_x + 0E_y + 0E_z = 0 \\
& \left[-\frac{e}{c} B_0 - k_x k_y \frac{i\gamma P}{2\omega n} \right] v_{ix} + \left[iM\omega - k_y^2 \frac{i\gamma P}{2\omega n} \right] v_{iy} - k_z k_y \frac{i\gamma P}{2\omega n} v_{iz} + 0 v_{ex} + 0 v_{ey} + 0 v_{ez} \\
& + 0E_x + eE_y + 0E_z = 0 \\
& -k_x k_z \frac{i\gamma P}{2\omega n} v_{ix} - k_z k_y \frac{i\gamma P}{2\omega n} v_{iy} + \left[iM\omega - k_z^2 \frac{i\gamma P}{2\omega n} \right] v_{iz} + 0 v_{ex} + 0 v_{ey} + 0 v_{ez} \\
& + 0E_x + 0E_y + eE_z = 0 \\
& 0 v_{ix} + 0 v_{iy} + 0 v_{iz} + \left[im\omega - k_x^2 \frac{i\gamma P}{2\omega n} \right] v_{ex} - \left[\frac{e}{c} B_0 + k_x k_y \frac{i\gamma P}{2\omega n} \right] v_{ey} - k_z k_x \frac{i\gamma P}{2\omega n} v_{ez} \\
& - eE_x + 0E_y + 0E_z = 0 \\
& 0 v_{ix} + 0 v_{iy} + 0 v_{iz} + \left[\frac{e}{c} B_0 - k_x k_y \frac{i\gamma P}{2\omega n} \right] v_{ex} + \left[im\omega - k_y^2 \frac{i\gamma P}{2\omega n} \right] v_{ey} - k_z k_y \frac{i\gamma P}{2\omega n} v_{ez} \\
& + 0E_x - eE_y + 0E_z = 0 \\
& 0 v_{ix} + 0 v_{iy} + 0 v_{iz} - k_x k_z \frac{i\gamma P}{2\omega n} v_{ex} - k_z k_y \frac{i\gamma P}{2\omega n} v_{ey} + \left[im\omega - k_z^2 \frac{i\gamma P}{2\omega n} \right] v_{ez} \\
& + 0E_x + 0E_y - eE_z = 0 \\
& -i \frac{4\pi}{c^2} \omega n e v_{ix} + 0 v_{iy} + 0 v_{iz} + i \frac{4\pi}{c^2} \omega n e v_{ex} + 0 v_{ey} + 0 v_{ez} + (k_y^2 + k_z^2) E_x - k_x k_y E_y - k_x k_z E_z = 0
\end{aligned}$$

$$0 v_{ix} - i \frac{4\pi}{c^2} \omega n e v_{iy} + 0 v_{iz} + 0 v_{ex} + i \frac{4\pi}{c^2} \omega n e v_{ey} + 0 v_{ez} - k_y k_x E_x + (k_x^2 + k_z^2) E_y - k_y k_z E_z = 0$$

$$0 v_{ix} + v_{iy} - i \frac{4\pi}{c^2} \omega n e v_{iz} + 0 v_{ex} + 0 v_{ey} + i \frac{4\pi}{c^2} \omega n e v_{ez} - k_z k_x E_x - k_z k_y E_y + (k_x^2 + k_y^2) E_z = 0$$

This set of equations yields the dispersion relation for all three unique modes, in a warm plasma, with an arbitrary \mathbf{k} direction. The components have been written here in a form suggestive of a matrix. The coefficients of these nine variables may be arranged in a matrix. For nontrivial solutions, the determinant of the coefficients must be zero.

A physical picture of the Alfvén wave

A simple case has $\mathbf{k} = k \hat{z}$, $\mathbf{B}_0 = B_0 \hat{z}$, $\mathbf{E} = E \hat{x}$ (the wave electric field) and no pressure gradient force (cold plasma approximation). The particle velocities and wave fields for this case will be described below.

A physical picture of the Alfvén wave may be developed by first showing the dependence of particle velocities on the magnetic field (\mathbf{B}_0) and the wave electric field (Figure 4-1). The ion equations of motion without pressure are:

$$iM\omega v_{ix} + \frac{e}{c} B_0 v_{iy} + e E_x = 0$$

$$-\frac{e}{c} B_0 v_{ix} + iM\omega v_{iy} + e E_y = 0$$

$$iM\omega v_{iz} + e E_z = 0.$$

Cramer's rule may be used to find v_{ix} and v_{iy} . They are:

$$v_{ix} = \frac{-ieE_x M\omega + eE_y eB_0/c}{-M^2\omega^2 + e^2 B_0^2/c^2}$$

$$v_{iy} = \frac{-ieE_y M\omega - eE_x eB_0/c}{-M^2\omega^2 + e^2 B_0^2/c^2}$$
(4-7)

The electron velocities may be found by letting $e \rightarrow -e$ and $M \rightarrow m$. If the low frequency limit is taken, where $M^2\omega^2 \ll e^2 B_0^2/c^2$, the velocities of both electrons and ions are consistent with an oscillating $\mathbf{E} \times \mathbf{B}_0$ drift, due to the wave electric field. If this limit is not taken, there will be velocity components in the direction of the wave electric field.

This shows how particle motion is related to the wave electric field and \mathbf{B}_0 . Next, the role of the wave magnetic field will be displayed. The wave magnetic field \mathbf{b} is in phase with the electric field :

$$b_x = \frac{c}{\omega} (k_y E_z - k_z E_y) \rightarrow -\frac{c}{\omega} k_z E_y$$

$$b_y = \frac{c}{\omega} (k_z E_x - k_x E_z) \rightarrow \frac{c}{\omega} k_z E_x$$
(4-8)

Note first that in the low frequency limit, \mathbf{b} is 180° out of phase with particle velocities, because the electric field components in (4-7) and (4-8) have the opposite signs. Also, the velocities in this limit maximize at the same time as the wave fields, but point in opposite directions (see Figure 4-1). The result is that the magnetic field is undisturbed by the wave at maximum plasma displacement, and is most disturbed as plasma rushes across the equilibrium position. The field line and mass appear to move together as a loaded string (Figure 4-2).

The restoring force for this plasma oscillator is the $\mathbf{J}_p \times \mathbf{B}_0$ force of a polarization current that arises from the difference in ion and electron masses. This follows from the

expressions for ion and electron velocities. From equation (4-7), the x component of the current is, in the low frequency limit :

$$J_{px} = ne(v_{ix} - v_{ex})$$

$$= ne \left[\frac{-ieE_x M\omega + eE_y eB_0/c}{e^2 B_0^2/c^2} - \frac{ieE_x m\omega + eE_y eB_0/c}{e^2 B_0^2/c^2} \right]$$

$$J_{px} = \frac{-in(M+m)\omega E_x}{B_0^2/c^2} .$$

With this, the restoring force is :

$$F = \frac{\rho c^2}{B_0^2} \frac{dE}{dt} \times B_0 ,$$

where ρ is the total mass density: $\rho = \rho_i + \rho_e$. The i in the velocity expression (4-7) shows that this force is 90° out of phase with the electric field and plasma velocity, in the same manner as a simple harmonic oscillator.

**Fast and Alfvén modes in a cold plasma in the low frequency limit;
k not parallel to B_0**

This case allows a straightforward derivation of the dispersion relations for both the Alfvén and fast modes. If the low frequency limit is not applied, and/or the case of a warm plasma is considered, the derivation is lengthier; so for these cases, only results will be presented.

The Alfvén mode is the one just discussed in terms of a physical picture. In that case, k was restricted to the z axis, parallel to B_0 , and the low frequency approximation was applied. If k is allowed to have a component perpendicular to B_0 , however, another mode appears. The second mode is the fast mode. In this section the dispersion relations

will be derived. In later sections, it will be shown that these two modes have different phase speeds and that one is guided by the local magnetic field, while the other is isotropic.

Both modes may be derived in the low frequency limit ($\omega \ll \Omega_i$), with an arbitrary direction for \mathbf{k} as follows. If $\mathbf{k} = k_x \hat{x} + k_y \hat{y} + k_z \hat{z}$, the force equations (the first six of the matrix above) may be arranged to give particle velocities as a function of the electric field. These velocities may be used to write the components of \mathbf{J} in the wave equation (last three equations in the matrix) in terms of \mathbf{E} , ω and \mathbf{k} , with $\mathbf{B}_0 \parallel z$. The ion velocities have been worked out above (equation 4-7). In the low frequency limit, $M^2 \omega^2 \ll e^2 B_0^2 / c^2$, which is true for ions and electrons. Using $m \ll M$, and beginning with the x component, the currents are:

$$\begin{aligned} i \frac{4\pi}{c^2} \omega J_x &= i \frac{4\pi}{c^2} \omega n e (v_{ix} - v_{ex}) \\ &= i \frac{4\pi}{c^2} \omega n e \left[\frac{(-ieE_x M \omega + eE_y e B_0 / c) - (ieE_x m \omega + eE_y e B_0 / c)}{e^2 B_0^2 / c^2} \right] \\ &= \frac{4\pi}{c^2} \omega^2 \frac{nM}{B_0^2 / c^2} E_x \end{aligned}$$

$$i \frac{4\pi}{c^2} \omega J_x = \frac{\omega^2}{V_A^2} E_x$$

where $V_A = \frac{B_0}{\sqrt{4\pi n M}}$ (the Alfven speed). The y component of current is :

$$\begin{aligned}
 i \frac{4\pi}{c^2} \omega J_y &= i \frac{4\pi}{c^2} \omega n e (v_{iy} - v_{ey}) \\
 &= i \frac{4\pi}{c^2} \omega n e \left[\frac{(-ieE_y M \omega - eE_x eB_0/c) - (ieE_y m \omega - eE_x eB_0/c)}{e^2 B_0^2 / c^2} \right]
 \end{aligned}$$

$$i \frac{4\pi}{c^2} \omega J_y = \frac{\omega^2}{V_A^2} E_y .$$

Finally, from the equations of motion for electrons and ions, the current along the z axis is :

$$\begin{aligned}
 i \frac{4\pi}{c^2} \omega J_z &= \frac{4\pi}{c^2} \omega n e (v_{iz} - v_{ez}) \\
 &= \frac{4\pi}{c^2} \omega n e \left[\frac{-eE_z}{iM\omega} - \frac{eE_z}{im\omega} \right] \\
 &\approx - \frac{4\pi}{c^2} \omega n e \frac{eE_z}{im\omega} \\
 J_z &\approx \frac{ne^2 E_z}{m\omega} .
 \end{aligned}$$

J_z will be finite only if E_z is small, because the electron mass is small (see, for example, Hughes & Southwood, 1976).

The wave equation's x and y components are (with $E_z = 0$)

$$-i \frac{4\pi}{c^2} \omega J_x + (k_y^2 + k_z^2) E_x - k_x k_y E_y = 0$$

$$-i \frac{4\pi}{c^2} \omega J_y - k_y k_x E_x + (k_x^2 + k_z^2) E_y = 0 .$$

With the current terms, the components become

$$\left(-\frac{\omega^2}{V_A^2} + k_y^2 + k_z^2 \right) E_x = k_x k_y E_y \quad (4-9)$$

$$\left(-\frac{\omega^2}{V_A^2} + k_x^2 + k_z^2\right) E_y = k_y k_x E_x \quad (4-10)$$

The determinant of the coefficients must be zero for nontrivial solutions, so we have

$$\left(-\frac{\omega^2}{V_A^2} + k_y^2 + k_z^2\right) \left(-\frac{\omega^2}{V_A^2} + k_x^2 + k_z^2\right) - k_x^2 k_y^2 = 0 .$$

We may define $k_{\parallel} = k_z$ and $k_{\perp} = k_x^2 + k_y^2$, so that $k^2 = k_{\perp}^2 + k_{\parallel}^2$.

With these substitutions, the determinant becomes

$$\left[\frac{\omega^2}{V_A^2} - k_{\parallel}^2 \right] \left[\frac{\omega^2}{V_A^2} - k^2 \right] = 0 \quad (\text{Cross, 1988}),$$

which yields two dispersion relations:

$$\omega = k_{\parallel} V_A \quad (\text{Alfven mode; also called shear, torsional, oblique or transverse}) \quad (4-11)$$

and

$$\omega = k V_A \quad (\text{fast mode; also called compressional or isotropic}). \quad (4-12)$$

Fast and Alfven modes in a cold plasma, without the low frequency limit

If the low frequency approximation is not made, then the phase speed dependence on wave frequency becomes clear. This is the subject of this section. The dispersion relation for the two modes without the low frequency limit is (for the special case of $\mathbf{k} \parallel \mathbf{B}_0$):

$$\frac{\omega^2}{k^2} = V_A^2 \left[1 \pm \frac{\omega}{\Omega_i} \right] \quad (\text{Dawson, 1966}), \quad (4-13)$$

where the upper sign is for the fast mode, and the lower for the Alfven mode. Note that the phase speed of the fast mode is always greater than that of the Alfven mode, and also

increases with wave frequency. On the other hand, the Alfvén mode phase speed decreases with increasing wave frequency.

It is also clear from (4-13) that the Alfvén mode will stop propagating when $\omega \geq \Omega_i$, because the phase speed becomes imaginary. However, the fast mode will propagate at these frequencies. This opposite behavior is due to resonance of the Alfvén mode with ions. The Alfvén mode is left polarized, so the electric field has counter clockwise rotation, looking parallel to \mathbf{B}_0 (Chen, 1974), which is the same sense as ion cyclotron motion in a magnetic field.

The dispersion relation (4-13) clearly shows the upper frequency limit for the Alfvén mode as the ion cyclotron frequency, while the fast mode can propagate at higher frequencies, up to the electron cyclotron frequency. This is due to resonances arising from the rotation sense of ions and electrons in a magnetic field. The ion rotation matches the left polarized Alfvén mode, while electrons match the fast mode polarization. A "cutoff" frequency exists for the Alfvén mode. This will be discussed below, in the section on plasmas with multiple ion species. The cutoff frequency is (for $\omega_{pe} \ll \Omega_e$ and $\omega_{pi} \ll \Omega_i$):

$$\omega_{co} = \Omega_i + \frac{\omega_{pi}^2}{\Omega_i} \quad (\text{Swanson, 1989})$$

where ω_{pi} is the ion plasma frequency, $\omega_{pi} = (4\pi ne^2/M)^{1/2}$ (cgs units), and $\omega_{co} > \Omega_i$. This cutoff frequency was derived by keeping the displacement current, which is often disregarded at ULF frequencies. The displacement current becomes significant at high phase speeds, however, and the phase speed approaches infinity near a cutoff. The effect of the displacement current on the magnetic field may be quickly shown as follows. Combining

$$ikB = \frac{4\pi}{c} J - \frac{i\omega}{c} E$$

with

$$kE = \frac{\omega}{c} B ,$$

we have

$$B = \frac{4\pi}{c} J - \frac{\omega^2}{k^2 c^2} B .$$

The second term on the right hand side, which arises from the displacement current, becomes important for high phase speeds.

Fast, Alfvén and slow modes in a warm plasma

If the warm plasma case is chosen, the pressure gradient force terms will remain in the equations of motion for the electron and ions, since $\nabla P = k_B T \nabla n$, which depends on temperature. This introduces the sound speed into the dispersion relation. There are three modes in the low frequency limit for a warm plasma, which are the ω^2/k^2 roots of the zero determinant condition (Cross, 1988) :

$$\left[\frac{\omega^2}{k^2} - V_A^2 \cos^2 \theta \right] \left[\frac{\omega^4}{k^4} - \frac{\omega^2}{k^2} (c_s^2 + V_A^2) + c_s^2 V_A^2 \cos^2 \theta \right] = 0 \quad (4-14)$$

where $c_s^2 = \gamma P / \rho$ (square of the sound speed).

From the first bracketed term, the first dispersion relation is

$$\frac{\omega}{k} = V_A \cos \theta , \quad (4-15)$$

where θ is the angle between \mathbf{k} and \mathbf{B}_0 . This is called the "torsional", or Alfvén, wave, and is unaffected by the pressure (Cross, 1988).

The second bracketed term yields the other two modes. One may write

$$\begin{aligned} \frac{\omega^2}{k^2} &= \frac{(c_s^2 + V_A^2)}{2} \pm \frac{1}{2} \sqrt{(c_s^2 + V_A^2)^2 - 4c_s^2 V_A^2 \cos^2 \theta} \\ &= \frac{(c_s^2 + V_A^2)}{2} \pm \frac{1}{2} \sqrt{c_s^4 + V_A^4 + 2c_s^2 V_A^2 (1 - 2\cos^2 \theta)} \end{aligned} \quad (4-16)$$

At $\theta = 0^\circ$,

$$\frac{\omega^2}{k^2} = \begin{cases} c_s^2 \\ V_A^2 \end{cases} \quad (4-17)$$

The fast wave phase speed is the greatest of the two, and the slow wave speed is the smallest. At $\theta = 90^\circ$,

$$\frac{\omega^2}{k^2} = \begin{cases} (c_s^2 + V_A^2) & \text{(fast wave)} \\ 0 & \text{(slow wave)} \end{cases} \quad (4-18)$$

If $c_s \ll V_A$, the dispersion relation for the fast and slow modes may be written as :

$$\frac{\omega}{k} = c_s \cos \theta \quad \text{(slow wave),} \quad (4-19)$$

and

$$\frac{\omega}{k} = V_A \quad \text{(fast wave).}$$

If more terms are kept in (4-16), these relations may be rewritten as:

$$\frac{\omega^2}{k^2} = \frac{c_s^2}{2} (1 + \cos 2\theta) \quad \text{(slow wave),}$$

and

$$\frac{\omega^2}{k^2} = V_A^2 + \frac{c_s^2}{2} (1 - \cos 2\theta) \quad (\text{fast wave}).$$

These expressions reduce to the 0° and 90° cases above (4-17, 4-18), in which no approximation was made.

The fast wave is isotropic, while the Alfvén (4-15) and slow (4-19) waves are field-guided, which will be shown below. Although these dispersion relations were derived for the low frequency limit, the two guided modes are still guided if this limit is not taken, as long as the medium is collisionless (Dawson, 1966; Cross, 1988). The fast mode does not have the same phase speed in all directions, but it may propagate in any direction. Cross (1988) diagrams the phase speeds vs. the angle between \mathbf{k} and \mathbf{B}_0 .

The slow wave may propagate perpendicular to \mathbf{B}_0 only if the ion collision frequency is on the order of the wave frequency (see Dawson, 1966). This will be covered further in the section on ionospheric modification of micropulsations.

The sound speed may be estimated for the plasmasphere where cold plasma thermal energies are a few eV. Assuming three degrees of freedom in the particles ($\gamma=5/3$), we have :

$$c_s^2 = \frac{\gamma P}{\rho} \approx \frac{5}{3} \frac{n k_B T}{n M} \approx 10^8 \text{ m}^2/\text{s}^2, \text{ or, } c_s \approx 10^4 \text{ m/s.}$$

For comparison, at $3 R_E$ in the equatorial plane, where the electron density is approximately 500/cc (see Kelley, 1989), and the magnetic field is approximately 0.01 gauss (T89 model, D. Larson, pc; or about 1/9 of the Earth's surface magnetic field), the Alfvén speed, $B_0 / \sqrt{4\pi n M}$, is approximately 10^6 m/s, 100 times greater than the sound speed.

Group velocity : the isotropic and field-guided nature of the modes

The propagation direction of a localized wave packet is described by its group velocity . Calculation of the group velocity shows that the Alfvén (transverse) mode is field-guided, while the fast mode is isotropic. From Cross (1988),

$$\mathbf{V}_g = \nabla_{\mathbf{k}} \omega = \frac{\partial \omega}{\partial k_x} \hat{x} + \frac{\partial \omega}{\partial k_y} \hat{y} + \frac{\partial \omega}{\partial k_z} \hat{z} .$$

The component of group velocity parallel to \mathbf{B}_0 for the two modes in a *cold* plasma, whose phase velocity is given by equation (4-13), is :

$$|\mathbf{V}_g|_{\parallel} = V_A \frac{\left[1 \pm \frac{\omega}{\Omega_i}\right]^{3/2}}{1 \pm \frac{\omega}{2\Omega_i}} \quad (\text{Dawson, 1966}) .$$

If the derivative of \mathbf{V}_g with respect to ω is taken, it is found that the group (and phase, as shown above) velocities increase with frequency for the fast mode ($\partial \mathbf{V}_g / \partial \omega > 0$), but *decrease* with increasing frequency for the Alfvén mode. This is apparent in the spectrograms of "pearls", or discrete pulses in the 0.2-5.0 Hz Pc1 band, about two minutes apart. The pulses first arrive as vertical lines on a frequency-time spectrogram, broadband in frequency, narrow in time. As successive pulses are seen, the vertical lines tip over, so that higher frequencies arrive last. The waves are thought to follow the magnetic field of the Earth, alternately mirroring from both hemispheres. The higher frequencies of these waves travel slowest, so they arrive later each time the wave packet reflects from the ionosphere.

The fast wave may propagate in all directions with the same speed (V_A), since the group velocity at low frequencies is

$$\mathbf{V}_g = \frac{\partial \omega}{\partial \mathbf{k}} \hat{\mathbf{k}} = V_A \hat{\mathbf{k}} .$$

The Alfvén and slow waves only propagate parallel to the magnetic field, however, since

$$\omega = kV_A \cos\theta$$

$$\mathbf{V}_g = \frac{\partial\omega}{\partial\mathbf{k}} \hat{\mathbf{k}} + \frac{1}{k} \frac{\partial\omega}{\partial\theta} \hat{\boldsymbol{\theta}} \quad (\text{Swanson, 1989})$$

$$= V_A \cos\theta \hat{\mathbf{k}} - V_A \sin\theta \hat{\boldsymbol{\theta}} .$$

The dot product of \mathbf{V}_g with the magnetic field vector is:

$$\begin{aligned} \mathbf{V}_g \cdot \mathbf{B}_0/|\mathbf{B}_0| &= (V_A \cos\theta)(\mathbf{k} \cdot \mathbf{B}_0/|\mathbf{B}_0|) + (-V_A \sin\theta)(\hat{\boldsymbol{\theta}} \cdot \mathbf{B}_0/|\mathbf{B}_0|) \\ &= (V_A \cos\theta)(\cos\theta) + (-V_A \sin\theta)(-\cos(90-\theta)) \\ &= V_A . \end{aligned}$$

The group velocity of the Alfvén mode has magnitude V_A parallel to the magnetic field.

Another, less general way to show this is to say that $\omega = V_A k_{\parallel}$, so that $(\partial\omega/\partial k_{\perp}) = 0$. The wavenormal \mathbf{k} of the Alfvén mode may be at an angle θ to \mathbf{B}_0 , but the group velocity is not parallel to \mathbf{k} .

On the other hand, in the cold plasma case, the fast wave group velocity is always in the \mathbf{k} direction, because there is no θ dependence. This makes the fast wave isotropic. In the warm plasma case, the phase speed of the fast wave does depend on θ (see 4-17 and 4-18), but the group velocity is not necessarily parallel to the magnetic field.

Polarization of the fast and Alfvén modes in a cold plasma

The polarization of the Alfvén and fast modes is discussed in the low-frequency limit by Denisse & Delcroix (1963) and Cross (1988). The polarization of a mode is the ratio of E_x to E_y . From the first component of the wave equation (4-9), the ratio of E_x to E_y is

$$\frac{E_x}{E_y} = \frac{k_x k_y}{\left[-\frac{\omega^2}{V_A^2} + k_y^2 + k_z^2 \right]}$$

The dispersion relation for the Alfvén mode in the low frequency limit, equation (4-11), may be substituted to find the polarization for that mode. This gives :

$$\frac{E_x}{E_y} = \frac{k_x k_y}{\left[-\frac{\omega^2}{V_A^2} + k_y^2 + \frac{\omega^2}{V_A^2} \right]} = \frac{k_x}{k_y}$$

From this, it may be concluded that if \mathbf{k} is confined to the x - z plane, then for the Alfvén mode, $E_y \rightarrow 0$. This means that the electric field vector for the low-frequency Alfvén mode is confined to the \mathbf{k} - \mathbf{B}_0 plane.

The polarization for the low-frequency fast mode is derived by using the fast mode dispersion relation (4-12) instead. In that case,

$$\frac{E_x}{E_y} = \frac{k_x k_y}{(-k^2 + k_y^2 + k_z^2)} = -\frac{k_y}{k_x},$$

so that $E_x \rightarrow 0$ for \mathbf{k} in the x - z plane. In the low frequency limit, then, the fast mode electric field is perpendicular to the \mathbf{k} - \mathbf{B}_0 plane. This is the opposite of the Alfvén mode. When $\mathbf{k} \perp \mathbf{B}_0$, this makes the $\mathbf{E}_{\text{wave}} \times \mathbf{B}_0$ motion of the plasma parallel to \mathbf{k} , which gives the fast mode a compressional nature.

Circular polarization in a cold plasma

If $\mathbf{k} \parallel \mathbf{B}_0$, circular polarization can occur, since there is no \mathbf{k} - \mathbf{B}_0 plane. If the low frequency approximation is not used, the polarization for the Alfvén and fast modes can be derived from the ratio of electric field components. If they are linearly polarized, with no phase difference, this ratio will be 1. A phase difference will be represented by -1, for a π radian phase difference, or a complex number for any other phase difference. For

example, if the ratio is $\pm i$, there is a $\pi/2$ difference, since the electric field has a harmonic variation. The $M^2 \omega^2$ terms may not be neglected in the ion velocity expressions above (4-7). When they are included in the y component of the wave equation, with $\mathbf{k} = k \hat{z}$, the ratio of E_x to E_y is

$$\frac{iE_x}{E_y} = \frac{\Omega_i}{\omega} - \frac{(\Omega_i^2 - \omega^2)V_A^2 k^2}{\Omega_i \omega^3} = \pm 1 \quad (\text{Dawson, 1966}) .$$

The dispersion relation (4-13) that does not arise from a low frequency approximation was used. The upper sign refers to the fast mode, and the lower to the Alfvén mode. The +1 means that

$$E_y e^{i(\mathbf{k}\cdot\mathbf{r} - \omega t)} = e^{i(\mathbf{k}\cdot\mathbf{r} - \omega t + \pi/2)} E_x ,$$

so that E_y is ahead of E_x by $\pi/2$, which is right circular polarization (cw rotation of the electric field vector) for the fast wave. The Alfvén wave is left circularly polarized when $\mathbf{k} \parallel \mathbf{B}_0$, which allows it to resonate with ions gyrating in a magnetic field.

Propagation in the presence of multiple ion species in a cold plasma

If more than one type of ion is present, the Alfvén mode may be found at a higher frequency than the lowest ion cyclotron frequency, and the right polarized mode is magnetic field-guided in certain frequency bands.

The effect of multiple ion species on the dispersion relation and wave polarization will be discussed in this section. They may be accounted for by modification of the single ion equations (Dawson, 1966). When this is done, the current density becomes:

$$\mathbf{J} = e(\sum n_i \mathbf{v}_i - n_e \mathbf{v}_e) ,$$

and charge neutrality requires:

$$n_e = \sum n_i .$$

If $\omega \ll \Omega_e$ and $\Omega_i \ll \Omega_e$, the velocities of the ions and electrons may again be expressed in terms of electric field. The dispersion relation will look the same as for the single ion species case if two changes are made. A composite ion gyrofrequency replaces the single ion gyrofrequency:

$$\Omega_{\text{com}} = \frac{\sum \frac{n_i \Omega_j}{\Omega_j^2 - \omega^2}}{\sum \frac{n_i}{\Omega_j^2 - \omega^2}} ,$$

which becomes the j^{th} gyrofrequency when ω approaches Ω_j . The composite Alfvén velocity is (quoted from Dawson (1966) in MKS units):

$$V_{\text{com}}^2 = \frac{B_0^2 \sum \frac{n_i}{M_j (\Omega_j^2 - \omega^2)}}{\mu \sum \frac{n_i}{\Omega_j - \omega} \sum \frac{n_i}{\Omega_j + \omega}} \quad (\text{Dawson, 1966}) .$$

Special frequencies due to the presence of heavy ions

Below every ion gyrofrequency, there will be other special frequencies introduced because of the presence of the next more massive ion. These are the crossover, the cutoff and the bi-ion hybrid frequencies. In a plasma with H⁺ and other ions, the H⁺ gyrofrequency will be the highest. The gyrofrequency is called a resonance, since ions may pass energy to a left-circularly polarized wave, or vice versa, when $\omega = \Omega_j$, the j^{th} ion gyrofrequency.

One of the frequencies created by the presence of multiple ion species is the zero-current frequency, or when $\Omega_{\text{com}} = 0$, which occurs at

$$\sum \frac{n_j \Omega_j}{\Omega_j^2 - \omega^2} = 0. \quad (\text{Dawson, 1966})$$

At this frequency, also called the bi-ion hybrid in literature (for example, Perraut et al., 1984), there will be no current parallel to the transverse wave electric field. Only the fast mode may propagate here (Dawson, 1966, unless $\mathbf{k} \perp \mathbf{B}_0$ (Rauch & Roux, 1982, Perraut et al., 1984, Roux et al., 1982)). This is discussed further in the next section. Above this frequency, the fast mode is guided by the magnetic field, but below, the fast mode is not guided. If the two ions are H^+ and He^+ , the bi-ion hybrid frequency is given by Young et al. (1981):

$$f_{\text{bi}} = \Omega_{\text{He}^+} \sqrt{\frac{1 + 3\eta}{1 + 3\eta/4}},$$

where η is the concentration of He^+ ($\eta = N_{\text{He}^+}/N_{\text{total}}$), and N_{total} is the density of both hot and cold ions (Perraut et al., 1984).

A cutoff frequency will occur when

$$\sum \frac{n_j}{\Omega_j - \omega} = 0 \quad (\text{Dawson, 1966}),$$

which makes the phase speed infinite (see Ichimaru, 1973; and Dawson, 1966). This sum involves positive and negative terms because ω may be between gyrofrequencies.

Another expression for the cutoff is given by Young et al., (1981). The ion gyrofrequency just below the cutoff, and the concentration of that ion determine the cutoff frequency :

$$f_{\text{CF}} = \Omega \sqrt{1 + 3\eta} \quad (\text{Young et al., 1981})$$

Finally, the crossover frequency is defined by

$$\Omega_{\text{com}} \rightarrow \infty ,$$

which takes place when the sum

$$\sum \frac{n_i}{\Omega_j^2 - \omega^2} = 0 \quad (\text{Dawson, 1966}) .$$

At this frequency, the polarization of the wave changes to the opposite sense (left to right or vice versa). The faster mode is always isotropic in the vicinity of this frequency, regardless of polarization (Dawson 1966). Above this frequency, the isotropic mode has the opposite polarization for propagation parallel to the magnetic field as below. The same is true for the field-guided mode. At the crossover frequency, the polarization of the wave is linear.

It is necessary for the wavenormal \mathbf{k} to have some component perpendicular to \mathbf{B}_0 for the polarization switch to occur (Young et al., 1981); otherwise, the left and right polarized modes will not couple. Even if \mathbf{k} and \mathbf{B}_0 are initially parallel at the equator, where wavegrowth is expected to occur (see section below on wavegrowth), the angle between them will increase as the left polarized wave propagates away from the equator (Young, et al., 1981).

Another expression for the crossover frequency, is given by Young et al. (1981). The ion gyrofrequency just below the crossover, and the concentration of that ion determine the crossover frequency :

$$f_{\text{CR}} = \Omega \sqrt{1 + 15\eta} \quad (\text{Young et al., 1981, with reference to Smith \& Brice, 1964}).$$

Implications of multiple ion species for micropulsations

Micropulsations are thought to be Alfvén waves that are amplified in the left-polarized mode near the equator, and propagate to the ground. A guided, left polarized wave, after resonance and amplification by energetic ions, will pass through the crossover and become a guided, right polarized wave. This wave, moving into a region of increasing magnetic field, will reach a point where the local bi-ion frequency matches the wave frequency. The wave will become unguided and the wave normal will quickly become perpendicular to \mathbf{B}_0 . Then, at a frequency slightly below the bi-ion frequency, when $\mathbf{k} \perp \mathbf{B}_0$, the group velocity parallel to \mathbf{B}_0 goes to zero, and the wave is reflected (Rauch & Roux, 1982). It will then return to a guided mode, and reflect from the bi-ion frequency region in the opposite hemisphere. In the case of H^+ and He^+ as the major constituents, the wave may tunnel through their bi-ion hybrid frequency if the He^+ concentration is only a few percent (Perraut et al., 1984). This means that waves amplified at the equator, between the H^+ and He^+ gyrofrequencies, *will not reach the ground* unless the He^+ density is low enough along their magnetic field path to ground.

The bi-ion hybrid frequency, or zero-current frequency, is important for the interpretation of micropulsation observations. When micropulsation studies are combined with spacecraft measurements, the importance of heavy ions to wave propagation can be determined.

The propagation of ULF waves in a H^+ , He^+ plasma in the magnetosphere has been discussed by Rauch & Roux (1982), who did ray tracing, and Young et al. (1981), Roux et al. (1982) and Perraut et al. (1984), who studied propagation in light of their GEOS 1 and 2 spacecraft measurements. They describe three classes of waves that are distinguished by the characteristic frequencies described above. Class III waves are

described above. They can exist from a frequency of zero up to the H^+ gyrofrequency, and are sensitive to the bi-ion hybrid frequency and the crossover.

Class I waves are amplified below the local He^+ gyrofrequency and are left polarized. As they move toward the ground, the local He^+ gyrofrequency increases further above the wave frequency, so these waves never encounter the bi-ion hybrid or crossover frequencies due to the He^+ ions. They can easily reach the ground, and the Pc1/2 in this study are in this class.

Class II waves exist above the cutoff due to the He^+ ions, so these waves are already above the local He^+ gyrofrequency. They can only be amplified by resonance with H^+ ions. Above the cutoff, but below the crossover, they are left polarized. Above the crossover, they are fast waves that are right polarized when $k \parallel B_0$. The crossover does not make them guided, it just switches their polarization. For this reason, these waves are unguided, regardless of polarization, and hence are not greatly amplified. They propagate away toward regions of weaker B_0 , since they only exist above the cutoff (Rauch & Roux, 1982). These classes will be discussed below in regard to ground observations in this study.

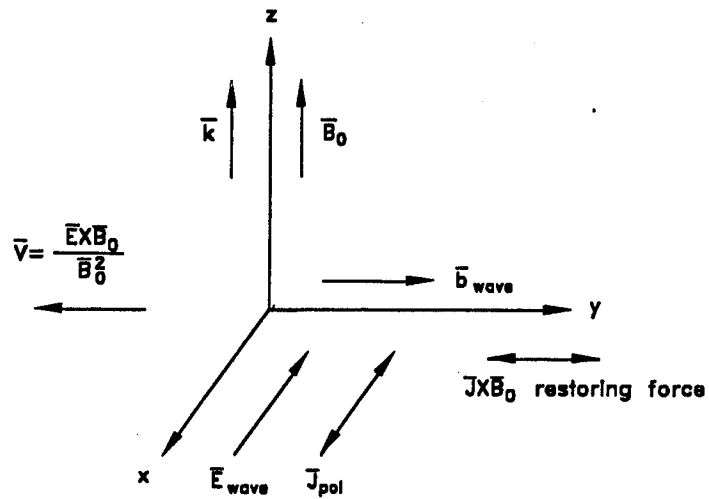


Figure 4-1. The slow mode with $\bar{k} \parallel \bar{B}_0$, in the low frequency limit. \bar{E} may have x and y components, but it has been aligned with the x axis for simplicity in the figure.

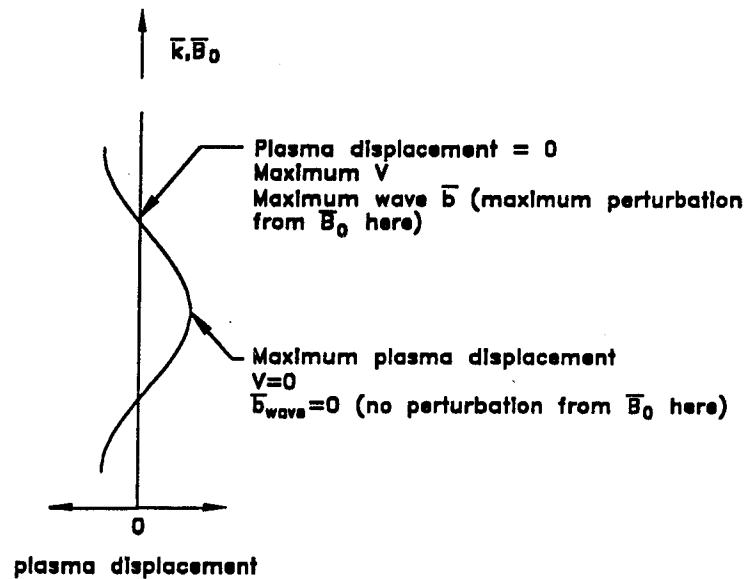


Figure 4-2. The plasma displacement and local magnetic field perturbation as a slow mode, low frequency Alfvén mode propagates parallel to \bar{B}_0 .

Chapter 5

Ionospheric Modification of Micropulsations

Introduction

All ground observations of waves from the magnetosphere are made after the waves have passed first through the ionosphere. As a wave approaches the Earth, the increasing magnetic field strength, the changing ion density and even the tilt angle the field makes with the ground all modify the propagation of the wave and alter the magnetic signature on the ground. When an Alfvén wave follows the Earth's magnetic field toward the ground, its energy splits into three branches at the ionosphere. It is mostly reflected, but some is transmitted to the ground, and some transported horizontally. The horizontal transport, or ducting, carries some energy beyond the region of the incident wave. Some of the ducted energy always escapes from the duct, partly by a Poynting loss, and partly by dissipative loss. The ducted wave fields are evanescent below the duct, but the wavelengths are long compared to the altitude of the duct, so the initial disturbance may be seen up to at least one or two thousand kilometers away (Hayashi, 1981). For the transmitted waves, certain polarization patterns are expected, depending on how far away the observations are made (Fujita & Tamao, 1988, Greifinger, 1972b).

Directly beneath the incident disturbance, the transmitted magnetic field is rotated by 90° from the initial Alfvén wave. This is due to the finite conductivity of the ionosphere and the lack of currents in the atmosphere (Hughes, 1974; Nishida, 1978). This finite conductivity is also responsible for coupling the incident Alfvén wave, which follows the Earth's magnetic field toward the Earth from the magnetosphere, to the fast or isotropic

wave, which carries energy away in the ionospheric duct, perpendicular to the Earth's field.

Another contribution to the ground observation comes from the fact that the magnetic field of the Earth intersects the surface at an angle. The incident Alfvén wave induces field-aligned currents because it is localized in space. These currents add an East-West magnetic component to the ground observation which increases in magnitude with the tilt of the Earth's field (Tamao, 1986).

The Incident Wave

All these processes can be illustrated by following an Alfvén wave as it arrives at the ionosphere. There, the Pedersen and Hall conductivities cause the rotation of the wave magnetic field below the ionosphere and couple the Alfvén to the fast wave. Suppose an Alfvén wave, with $k^2 = k_x^2 + k_z^2$, and with a wave electric field in the $\mathbf{k}-\mathbf{B}_0$ (or $x-z$) plane, is incident downward on the ionosphere (see Figure 5-1). \mathbf{B}_0 points downward, parallel to the z axis. The x axis is in the meridian, North-South. A fast wave in this arrangement, such as the one induced by coupling in the ionosphere, would have an electric field perpendicular to the $\mathbf{k}-\mathbf{B}_0$ plane (Dawson, 1966). E_x represents the Alfvén wave, and E_y the fast wave, but all variations in the $x-y$ plane go as $e^{ik_x x}$. Other plane waves, with $e^{iky y}$ dependence, may be added in a Fourier sum to represent any localized Alfvén disturbance (Greifinger, 1972b).

Pedersen and Hall conductivities and currents

To show how waves propagate at different altitudes, it is necessary to account for height-dependent conductivities. Their effect may be shown by combining conductivity relations

between \mathbf{E} and \mathbf{J} with the wave equation. In the ionospheric E-layer, the Hall conductivity links the Alfvén and fast modes. Starting with Maxwell's equations, in gaussian units, we have (following Greifinger & Greifinger, 1968):

$$\nabla \times \mathbf{B} = \frac{4\pi}{c} \mathbf{J} + \frac{1}{c} \frac{\partial \mathbf{E}}{\partial t} \quad (5-1)$$

and

$$\nabla \times \mathbf{E} = - \frac{1}{c} \frac{\partial \mathbf{B}}{\partial t} \quad (5-2)$$

and, as in chapter 5, by taking $\partial/\partial t$ of the first and $\nabla \times$ of the second, the wave equation results:

$$\nabla \times \nabla \times \mathbf{E} = \nabla(\nabla \cdot \mathbf{E}) - \nabla^2 \mathbf{E} = - \frac{4\pi}{c^2} \frac{\partial \mathbf{J}}{\partial t} . \quad (5-3)$$

The conductivities are derived from the equations of motion for ions and electrons, along with the definition of current density. When these equations of motion are written in terms of \mathbf{E} and \mathbf{v} , and the definition of current density $\mathbf{J} = n_e e(\mathbf{v}_i - \mathbf{v}_e)$ (Dawson, 1966) is used, it is found that

$$J_x = \sigma_P E_x - \sigma_H E_y$$

$$J_y = \sigma_P E_x + \sigma_H E_y$$

$$J_z = \sigma_0 E_z$$

when the magnetic field is directed along the z axis. This means that the current \mathbf{J} may be written as $\mathbf{J} = \boldsymbol{\sigma} \cdot \mathbf{E}$, where $\boldsymbol{\sigma}$ is a tensor composed of Hall (σ_H), Pedersen (σ_P) and direct (σ_0 , along the magnetic field) conductivities. The conductivity tensor is, then :

$$\sigma = \begin{bmatrix} \sigma_P & -\sigma_H & 0 \\ \sigma_H & \sigma_P & 0 \\ 0 & 0 & \sigma_0 \end{bmatrix},$$

and in general,

$$\mathbf{J} = \sigma_0 \mathbf{E}_{\parallel} + \sigma_P \mathbf{E}_{\perp} + \sigma_H \frac{\mathbf{E}_{\perp} \times \mathbf{B}_0}{B_0} \quad (\text{Nishida, 1978}),$$

where parallel and perpendicular components are relative to the Earth's field \mathbf{B}_0 . For altitudes between 200 and 1000 km (the ionosphere and above), conductivity parallel to the magnetic field, σ_0 , is several orders of magnitude greater than either the Pedersen (σ_P) or Hall (σ_H) conductivities (Kelley, 1989). For midday at sunspot minimum, the Hall conductivity maximizes near 120 km and falls off by an order of magnitude at altitudes approximately 40 km above and below. This provides a relatively narrow range of altitude in which the screening process and coupling of Alfvén and fast modes can take place (see Greifinger & Greifinger, 1968, and Fujita & Tamao, 1988). The Pedersen conductivity maximizes about 20 km higher and falls off more gradually with altitude (Hughes, 1974).

Nishida (1978) and Greifinger & Greifinger (1968) show ionospheric conductivity forms, which involve collision and gyrofrequencies for electrons and ions. They are, including the ion collision frequency (from Greifinger & Greifinger, 1968):

$$\sigma_P \approx \frac{ic^2 \omega}{4\pi V_A^2} \frac{(1 + i\nu_i/\omega)}{\{1 + [(\nu_i - i\omega)^2 / \Omega_i^2]\}} \quad (5-4)$$

$$\sigma_H \approx i \frac{\omega}{\Omega_i} \left(1 + i \frac{\nu_i}{\omega}\right) \sigma_P, \quad (5-5)$$

where Ω_i is the ion gyrofrequency, ω is the wave frequency and ν_i is the ion-neutral collision frequency.

Pedersen currents are parallel to the electric field, while the Hall current is perpendicular. In the lower ionosphere, the ion collision frequency (with neutrals and electrons) is larger than the wave frequency, but approximately the same as the ion gyrofrequency. On the other hand, the electron collision frequency is less than the electron gyrofrequency (Kelley, 1989), so the Hall conductivity in the *lower* ionosphere,

$$\sigma_H = \frac{n_e e}{B_0} \left[\frac{\Omega_i^2}{\Omega_i^2 + \nu_i^2} - \frac{\Omega_e^2}{\Omega_e^2 + \nu_e^2} \right],$$

is negative (Nishida, 1978). This is also true for the real part of (5-5) in the same region, where terms in ω/ν_i are negligible. This means that a conventional current equivalent to this Hall current is in the $-\mathbf{E} \times \mathbf{B}$ direction. The collisions inhibit the ion motion, leaving the electrons to $\mathbf{E} \times \mathbf{B}$ drift, which results in a net current.

Since the conductivities are derived from the equations of motion for ions and electrons, the terms in the conductivity expressions depend on what forces are significant in the regime of interest. For example, the rate of momentum transfer by collision, from ions to neutrals, is only important at certain altitudes (see Kelley, 1989 and Nishida, 1978). Above those altitudes, terms in ν_i/ω are negligible.

The incident wave as it approaches the ionosphere from above

Now that the wave equation may be written in terms of the conductivities at different altitudes, the waves may now be followed down through the ionosphere into the atmosphere. At the interface between any two regions, such as the ionosphere and atmosphere, the wave electric and magnetic fields on both sides are matched to each other. This process determines coefficients and yields reflection coefficients. When the tangential magnetic fields are different, there are currents in the plane of the interface:

$$B_{x2} - B_{x1} = \frac{4\pi}{c} K_x = \frac{4\pi}{c} (\Sigma_P E_y - \Sigma_H E_x)$$

$$B_{y2} - B_{y1} = \frac{4\pi}{c} K_y = \frac{4\pi}{c} (\Sigma_P E_x + \Sigma_H E_y)$$

The assumption of harmonic field variations provides the following substitutions:

$$\partial/\partial t \rightarrow -i\omega \quad \text{and} \quad \nabla_x \rightarrow ik_x, \quad \text{where } \mathbf{k} = k_x \mathbf{x} + k_z \mathbf{z}$$

$$\text{and } \partial/\partial z \rightarrow ik_z, \quad \text{so that } k_z = -i \partial/\partial z.$$

With these, the components of equation (5-3) become

$$-k_x (k_x E_x + k_z E_z) + (k_x^2 + k_z^2) E_x = \frac{4\pi}{c^2} i\omega J_x = \frac{4\pi}{c^2} i\omega (\sigma_P E_x + \sigma_H E_y) \quad (5-6)$$

$$(k_x^2 + k_z^2) E_y = \frac{4\pi}{c^2} i\omega J_y = \frac{4\pi}{c^2} i\omega (-\sigma_H E_x + \sigma_P E_y) \quad (5-7)$$

$$-k_z (k_x E_x + k_z E_z) + (k_x^2 + k_z^2) E_z = \frac{4\pi}{c^2} i\omega J_z = \frac{4\pi}{c^2} i\omega \sigma_0 E_z. \quad (5-8)$$

Greifinger and Greifinger (1968) note that E_z is approximately zero below 1000 km because of the high parallel conductivity σ_0 (see also Hughes & Southwood, 1976a).

Note also in the z component that even if $E_z \approx 0$,

$$\nabla_z (\nabla \cdot \mathbf{E}) - \nabla^2 E_z = \frac{4\pi}{c^2} i\omega J_z \rightarrow \frac{\partial}{\partial z} \left(\frac{\partial}{\partial x} E_x + \frac{\partial}{\partial y} E_y \right) = \frac{4\pi}{c^2} i\omega J_z, \quad (5-9)$$

and there will be a field-aligned current if there is a variation in E_x or E_y in the horizontal (x-y) direction. This variation could arise from a wavenormal \mathbf{k} that is not parallel to the z axis, so that a k_x or k_y exists. Nishida (1964) gives an example of this, as he treats a sum of non-vertically propagating waves (a Fourier representation of the electric and magnetic fields). It could also arise from a localized disturbance, in which the horizontal electric field goes to zero over a finite distance. Greifinger (1972a) noted the few hundred kilometer extent of micropulsation disturbances and suggested that they are composed of

a superposition of plane waves, with a distribution of amplitudes and phases. Given harmonic variations in z and x , J_z would be out of phase with the wave electric field by $\pi/2$.

Wave-mode coupling in the ionosphere

If the x and y components of the wave equation are rearranged, we have

$$\left[\frac{\partial^2}{\partial z^2} + \frac{4\pi}{c^2} i\omega\sigma_P \right] E_x + \frac{4\pi}{c^2} i\omega\sigma_H E_y = 0 \quad (5-10)$$

$$\left[\frac{\partial^2}{\partial z^2} - k_x^2 + \frac{4\pi}{c^2} i\omega\sigma_P \right] E_y - \frac{4\pi}{c^2} i\omega\sigma_H E_x = 0 \quad (5-11)$$

Note that the Hall conductivity couples E_x and E_y . At altitudes where the Hall conductivity is *small*, the magnitude of E_x is not related to that of E_y and the two components are uncoupled. There, (5-10) becomes an equation for the Alfvén wave (E_x), and (5-11) becomes an equation for the fast wave (E_y). This is because the fast wave electric field is perpendicular to the \mathbf{k} - \mathbf{B}_0 plane, and the Alfvén wave electric field is in that plane (Dawson, 1966). An Alfvén wave propagating down the field toward the ionosphere will reach the altitude range where the Hall conductivity is increased by ion-neutral collisions (Greifinger & Greifinger, 1968) at the E-layer, near 120 km. Coupling of the two modes occurs there, so the reflected waves consist of both an Alfvén and a fast wave.

Dawson (1966) suggests how the presence of collisions can couple a wave which propagates along the magnetic field (Alfvén) to a ducted fast wave which can propagate perpendicular to the magnetic field. He includes ion-electron collisions in the derivation of the dispersion relation for Alfvén waves. The collision frequency ν_{ie} becomes important when it approaches the wave frequency, while $\omega \gg m_e \nu_{ie} / m_i$ and $\nu_{ie} \ll \Omega_e$. This

occurs below 20,000 km. The Hall and Pedersen conductivities are not changed under these circumstances, but the parallel conductivity goes from

$$\frac{in_e e^2}{m_e \omega} \quad \text{to} \quad \frac{in_e e^2}{m_e (\omega + i\nu_{ie})},$$

which has the effect of changing the electron mass:

$$m_e \rightarrow \frac{m_e (\omega + i\nu_{ie})}{\omega} \quad (\text{Dawson, 1966}).$$

In this case, the Alfvén wave can have a real wave normal component perpendicular to the steady magnetic field. In this case, for propagation perpendicular to the field,

$$\frac{k^2}{\omega^2} \approx \frac{\omega_p \nu_{ie}}{2c\omega^2} + \frac{i\omega_p}{c\omega},$$

instead of

$$\frac{k}{\omega} = \frac{-i\omega_p}{c\omega}.$$

The real part becomes large as ν_{ie}/ω becomes large.

Reflectivity of the ionosphere

The Poynting flux of the incident Alfvén wave is substantially reflected. Hughes & Southwood (1976a) give the dayside reflection as at least 97%, and the nightside as 40-70% (at sunspot minimum and maximum, respectively). An Alfvén mode is reflected, with an oppositely directed electric field, because the wave reflects from a medium with a higher index of refraction. A fast mode, in which the electric field is perpendicular to the $\mathbf{k}\text{-}\mathbf{B}_0$ plane, is also reflected, and is vertically evanescent, so it carries no energy flux (Hughes & Southwood, 1976a). The reflectivity of the ionosphere depends on

$$-\left[\frac{c}{V_A} - \frac{4\pi\Sigma_P}{c} \right]^2 \left[\frac{c}{V_A} + \frac{4\pi\Sigma_P}{c} \right]^{-2},$$

where for good conductivity, as on the dayside, $\Sigma_P \gg c^2 / 4\pi V_A$. These are approximately equal for poor, nightside conductivity (Hughes & Southwood, 1976a). Consequently, the Poynting flux transmitted into the ionosphere is relatively small. The electric field magnitude does not change much through the ionosphere (Nishida, 1964), and in fact, since the E-layer is thin compared to the wavelength, some authors treat the ionosphere as a thin surface. The tangential components of the electric field are conserved across this surface (Hughes, 1974; Nishida, 1964).

The rotation of the magnetic field as seen on the ground

Although most of the incident Alfvén wave energy is reflected, some is ducted horizontally in the ionosphere and some penetrates to the ground via the Hall current. The wave magnetic field observed on the ground, from the incident Alfvén wave, is perpendicular to the wave magnetic field *above* the ionosphere. This 'rotation' process is caused by the Pedersen and Hall currents.

Beneath the ionosphere, the magnetic field of the Pedersen current is antiparallel to that of the incident Alfvén wave. This opposition greatly reduces the magnitude of the incident wave magnetic field at the ground. However, the Hall current creates a magnetic field perpendicular to both of these, and this is seen on the ground (see Hughes & Southwood, 1976a).

Cancellation of the wave \mathbf{b} at the ground by the Pedersen current at the ionosphere is realizable for low frequency waves. The phase of the wave at the E-layer is not much different from the phase at the ground because of the long wavelengths of ULF. For a 0.1 Hz wave, the wavelength is at least 1000 km, since the Alfvén speed is at least 10^5

m/s (Dawson, 1966). This is approximately 10 times the height of the E-layer above the ground. Moreover, the magnetic field from the Pedersen sheet current probably does not change much with height below the ionosphere, since the field at a point above a current sheet of infinite extent depends only on the magnitude of the current/unit width, not on the height.

The role of the Pedersen and Hall conductivities is shown more explicitly by Fujita & Tamao (1988). The fields seen on the ground are explained in terms of height-integrated conductivities and the incident Alfvén and induced fast mode electric fields. The height-integrated conductivity is the conductivity σ integrated over the height of the current layers (Hughes, 1974). For the Hall current:

$$\Sigma_H = \int \sigma_H dz ,$$

and Σ_P (Pedersen) is similarly defined. The current layers could be the E-region (Fujita & Tamao, 1988). The units of σ are $\text{ohm}^{-1}\text{m}^{-1}$ (mks units), which gives amps/m^2 when multiplied by the electric field in volts/m. The units of Σ are ohm^{-1} , so the product of Σ and E results in current/m (or current/unit horizontal width).

The magnetic field below the ionosphere depends on the Hall current from the incident Alfvén wave, and both the magnetic field and the Pedersen current of the induced fast mode wave (Fujita & Tamao, 1988). Fujita & Tamao (1988) match the tangential electric and magnetic fields at the atmosphere-ducting layer interface (that is, across the thin E-layer), taking the surface currents into account, and derive the following (mks units):

$$\hat{\mathbf{z}} \times (\delta\mathbf{B}_{\text{atmos}} - \delta\mathbf{B}_f)/\mu_0 = \Sigma_P \delta\mathbf{E}_f + \Sigma_H \hat{\mathbf{z}} \times \delta\mathbf{E}_{tr} \quad (5-12)$$

$$(-\hat{\mathbf{z}} \times \delta\mathbf{B}_{tr})/\mu_0 = \Sigma_P \delta\mathbf{E}_{tr} + \Sigma_H \hat{\mathbf{z}} \times \delta\mathbf{E}_f, \quad (5-13)$$

where the subscript *tr* refers to the Alfvén wave, and the *f* to the fast wave. The magnetic field seen on the ground is $\delta\mathbf{B}_{\text{atmos}}$, and is described by equation (5-12). It arises from the Hall current of the Alfvén wave and the Pedersen current of the fast wave. It is polarized in the direction of the incident Alfvén wave's \mathbf{k} projection in the xy plane (Greifinger, 1972a). Beneath the wave injection point in the E-layer, the Hall current associated with the Alfvén wave produces the magnetic field variations. These are seen on the ground in what Fujita & Tamao (1988) call the central region, where the incident Alfvén mode is dominant. The radius of the central region is approximately equal to 1/3 the thickness of the ducting layer.

An intermediate region below the E-layer extends from the outer limit of the central region to a distance where the ducted fast wave is dominant. In the intermediate region, the *Pedersen* current of the induced fast wave produces the magnetic field variation on the ground.

The cancellation of the magnetic field of the incident Alfvén wave, described by equation (5-13), is carried out by the Pedersen current of the incident Alfvén wave and the Hall current of the induced fast wave. (Pedersen cancellation dominates in central region - Fujita & Tamao, 1988) The Pedersen current is part of a circuit that also includes the field-aligned current of the localized Alfvén wave and the cross-field polarization drift current in the magnetosphere (Fujita & Tamao, 1988); i.e., $\mathbf{j} = (\rho/B^2) \partial\mathbf{E}/\partial t$ (Chen, 1974).

Although it does not give as much information as the work of Fujita & Tamao (1988), a simple way to conclude that the incident Alfvén wave field is cancelled in the atmosphere

comes from an argument by Nishida (1978). In the atmosphere, there should be no vertical (or any other) currents. The displacement current, $\partial\mathbf{E}/\partial t$, is negligible because of the low frequencies of ULF, so $\nabla\times\mathbf{b} = 0$. In the example above, the incident Alfvén wave electric field is $\mathbf{E} = E_x \mathbf{x}$, and the magnetic field is $\mathbf{b} = b_y \mathbf{y}$. The z component of $\nabla\times\mathbf{b}$, given the wave in example above, is:

$$\mu_0 J_z = 0 = \frac{\partial b_y}{\partial x} - \frac{\partial b_x}{\partial y} = \frac{\partial b_y}{\partial x} = ik_x b_y ,$$

therefore, $b_y = 0$.

In the case of localized fast mode incidence, in which the electric field has a spatial variation in the horizontal (ionospheric) plane, the polarization axis of the magnetic field seen on the ground is not rotated. The ground magnetic field is from the Pedersen current of the incident fast wave, the same current that almost shields the wave magnetic field from the ground. The fast wave's Hall current carries part of the induced Alfvén wave's field-aligned current and has no magnetic effect on the ground (Fujita & Tamao, 1988) as in equation (5-13). Nishida (1964) also shows the lack of axis rotation of an incident fast wave magnetic field as seen on the ground.

The magnitude of the magnetic field component on the ground is related to the Alfvén wave \mathbf{b} in the magnetosphere as:

$$b_g/|b| = -e^{-kh} (\Sigma_H/\Sigma_P)[1 + (kd/2)] \quad (\text{Hughes and Southwood, 1976a})$$

where h is the height where the Hall conductivity is no longer important, and d is the thickness of the Hall conducting region. The ratio of the height integrated conductivities is always near unity (Hughes, 1974), ranging from 0.28 at night during sunspot maximum to 1.23 during the day at sunspot minimum; $h \approx 120$ km, and $d \approx 20$ km (Hughes and Southwood, 1976a). For small ionospheric wavenumbers, $k < 0.01$ km⁻¹,

the magnetic field on the ground has a *magnitude* similar to the wave magnetic field in the magnetosphere. Otherwise, the ground magnitude is reduced exponentially from the magnetospheric value.

Ducting

Introduction

The coupling of the Alfvén and fast modes affects the way energy ducts away and the way it leaks from the duct itself, in addition to creating the magnetic field perturbation seen on the ground. The ducting fast mode can couple to the Alfvén mode every time it reflects from the E-layer duct floor. The field-aligned Alfvén wave can then carry some energy up through the Alfvén speed-gradient ceiling of the duct.

After the Alfvén wave is incident on the ionosphere, some energy is ducted horizontally in a duct bounded above by a sharp increase in Alfvén speed with height, and below by another sharp speed increase and the E-layer (see Figure 5-1). The speed variations arise because the Alfvén speed,

$$V_A = \frac{B}{\sqrt{\mu_0 \rho}} \quad (\text{Chen, 1974})$$

depends on the mass density of the ions, ρ , and the Earth's magnetic field B_0 . The magnetic field changes monotonically with altitude, but charged particle density maximizes in the ionosphere (see Kelley, 1989).

The Alfvén speed minimum is located at about 400 km (Greifinger & Greifinger, 1968, with data from Sims & Bostick, 1963; Dawson, 1966), and the ducted wave is totally internally reflected because of the high index of refraction inside the duct compared to the low index outside; a situation similar to light in an optical fiber.

Evanescence of the ducted wave above and below the duct

The part of the ducted fast wave that is transmitted through the upper and lower boundaries of the duct is evanescent. The same is true for the electric field of the Alfvén wave that is transmitted through the lower boundary into the atmosphere. The evanescence of the transmitted part will be discussed in this section. The reason for this in the atmosphere is that the conductivities decrease. Consequently, the terms

$$4\pi i \omega \sigma_P / c^2 \quad \text{and} \quad i 4\pi \omega \sigma_H / c^2$$

both become very small in equations (5-10) and (5-11). The result for the fast wave (5-11) can be seen easily :

$$\left[\frac{\partial^2}{\partial z^2} - k_x^2 + \frac{4\pi i \omega \sigma_P}{c^2} \right] E_y - \frac{4\pi i \omega \sigma_H}{c^2} E_x = 0$$

which becomes

$$\left[\frac{\partial^2}{\partial z^2} - k_x^2 \right] E_y = 0 ,$$

the solution to which is an evanescent exponential in z , subject to the condition of a zero or near zero electric field at the highly conductive earth (Greifinger & Greifinger, 1968).

The Alfvén wave is also evanescent in the atmosphere. Note that the E_z term may be kept in the atmosphere (Hughes & Southwood, 1976a). This does not change the circumstances for the fast wave because there is no k_y in this case (see equations 5-6 and 5-7), but it does affect the Alfvén wave electric field. If conductivities become negligible in the atmosphere, equation (5-6) becomes:

$$-\frac{\partial^2}{\partial z^2} E_x + ik_x \frac{\partial}{\partial z} E_z = 0 . \quad (5-14)$$

If $\nabla \cdot \mathbf{E} = 0$ in the atmosphere (zero charge density), we have

$$ik_x E_x + \frac{\partial}{\partial z} E_z = 0 \quad (\nabla \cdot \mathbf{E} = 0) . \quad (5-15)$$

Using (5-15) in (5-14), we have

$$\frac{\partial^2}{\partial z^2} E_x = ik_x \frac{\partial}{\partial z} E_z = k_x^2 E_x$$

so that

$$E_x \propto \exp(\pm k_x z) .$$

The combination of these functions is subject to the boundary condition that $E_x = 0$ at the ground (following Hughes & Southwood, 1976a), so the Alfvén wave is evanescent below the ionosphere. When a conductivity model is used, it is found that the Alfvén wave electric field decay occurs mostly below an altitude of 50 km, according to Hughes & Southwood (1976a) calculations (see their Figure 3, for example). The evanescent nature of the wave means that disturbances whose amplitudes are still large enough at the ground to be measured, despite the exponential decay with height, must have *horizontal* scales (k_x) longer than the thickness of the neutral atmosphere (Hughes & Southwood, 1976a).

The fast mode wave that is transmitted through the top of the duct is evanescent also (the Alfvén mode is not). Fast mode decay is due to the low frequency of the micropulsations and the projection of the wavenormal \mathbf{k} in the plane of the ionosphere. If the time and space variations of the fields are given by

$$\exp(i(k_x x + k_y y + k_z z - \omega t)) ,$$

then the phase speed of the wave is

$$k_x^2 + k_y^2 + k_z^2 = \omega^2 / V_A^2 .$$

Let the Alfven speed be V_D in the ducting layer (near the Alfven speed minimum) and V_M in the magnetosphere (near the sharp increase in Alfven speed). If the frequency is low, such as $(0.1 \times 2\pi)$ rad/s, and the projection of \mathbf{k} in the E-layer x - y plane has $k_y = 0$, then

$$k_x^2 + k_z^2 = \omega^2 / V_D^2 \quad (\text{ducting layer}), \text{ and}$$

$$k_x^2 + k_z^2 = \omega^2 / V_M^2 \approx 0 \quad (\text{magnetosphere})$$

where since $V_M \gg V_D$.

In the magnetosphere, then, $k_z^2 \approx -k_x^2$, since k_x is real for all the above calculations involving wave propagation. This means that the induced fast wave is evanescent in the vertical (z) direction upon transmission through the upper boundary of the duct (see Nishida, 1964; and Hughes, 1974). As long as $V_D k_{x\text{real}} < \omega < V_M k_{x\text{real}}$, the ducted fast wave will be vertically evanescent in the magnetosphere, and simultaneously vertically propagating in the ducting layer (Fujita, 1988).

Note from equations (5-10) and (5-11) that when the fast and Alfven waves are uncoupled in regions of low Hall conductivity and small E_z , the fast mode (equation 5-11) is different from the Alfven mode because of the \mathbf{k} projection in the xy E-layer plane. The coupling due to the Hall conductivity and this *projected* \mathbf{k} component, k_x , create the fast wave with the same k_x as the incident Alfven wave, but not the same k_z . For the Alfven mode: $k_z = \omega/V_A \ll k_x$, which propagates vertically (see Hughes, 1974; and Fujita, 1988).

Propagation in the duct

Some aspects of duct propagation will be touched upon next. For the induced fast wave whose wavelength is on the order of the ionospheric thickness or less, the wave is ducted in a region at the Alfvén speed minimum, and has a phase speed of approximately the Alfvén minimum. The duct is bounded on the top where the Alfvén speed rises sharply (about 1000 km) and on the bottom by the E-layer (100 km) and another increase in Alfvén speed. Ideally, only certain fundamental and harmonic bands exist for waves that travel in the duct. Poynting losses (Fujita, 1988) occur at the upper duct 'surface' as the induced Alfvén wave escapes upward. Fast waves will be observed on the ground far from the injection site via Pedersen currents in the E-layer. Under ideal circumstances, certain polarization patterns are expected on the ground, depending on the horizontal distance from the injection site.

At high frequencies, most of the Poynting flux is contained in the duct above the E-layer (see Figure 5, Fujita, 1988). As the frequency of the fast wave decreases, more of the Poynting flux is above the upper duct 'wall'. At frequencies near the lower cutoff for the duct, the energy is transported by a vertically evanescent boundary wave along the top of the duct (Fujita, 1988). The vertical wavenumber of the evanescent wave becomes small (large vertical wavelength) above the top surface of the duct :

$$k_z^2 = \omega^2/V_M^2 - k_x^2 \rightarrow 0 ,$$

because $k_x^2 \rightarrow \omega^2/V_M^2$ in the magnetosphere (Fujita, 1988) at altitudes above the sharp increase in Alfvén speed.

Within the duct, only waves in certain harmonic frequency bands may propagate. This is a consequence of the limited vertical dimension of the duct, the matching of tangential electric and magnetic fields across the duct surfaces, and the finite thickness of the

atmospheric layer. The lowest frequency of the lowest band depends on daylight and solar activity because of the effect these have on the dimensions of the ionosphere (see Greifinger & Greifinger's (1968) Table 1). For example, in the day at sunspot maximum, the lowest band low-frequency cutoff is calculated as 0.10 Hz, vs. 0.36 Hz for the night at sunspot minimum (Greifinger & Greifinger, 1968). The presence of a finite thickness atmosphere over conducting earth leads to the nonzero low-frequency cutoff, but these bands have no high frequency cutoff. Minimum attenuation takes place near the lowest frequency cutoff in any band (or harmonic; see Fujita, 1988; Greifinger & Greifinger, 1968).

The fast wave reflects from the top and bottom of the duct as it propagates away from the central region. At the low frequency cutoff, the vertical wavelength of the fast wave is $4D/(2j - 1)$, where D is the thickness of the duct, and j is the harmonic. The electric field intensity has a node (approximately) at the conducting E-layer and an antinode at the upper surface of the duct (Fujita, 1988).

Losses in the duct

Losses in the duct are partly due to dissipative "Joule" losses in the E-layer (via the Pedersen current, so $\mathbf{J} \cdot \mathbf{E}_{\text{fast}} > 0$) and the solid Earth, and partly to a Poynting loss as energy is carried away by waves escaping the duct. Each time the fast wave reflects from the E-layer, it can recouple to an Alfvén wave (via the Hall current of the fast wave, Fujita, 1988), which may then carry energy up the field line. Some of this will be reflected, but the rest will go through into the magnetosphere as the Poynting loss. In addition, the Pedersen current of the fast wave creates an observable signal on the ground, far from the central region (a Joule loss). Overall, the Poynting loss accounts for less than 15% of the total, unless $\Sigma_H/\Sigma_P > 10$ and $\mu_0 V_D \Sigma_P < 0.1$. In this case, the

Poynting loss becomes about three times greater than the ionospheric Joule loss (Fujita, 1988).

When the two conductivities are comparable, the ionospheric Joule loss contributes most to the attenuation of the ducted wave. This loss depends on the Pedersen conductivity (Fujita, 1988), which is highest during the day (Kelley, 1989).

The relative heights of the conductivity maxima and the electric field amplitude are also important. When the maxima in the electric field and Pedersen conductivity coincide, the Joule loss is maximized (Fujita, 1988). The maximum Poynting loss will occur when the maximum fast wave electric field intensity is at the maximum Hall conductivity altitude.

The standing wave nature of the induced Alfvén wave in the duct can create a frequency-dependent attenuation. If the duct thickness is half a wavelength ($\omega D/V_A = j\pi$, where j is an integer), the magnetic field of the induced, standing Alfvén wave nearly cancels at the E-layer. Since the two waves couple as $-\mathbf{b}_\alpha/\mu_0 = \Sigma_H \mathbf{E}_f$, where 'tr' and 'f' refer to the Alfvén and fast wave (Fujita, 1988), the reduced magnetic field inhibits coupling and reduces Poynting loss under those resonant conditions.

Off-meridian propagation

Greifinger & Greifinger (1973) found that coupling between the fast and Alfvén waves caused attenuation of ducted waves traveling in off-meridian directions. Their calculations showed a resonance-type pattern that depended on magnetic latitude and ionospheric parameters. They concluded that attenuation was significant for propagation directions other than N-S or E-W. Tepley et al. (1965) found a restricted longitudinal span over which pearls (pulsed Pc1) were detected, compared to the range in latitude. Berthold et al. (1960) examined signals from the high altitude nuclear explosion ARGUS-3 that were

thought to be ducted. They fell off in amplitude when observed off the geomagnetic meridian that passed through the point of detonation. Manchester (1968) observed waves propagating both toward and away from the equator at calculated speeds that agreed with corresponding Alfvén speeds. It was concluded that the waves were traveling approximately parallel to the geomagnetic meridian. All of these suggest that the ducted wave traveling parallel to the meridian would suffer the least attenuation.

The contribution to ground observations from field-aligned currents

The Earth's magnetic field is not perpendicular to the ground, although at high latitudes it is approximately so. The tip angle of the field relative to the ground introduces two effects. First, the coupling between the fast and Alfvén modes is enhanced, which increases the Poynting loss (Fujita, 1988, and references therein). Second, the field-aligned currents are allowed to contribute to the magnetic field observed on the ground (Tamao, 1986).

A horizontally localized Alfvén wave guided downward by the Earth's magnetic field carries a field-aligned current. This is due to the variation of the horizontal electric field components, as shown above (equation 5-9). The field aligned current is out of phase with the wave electric field, and it can produce a magnetic field below the ionosphere. To do this, the current must have a component in the plane of the ionosphere, and there must be a variation of the wave electric field as a function of distance along the East-West axis (see Figure 5-2). This creates a variation in the N-S component of the field-aligned current. The magnitude of this current is 90° out of phase with the ionospheric Hall current along the E-W axis, so the ground magnetic field signatures from the two are also 90° out of phase. The ground magnetic field from the N-S component of the tipped, field-aligned currents is E-W.

Tamao (1986) calculated the contribution from the field aligned currents at 60° geomagnetic latitude for an ionospheric electric potential of:

$$\Phi(x,y,0) = \Phi_0 \exp[-(x/a)^2 - (y/b)^2]$$

where $a = b$ (horizontally isotropic). The contribution was 80% of the field due to the ionospheric current.

If the Earth's field were vertical, the Hall current from the wave electric field would be the only one to produce a magnetic disturbance on the ground under the incident wave. Since the Earth's field is tipped, the magnetic field from the field-aligned current is enhanced if the horizontal scale of the disturbance is shorter in the longitudinal than the latitudinal direction (Tamao, 1986).

Polarization patterns on the ground

The 'rotation' of the magnetic field by the action of the Pedersen and Hall currents will not affect the sense of circular polarization, but it will rotate the axis of the polarization ellipse by 90° (Hughes, 1974; Fujita & Tamao, 1988). A circularly polarized incident Alfvén wave may be represented with a Fourier series with wavenumbers in the x and y direction. Rotation of the wave magnetic field will occur for each component, and in a given hemisphere, all components will rotate in the same sense by 90°.

The polarization of the ground signal ideally depends on the horizontal distance from the injection source. Directly under an incident Alfvén wave, the magnetic field on the ground will be polarized the same way as the incident wave electric field (see for example, Greifinger, 1972b). The ducted wave is isotropic, or spherical (Tamao, 1964), and is right polarized when its wavenormal \mathbf{k} is parallel to \mathbf{B}_0 (Hayashi et al., 1981; Manchester, 1968; see Dawson, 1966). In the central region, the Alfvén wave amplitude

is largest, so the signal at the ground will be left polarized. Beyond the central region, a horizontal distance of about 30% of the duct thickness, the ducted wave amplitude will be larger than the incident Alfvén wave, so the polarization will have a right-hand sense (Greifinger, 1972b; Fujita & Tamao, 1988).

Greifinger (1972b) shows that the magnitude of the ducted signal magnetic field depends on $|b| \sim r^{-1/2} \exp(-r/\Lambda)$, where Λ is the attenuation length (very large at night, hence long distance propagation), and r is the horizontal radial distance from the injection center. On the other hand, the incident Alfvén wave depends on r^{-2} for distances where the fast wave amplitude dominates. Greifinger & Greifinger (1968) tabulate attenuation lengths, and these range from 650-950 km during the day, up to thousands of km at night. These attenuation lengths depend on collision frequencies.

Far from the central region, the polarization ellipse on the ground points toward the injection center (Fujita & Tamao, 1988). This was discussed by Baranskiy (1970), Greifinger (1972b) and used by Fraser & Summers (1972) and Fraser (1975) to locate the central region of Pc1 disturbances on the ground. Fraser & Summers (1972) used polarization measurements from low latitudes. They expected to be far enough from the central region that the polarization properties of the ducted wave would be dominant. This is because in the central region dominated by the incident wave, the ellipse major axis does *not* point to the source. Instead, it is perpendicular to the radial vector.

In the magnetosphere, the polarization *sense* has the same pattern as it does on the ground. The ellipse *axis pattern* is the opposite of that on the ground, though. The major axis points to the source in the central region and azimuthally in the distant region.

The polarization pattern does not always materialize, though. Hayashi et al. (1981) measured the amplitudes and polarizations of Pc1 events on the ground. They used thirteen stations across the auroral zone in a 30° (long.) by 15° (lat.) area. They found that

left hand polarization was observed outside the source region; in one case beyond a measurement of right hand polarization. At sites far from the center, polarization was predominantly linear. They concluded that left-hand polarization is not a sure sign of location in the central region, below the incident Alfvén wave. The source region size was estimated by the attenuation of the wave amplitude. Events in their study were seen by stations separated by 1000 km when one of them was at the source.

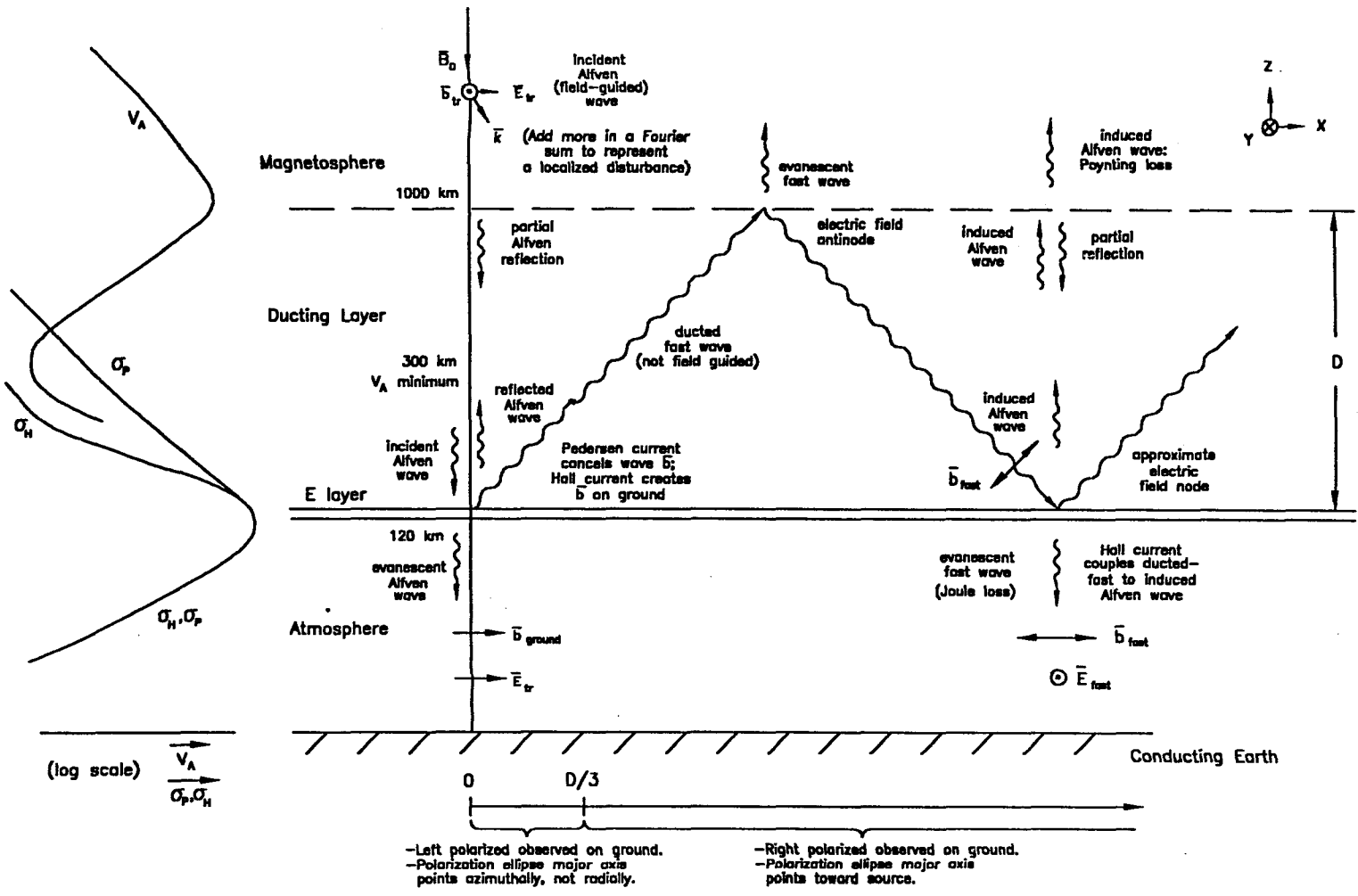
The proposition that the polarization ellipse major axis should point toward the source when observed on the ground, far from the source, seems reasonable when considering the simple example above. In that example, the fast wave electric field is in the y direction, so the *Pedersen current* of the fast wave creates a ground magnetic field parallel to the x axis.

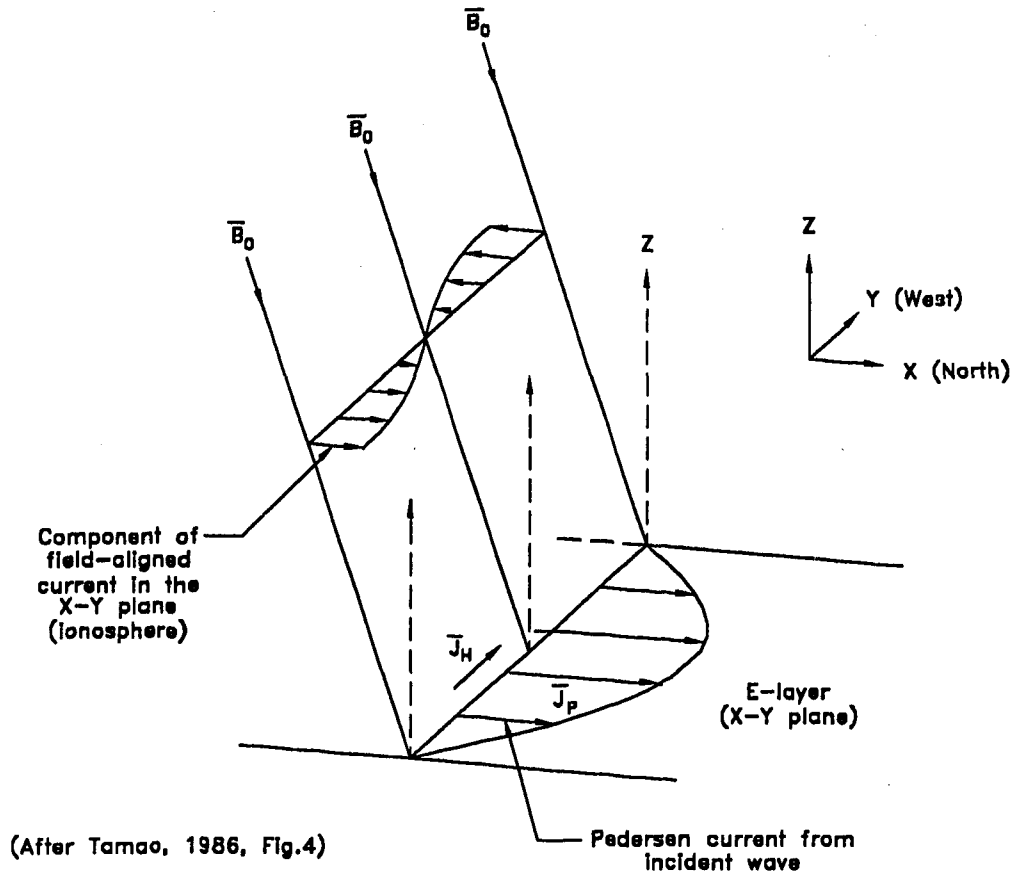
Since the wavenormal k is in the x - z plane, the wave magnetic field ($\omega \mathbf{b} = \mathbf{k} \times \mathbf{E}$) is also in that plane. However, only a component of \mathbf{b}_{fast} is in the *ionospheric plane*, so \mathbf{b}_{fast} does not fully cancel the Pedersen current's magnetic field on the ground. This is different from the situation of the incident Alfvén wave, where \mathbf{E}_A was in the x direction. That led to an incident Alfvén wave \mathbf{b}_A completely parallel to the ionospheric plane. Due to this orientation, the Pedersen current's magnetic field fully canceled the incident Alfvén wave \mathbf{b}_A .

The fast wave magnetic field is not rotated during passage through the bottom of the duct. Far from the source along the x axis, where the fast wave amplitude dominates, it is reasonable that the magnetic field observed on the ground should be along the x axis, pointing toward the source. In the case of elliptical polarization, where some Alfvén wave magnetic field is present due to recoupling, the major axis should still point along the x axis because of the dominant fast wave signal.

Ducting appears to play a significant role in the transmission of Pc1 waves above 0.4 Hz from their magnetospheric source to the auroral zone stations in this study. In fact, they may routinely duct from latitudes close to where plasmapause field lines intersect the Earth's surface, up to Sondre Stromfjord and South Pole latitudes. Meanwhile, the Pc1 that are amplified in the distant dayside magnetosphere may be blocked from directly reaching these high latitude stations by He⁺ ions in the magnetosphere. The lower frequency Pc1/2 are also likely to duct, but not as efficiently as the shorter wavelength Pc1. This will be discussed further in the wave growth and data analysis sections.

Figure 5-1. Wave fields from an incident Alfvén wave near the Earth, as modified by the ionosphere.





- Hall current J_H is also from the incident wave and its magnitude is in phase with the Pedersen current magnitude.
- The magnetic field from the field-aligned axis is along the Y-axis (E-W).
- The magnetic field from the ionospheric Hall current is along the X-axis (N-S).
- The field-aligned current is out of phase with the Hall current by 90° .

Figure 5-2. The currents contributing to the ground magnetic field signature of a field-aligned current are shown above. The current in the diagram is incident on the ionosphere E-layer.

Chapter 6

Wave growth

Introduction

Ion-cyclotron wave growth will be discussed in this section. This process involves a resonance between ions and cyclotron waves in which energy is passed to the waves. Energy can go to the particles under certain conditions, as well. In a plasma with many ion species, these two processes compete and create some frequency bands in which waves may grow and others in which they do not propagate. The dependence of the growth rate on the cold ion density, the local magnetic field (B_0), and ion speeds parallel and perpendicular to B_0 will be presented.

Ion-cyclotron resonance

The field-guided Alfvén mode can resonate and exchange energy with ions, since they both have the same rotation sense. The wave can become circularly polarized when $\mathbf{k} \parallel B_0$, since then \mathbf{E} is not confined to a \mathbf{k} - B_0 plane. Left circular polarization means a counterclockwise rotation of the electric field vector when looking parallel to B_0 (Chen, 1974). At resonance, a particle finds itself in an electric field over most of one orbit or more. At a given instant, the electric field everywhere points uniformly in one direction. As the electric field of the wave rotates, it increases or decreases a particle's tangential speed (v_{\perp}), depending on the dot product $\mathbf{v}_{\perp} \cdot \mathbf{E}$. Resonance may occur between charged particles and waves much lower than their gyrofrequencies through a Doppler shift of the gyrofrequency. The resonance condition may be expressed as (Arnoldy et al., 1988):

$$\omega = \Omega + \mathbf{k} \cdot \mathbf{v}, \quad (6-1)$$

where \mathbf{v} or v_{\parallel} is the charged particle velocity, ω is the wave frequency, \mathbf{k} is the wavenormal and Ω is the ion gyrofrequency. Ions satisfy this relation by meeting left polarized waves head-on. The condition then becomes:

$$\omega = \Omega - k|v_{\parallel}|,$$

which permits resonance of Pc1 waves with ions with tens of keV in energy (Gendrin et al., 1971).

Ions pursuing right polarized (fast) waves may resonate with waves whose frequencies are higher than the gyrofrequency of the ion, since the wave frequency would be Doppler shifted down to the gyrofrequency. Resonance may also be satisfied for electrons pursuing left polarized waves along the magnetic field (Ω has the opposite sign for electrons and ions), or meeting right polarized waves head-on.

Probable resonance mechanism for Pc1 micropulsations

The resonance consideration alone would suggest that electrons, ions and waves of both polarizations could be responsible for Pc1 seen on the ground. However, the resonance of left polarized waves with electrons is not as likely as resonance with ions because of the energy requirements. Resonance requires either relativistic energy electrons or keV ions, and there are many more such ions available than electrons (Gendrin et al., 1971).

The right polarized waves are isotropic, not guided, and so are less likely to be seen on the ground with amplitudes comparable to the guided mode (Tamao, 1964).

Consequently, they are not as efficient as the guided mode in transporting energy from the magnetosphere to the ground.

Other indications that Pc1 are from ions that resonate with left polarized waves come from the 'pearl', or pulsed Pc1. These are pulses detected about 1-2 minutes apart, and are seen alternately in opposite hemispheres. Their spectral shapes usually change, indicating that the higher frequencies travel more slowly than low, hence arrive later on each successive pulse. This behavior is consistent with a wave mode that follows the Earth's magnetic field, alternately mirroring from the northern and southern hemispheres. The dispersion shows that higher frequencies in the pulses travel slowest, which is the case for the guided mode, and opposite to the dispersion pattern of the isotropic (right polarized along \mathbf{B}_0) mode.

Wavegrowth in the presence of a distribution of ion velocities

The Doppler resonance condition will be satisfied by many ions over a range of velocities, because waves will have some finite frequency bandwidth and will not be monochromatic. The dispersion relation that describes wavegrowth in the presence of a distribution of ion velocities will be presented in this section.

The Vlasov equation is derived from a statistical average of many single particle distribution functions. It describes the macroscopic properties of the plasma, and tells how the distribution function changes in the presence of \mathbf{B}_0 and the wave fields. It does not include effects due to the discreteness of particles (Ichimaru, 1973). Nishida (1978) writes the first order approximation to the Vlasov equation (no collisions) :

$$\frac{\partial f_j}{\partial t} + \mathbf{v} \cdot \nabla_{\mathbf{r}} f_j + \frac{e_j}{m_j} (\mathbf{v} \times \mathbf{B}_0) \cdot \nabla_{\mathbf{v}} f_j + \frac{e_j}{m_j} (\mathbf{E} + \mathbf{v} \times \mathbf{b}) \cdot \nabla_{\mathbf{v}} F_j = 0 \quad ,$$

where $F_j + f_j$ is the distribution function for each of three species in the wave-perturbed plasma; $j = 1,2,3$ refers to cold protons, cold electrons and hot protons. F_j is the distribution function of the unperturbed species. \mathbf{B}_0 is parallel to the z axis. A Fourier

transformation is applied, which gives f_j , \mathbf{E} and \mathbf{b} (the wave fields) a harmonic dependence $\exp[i(kz - \omega t)]$. The wave \mathbf{b} is written in terms of \mathbf{E} by Faraday's law, and the perturbation part of the distribution function is then written as:

$$f_j = \frac{-i e_j E^\pm}{m_j (\omega - k v_{\parallel} \pm \Omega_j)} \left\{ \frac{\partial F_j}{\partial v_{\perp}} \left[1 - \frac{k v_{\parallel}}{\omega} \right] + \frac{k v_{\perp}}{\omega} \frac{\partial F_j}{\partial v_{\parallel}} \right\} \quad (\text{Nishida, 1978})$$

where

$$-E_x = \pm i E_y \equiv E^\pm ,$$

and the upper sign refers to a right polarized wave, the lower to a left polarized wave.

$E_z = 0$. The parallel speed v_{\parallel} is a signed quantity in this expression.

The definition of current density is combined with the wave equation to yield the dispersion relation (six equations for three unknown current components and three unknown electric field components). The current density arises from the wave-induced perturbation (f_j) in the distribution function :

$$\mathbf{j} = \sum_j n_j \mathbf{v} e_j \rightarrow \sum_j e_j \int \mathbf{v} f_j v_{\perp} dv_{\perp} d\theta dv_{\parallel} ,$$

where \mathbf{v} refers to the velocity of species j . The wave equation is:

$$i\omega\epsilon_0 \left[-\frac{c^2 k^2}{\omega^2} + 1 \right] \mathbf{E} = \mathbf{j} .$$

These equations lead to the dispersion relation (Nishida, 1978):

$$\frac{c^2 k^2}{\omega^2} = 1 + \frac{\pi}{\omega\epsilon_0} \sum_j \frac{e_j^2}{m_j} \int \frac{v_{\perp}^2 dv_{\perp} dv_{\parallel}}{\omega - k v_{\parallel} \pm \Omega_j} \left\{ \frac{\partial F_j}{\partial v_{\perp}} \left[1 - \frac{k v_{\parallel}}{\omega} \right] + \frac{k v_{\perp}}{\omega} \frac{\partial F_j}{\partial v_{\parallel}} \right\} .$$

The cold population distribution functions are represented by Maxwellians with thermal velocity v_{th} , and all cold components and electrons satisfy $\Omega_j \gg kv_{th,j}$ (Kozyra et al., 1984).

The hot populations are represented by a bi-Maxwellian, which has separate temperatures to describe motion parallel and perpendicular to the field:

$$F_{hot,j} = \left[\frac{m_j}{2\pi k_B T_{\perp}} \frac{m_j}{2\pi k_B T_{\parallel}} \right]^{1/2} \exp \left[- \frac{m_j v_{\perp}^2}{2k_B T_{\perp}} - \frac{m_j v_{\parallel}^2}{2k_B T_{\parallel}} \right],$$

where k_B is Boltzmann's constant. The integral above must be done for each species, and the imaginary part of ω , which gives the growth rate, comes out of the integral. The harmonic form used above with the Vlasov equation, $\exp[i(kz - \omega t)]$, may be expressed as

$$\exp[i(kz - (\omega_r + i\omega_i)t)] \rightarrow \exp[ikz - i\omega_r t + \omega_i t],$$

so the imaginary part gives exponential change in the wave amplitude. If $\omega_i > 0$, wave growth will result.

Kozyra et al. (1984) included ions heavier than protons in both hot and cold species. Also, instead of simply calculating the temporal growth rate (ω_i), Kozyra et al. (1984) calculated the convective growth rate ($S = \omega_{imag}/(\Omega_p V_{group})$). The argument was made that the convective growth rate was more important than the temporal growth rate because wave amplification depends on the time the wave spends in the amplifying region. The convective growth rate is:

$$\begin{aligned}
S &= \frac{\omega_i / \Omega_p}{\partial \omega_r / \partial k} = \frac{\omega_i / \Omega_p}{V_g} \\
&= \left\{ \sum_l \frac{\eta_{lw} \sqrt{\pi}}{M_l^2 v_{l\parallel}} [(A_l + 1)(1 - M_l X) - 1] \exp \left[\frac{-\frac{\eta_{lw} (M_l X - 1)^2}{M_l \beta_{lw} X^2}}{\frac{(1 + \delta)}{(1 - X)} + \sum_j \frac{(\eta_{jw} + \eta_{jc}) M_j}{1 - M_j X}} \right] \right\} \\
&\cdot \frac{1}{2X^2} \left[\frac{(1 + \delta)}{(1 - X)} + \sum_i (\eta_{iw} + \eta_{ic}) \frac{M_i}{1 - M_i X} \right]^{-1} \quad (\text{Kozyra et al., 1984}).
\end{aligned}$$

Summations over l include all ions, and summations over i and j include only ions heavier than H^+ . It is assumed that $\omega_r \gg \omega_i$ and only the field-guided mode is considered (Kozyra et al., 1984). The subscript w refers to warm components, and c refers to cold.

The variables in the expression are:

$$\beta_{lw} = \frac{8\pi n_{lw} k_B T_{l\parallel}}{B_0^2}, \text{ where } n_{lw} \text{ is the density of the warm species } l;$$

$$X = \frac{\omega_i}{\Omega_p}$$

$$\delta = \frac{\omega_{ppc}^2}{\omega_{ppw}^2}, \text{ the plasma frequencies of the cold and warm protons,}$$

$$M_j = \frac{m_j}{z_j m_p}$$

$$\eta_{jw(c)} = M_j \frac{\omega_{pjw(c)}^2}{\omega_{ppw}^2}$$

$v_{l\parallel}$ is the parallel thermal velocity of the energetic species l ,

$$A_l = \frac{T_{l\parallel}}{T_{l\perp}} - 1 \text{ is the anisotropy of species } l, \text{ and}$$

$T_{l\parallel}$ is the temperature of the component l measured parallel to B_0 .

The dependence of wavegrowth on anisotropy

In the expression for the convective growth rate above, the term

$$[(A_1 + 1)(1 - M_1 X) - 1] \quad (6-2)$$

must be greater than zero for $\omega_i > 0$ and growth to occur.

In a simple proton plasma, it is clear from (6-2) how the anisotropy affects wavegrowth, since it must be greater than a certain threshold value:

$$A > \frac{\omega_r}{\Omega_p - \omega_r} .$$

The minimum necessary anisotropy decreases for lower wave frequencies. On the other hand, for waves near the cyclotron frequency, ions must have nearly infinite anisotropy for growth to occur.

The effect of increasing anisotropy on wavegrowth has been plotted by Gendrin et al. (1971) and discussed by Kennel & Petschek (1966). Increased anisotropy increases wavegrowth for ion resonance with left circularly polarized waves. This requires $T_{\perp} > T_{\parallel}$, which is to say that large ion pitch angles ($\arctan(v_{\perp}/v_{\parallel})$) enhance wavegrowth. The resonance of ions with right polarized waves, as ions overtake the waves, requires $T_{\parallel} > T_{\perp}$ (Kennel & Petschek, 1966; Nishida, 1978).

Wave amplification has the effect of removing some of the perpendicular energy from the ions, consequently lowering their pitch angles. This is discussed in the case of an individual VLF electron-cyclotron resonance by Brice (1964). Electron cyclotron resonance is analagous to ion-cyclotron resonance discussed here, except that an electron resonates with a right-circularly polarized wave. He showed that the perpendicular energy of the electron decreases more than the amount passed to the wave, so the parallel energy

of the electron increases as the overall electron energy decreases. This means that the particle is scattered to a smaller pitch angle.

Inan et al. (1978) discussed pitch angle scattering in electron-coherent VLF interactions. The equations of motion of the electron in resonance with a cyclotron wave were derived there. They showed that cyclotron waves may change the pitch angle of a particle, by up to almost 100%, through the wave magnetic field, with a total particle energy change of a few percent. The magnetic field changes the pitch of the particle in the magnetosphere, but not its energy. Energy is exchanged via the wave electric field. Changes in v_{\parallel} , v_{\perp} and the initial phase angle between \mathbf{b}_{wave} and \mathbf{v}_{\perp} of the particle depend partly on the wave forces ($\mathbf{v}_{\perp} \times \mathbf{b}_{\text{wave}}$) and ($\mathbf{v}_{\parallel} \times \mathbf{b}_{\text{wave}} + \mathbf{E}_{\text{wave}}$), and partly on adiabatic pitch angle changes necessary to conserve magnetic moment along the field line. The change in gyrofrequency is important for determination of the wave-particle interaction time.

Marginally unstable wave frequency

In a composite of many ion masses, equation (6-2) also defines the marginally unstable wave frequency. Below this frequency (X_m), the energetic ions of species l may contribute to wavegrowth; above this frequency, the species l ions damp the wave (Kozyra et al., 1984). The marginally unstable wave frequency is below the gyrofrequency of species l and is:

$$X_m = \frac{\omega_{rm}}{\Omega_p} = \frac{A_l}{M_l(1 + A_l)},$$

where ω_{rm} is the real part of the wave frequency at the marginal limit, and the cyclotron frequency is used for normalization. For example, below the He⁺ marginal limit, wavegrowth comes from He⁺ and H⁺ ions. Above the He⁺ marginal limit, growth comes from H⁺, but there is damping from He⁺. The effect of the marginal instability, then, is

that wavegrowth in the higher frequency passbands, for example between the He⁺ and the H⁺ gyrofrequencies, is inhibited (Kozyra, 1984). Note that the marginal instability frequency limit for an ion depends only on anisotropy, and is raised as anisotropy increases (Kozyra et al., 1984).

The effects of an increased Doppler shift

An increased Doppler shift (from v_{\parallel}/V_A) in a pure proton plasma, with constant anisotropy also increases wavegrowth, but the frequency of maximum growth decreases (Gendrin, 1971). The increase in wavegrowth comes from the exponential dependence on T_{\parallel} . The decrease in the frequency at maximum growth is because a lower wave frequency is being raised to the gyrofrequency of the ion, which is fixed by B_0 and the ion mass, not the ion's parallel velocity.

The frequency bands of maximum growth

The wavegrowth in a multicomponent plasma tends to maximize just below the heavy ion gyrofrequencies. This is because the wavenumber k increases near a resonance (Kozyra et al., 1984), decreasing the phase speed and reducing the resonant energy of all ions whose marginally unstable frequencies are above the wave frequency. Resonant energy involves speed parallel to the magnetic field. The resonant energy for the energetic ion of species α in a cold, purely H⁺ plasma comes from the resonance condition (6-1), and

$E_{\text{res}} = 1/2 mV_{\text{res}}^2$; it is :

$$E_{r,\alpha} = \frac{1}{2} \frac{M_{\alpha}(\Omega_{\alpha} - \omega)^2}{k^2} \quad (\text{Kozyra et al., 1984}).$$

Another expression for resonant energy is given by Kozyra et al. (1984), for the case of multiple cold ion species. Reduction of the resonant parallel speed makes a difference in

wave growth because it allows lower energy ions to participate. This means more ions may participate, if their speeds have a Maxwellian distribution, as assumed here. For example, a wave just below the He gyrofrequency would have a low phase velocity and would receive energy from slower H⁺ ions than would otherwise contribute. Note also that in regions of increased magnetic field strength, the gyrofrequency Ω_α would be increased, which in turn would increase the resonant energy $E_{r,\alpha}$. This suggests that wave growth would be enhanced in regions of weaker B, since lower energy particles could participate.

When the expression for the real wave number k of the field-guided mode is imaginary, the range of frequencies in which this occurs is called a stop band. In the completely cold plasma case, the bands are bounded below by an ion gyrofrequency, and above by the cutoff due to that ion (Dawson, 1966). In these bands, no propagation, and consequently neither wavegrowth nor damping take place (Kozyra et al. 1984).

The effect of cold ion density on the growth rate

The presence of either cold or energetic heavy ions will create stop bands. In single energetic ion plasmas (H⁺, He⁺ or O⁺), the increase of cold plasma density will increase the growth. The phase speed of the wave will go down if ion density ρ goes up ($V_A = B_0/\sqrt{4\pi\rho}$). This will increase the Doppler shift (Halliday & Resnick, 1988), by shortening the wavelength, for an ion whose parallel speed was previously too low. The effect is to decrease the resonant energy, which allows more ions to participate in wavegrowth.

In the passband between the O⁺ cutoff and the He⁺ gyrofrequency, wavegrowth is affected by changes in these cold ion densities. An increase in the He⁺ density increases the convective growth rate in that passband and lowers the frequency of maximum

growth. However, an increase in the O⁺ density has the opposite effect (Kozyra et al., 1984). The same damping effect occurs above the He⁺ gyrofrequency when He⁺ or heavier ions are added to either warm or cold populations.

The effect of magnetic field on the growth rate

The effect of the magnetic field has been examined by Anderson et al. (1990), who took logarithmic derivatives ($\partial \ln S_{\max} / \partial \ln x$) of the expression for maximum growth rate with respect to magnetic field, anisotropy and particle densities in a pure proton plasma. The rate depends inversely on magnetic field, and is more sensitive to this than to warm or cold densities. It is reasonable for a strong inverse relation to magnetic field to exist, since the convective growth rate expression above depends on B₀ in the exponent, through the β ($\propto 1/B_0^2$) and X ($\propto 1/B_0$) terms. This would suggest enhanced growth with increasing radial distance from the Earth (Anderson et al., 1990).

It also suggests that the equatorial region at any radial distance would be favored for wavegrowth. A dipole field can be expressed as (Kelley, 1989)

$$|B(r, \theta)| = \frac{0.3 R_E^3}{r^3} (1 + 3 \sin^2 \theta)^{1/2}$$

where θ is the latitude and **B** is in gauss. This has its minimum value at the equator (zero latitude). The increase in magnetic field away from the equator also raises the resonant ion energy by increasing the difference between the cyclotron and wave frequencies (Kennel & Petschek, 1966). Increased Doppler shifting becomes necessary to resonate with the same wave further from the equator.

The implications for Pc1/2 micropulsations

An enhancement of wavegrowth just below the He⁺ gyrofrequency, at a distance of 6-7 Earth radii in the equatorial plane, may be responsible for Pc1/2 production. The He⁺ cyclotron frequency may form the sharp high frequency bound of these waves. The sharp low frequency bound typical of the Pc1/2 may be due to a sharp fall-off in wavegrowth below the He⁺ gyrofrequency. The wavegrowth just below the He⁺ gyrofrequency is mainly from H⁺ ions, suppressed in part by He⁺ ions. O⁺ may assist in creating this wavegrowth spectrum, but the fact that the Pc1/2 are seen on the ground, as discussed below, argues against large concentrations of O⁺ ions near the wavegrowth region. Otherwise, their presence could have the same blocking effect as the He⁺ ions appear to have.

Chapter 7

Results of data analysis

Introduction

The survey of the micropulsation data from 1986 has revealed distinctive patterns among waves in the 0.1-5.0 Hz range. The data is organized by a frequency of about 0.4 Hz. The patterns suggest that most of the waves above this frequency appear to come from L-shells near Siple, the plasmopause station. An L-shell is a surface formed by dipole field lines that would leave the Earth at the station's latitude. Below 0.4 Hz, most seem to come from L-shells between the plasmopause and the auroral zone. The conclusion is drawn that He⁺ ions along the path from the wave growth region to the ground are responsible for this organization. This study suggests, from ground-based observations alone, that He⁺ is modifying wave propagation. The patterns also identify the afternoon sector of the magnetosphere as the source region for the low-frequency branch.

The survey was also used, in conjunction with solar wind measurements and magnetic indices, to identify the mechanism that brings ions to the post-noon sector, far from the Earth, with the right pitch-angle distribution and energy to amplify Pc1/2 waves. Values of solar wind parameters, such as the pressure and magnetic field, were selected during the occurrence of Pc1/2 to look for a direct solar wind-magnetosphere energy source. Possible sources inside the magnetosphere, such as substorms and storms, were also examined through magnetic index values during and before the occurrence of Pc1/2 waves on the ground. The Pc1/2 appear to be amplified at L-shells between the

plasmopause and the auroral zone by ions that convect from the plasma sheet into the afternoon sector.

Indications that He^+ is important are provided by the diurnal occurrence pattern of the micropulsations, their event length and bandwidth distributions, and seasonal occurrence at opposite-hemisphere ground sites. Simultaneous observations from two stations at different latitudes, but in the same hemisphere, suggest that Pc1/2 come from higher L-shells than the waves above 0.4 Hz that are seen on the ground.

This is different from what is seen in space. For example, Fraser (1982) discussed wave spectra observed at ATS-6 ($L=6.6$), with power above and below a notch at the He^+ gyrofrequency. Anderson (1989) found that the outer magnetosphere, beyond $L=7$, was a stronger source of waves above the local He^+ gyrofrequency than the plasmopause region. Perraut (1984) concluded with a limited GEOS study that only about half of the waves above the local He^+ gyrofrequency would reach the ground at 70° magnetic latitude. Observations from this study will be discussed below, followed by the associative studies between Pc1/2 occurrence and the solar wind and magnetic indices.

Diurnal Occurrence Patterns

The Pc1/2 (0.1-0.4 Hz) Band

When all the unstructured events of 1986 at Sondre Stromfjord are superimposed on each other (Figure 7-1a), an intense diurnal variation appears for waves below 0.4 Hz. This frequency clearly organizes the wave data, since the diurnal pattern above 0.4 Hz is quite

different from that below. The peak occurrence for waves in the Pc1/2 band is between 1600 and 1800 UT.

The horizontal axis in Figure 7-1a is time of day in UT. It is divided into 20 minute segments. The vertical axis is the observed wave frequency, in 0.1 Hz steps, beginning at 0.1 Hz. The intensity of the grayscale is the number of times wave power was observed at Sondre Stromfjord, at a given wave frequency and 20 minute segment of the day in 1986.

At 1330 UT, Sondre Stromfjord is at local magnetic noon. This means that its geomagnetic longitude is subsolar, or on a line joining the center of the Earth and the Sun (Montbriand, 1970). The wave power counts in the Pc1/2 band were summed for each 20 minute segment of day and replotted as a line plot in local magnetic time, instead of UT, in Figure 7-1b. Also plotted are the counts from Siple and South Pole in the Pc1/2 band. When presented in local magnetic time, all three stations show a common post-noon peak occurrence for Pc1/2.

Sato & Saemundsson (1989) suggested that the emission intensity of Pc1/2 on the ground was linked to sunlight. They said that an increase in electron density in the topside ionosphere makes wave propagation from the magnetosphere through the ionosphere more efficient. Sunlight would create this increase on a seasonal and diurnal cycle. However, the diurnal pattern at South Pole, which has no solar day, rules out the possibility that sunlight enhancement of the ionosphere is responsible for the diurnal pattern. The South Pole observation means that the Pc1/2 source is in the afternoon sector of the magnetosphere, although it does not address the question of whether it is inside, or at the boundary layer.

The diurnal patterns for all unstructured waves at South Pole, Siple and McMurdo are shown in Figure 7-2. This has the same format as Figure 7-1a for Sondre Stromfjord

events. Each station plot is in UT, with local magnetic noon indicated. The Pc1/2 peak stands out in each case. South Pole, like Sondre Stromfjord, is near the auroral zone, with a magnetic latitude of -74.9° . Siple is close to the plasmopause, with a latitude of -61° . At a latitude of 80° , McMurdo is in the polar cap, where the magnetic field lines through the Earth's surface extend into interplanetary space, back to the Sun (Nishida, 1978).

McMurdo was surveyed from 9/13-9/17, 9/27-10/4 and 10/18-11/29, or 55 days in the local fall/winter season. Local summer is the most likely time to see the Pc1/2, as shown by Bolshakova et al (1980), Troitskaya et al., (1980), Heacock (1974) and Sato and Saemundsson (1989). The McMurdo survey did not include enough events to be as convincing as the other three, and Figure 7-2 is the only McMurdo data shown here. Nevertheless, the post-magnetic noon, Pc1/2 occurrence peak is quite clear.

The diurnal distributions for each station are shown by month in Figure 7-3. The Pc1/2 afternoon peak persists, regardless of season, in all three cases. This shows that the mechanism which produces the Pc1/2 in the afternoon operates independently of the mechanism that keeps most Pc1/2 from the winter hemisphere.

The trend for all Pc1/2 is for an afternoon maximum occurrence. However, some waves might come from other sources, such as the cusp or plasmopause. They might exhibit a different diurnal variation, which could be overwhelmed by the great number of Pc1/2 that have the afternoon peak occurrence. By selecting events with the right set of parameters, such as the Pc1/2 that are narrow band, or Pc1/2 with some pulse (pearl) structure, or just the lower frequency Pc2 waves, a different diurnal pattern might be apparent. This could suggest the source region for these waves. The diurnal patterns of some of these Pc1/2 band subsets are plotted in Figure 7-4 and described next.

Three subsets of Pc1/2 are the Pc2 waves (0.1-0.2 Hz), Pc1/2 with some periodically structured elements and Pc1/2 that are narrow-banded (≤ 0.1 Hz wide). Their diurnal patterns (Figure 7-4) are substantially similar to the Pc1/2 overall, but some possibly significant differences exist. Both the narrow-band Pc1/2 and the Pc2 have a postnoon peaks that are narrower in local time than for Pc1/2 overall.

At Sondre Stromfjord, the postnoon full-width half-maximum is 5.4 (± 0.5) hours for narrow-band Pc1/2, vs. 7 hours for *all* Pc1/2 at that station. At South Pole, the widths are 4.6 hours vs. 5.7, and at Siple, 6.0 vs. 8.6. The edge of the peak near noon generally shifts more than the edge near evening. The narrow-band Pc1/2 are shown in Figure 7-4c.

The Pc2 daily occurrence peaks are shown in Figure 7-4a. The full-width half maxima are narrow: 3.3 (± 0.5) hours at Sondre Stromfjord and Siple, and 5 hours at South Pole. The most dramatic narrowing is at Siple, compared to the Pc1/2 waves overall. Waves near 12-13 MLT may be of a higher frequency than waves later in the afternoon, because the low-frequency limit of the Pc2 seems to exclude events near 12-13 MLT.

Pc1/2 with some periodically structured elements are fewer in number than the other two subsets of Pc1/2, but they are spread more into the prenoon hours (Figure 7-4b). In these events, the structured elements occupy a relatively small part of the frequency-time area on a spectrogram, so overall, the events are considered unstructured. If the structured elements come from the same source region as these particular Pc1/2, they could provide some information through dispersion and travel time analysis (Gendrin et al., 1971). It could also be true that the Pc1/2 and the structured elements are produced simultaneously in different places. In that case, the associated Pc1/2 may appear more often near noon because the structured events preferentially occur there. See Figure 7-5 for the diurnal pattern of structured events.

The Importance of Structured Events and What They Suggest About the Source Region

The Pc1/2 classification includes events with structured elements as a minor part of the area on a frequency-time spectrogram. This type is known as "some str" in the database used for this work, and are considered unstructured. However, structured events, in which the periodic elements cover most of the area, are not included in Figures 7-1 and 7-4. There are relatively few such events in the Pc1/2 band, but there are enough to make a suggestion about source regions. The fraction of all events in the Pc1/2 band that are structured is: 6% at South Pole (37/601 events), 4% at Sondre Stromfjord (21/596), and 8% at Siple (53/641). Consequently, plots of *unstructured* Pc1/2 include nearly all events in the Pc1/2 band.

Siple has a greater fraction of structured events in the Pc1/2 band than the higher latitude stations. It is possible to estimate whether it is significantly greater. If it is, then two conclusions may be drawn. First, without knowing the origin of the structured features, it could be said that Siple is closer to their source than the higher latitude stations. Siple is close to the plasmopause, which is a source of Pc1 (Kozyra, 1984; Roth & Orr 1975, for example). Second, if structured events are observed in this band, then some Siple Pc1/2 may be from the plasmopause as well.

The above fractions are estimates of the fractions one would expect to find at these latitudes. It will be assumed that they are in fact the expected fractions, since we have only one survey. If the survey were repeated, with different stations at the same latitudes, the fractions might be somewhat different. This spread around the expected value might be described by binomial statistics, since only two outcomes are possible: structured and unstructured. With binomial statistics, there is a 96% chance that a measurement would

fall within two standard deviations of the expected value (Dowdy & Wearden, 1983). One standard deviation is: $\sigma = [n\pi(1-\pi)]^{1/2}$, where n is the total number of events in the band and π is the fraction that are structured (Dowdy & Wearden, 1983).

One may postulate that all three stations should have the same fraction of structured events in the Pc1/2 band, and then test that postulate. The postulate in fact is not true. Siple has a bigger fraction of structured events than the higher latitude stations, as will be shown next.

At Siple, one standard deviation in the *number* of structured events is 7, given that $n=53+588$, and 8% of these are structured. If there were 14 fewer structured events at Siple (two standard deviations), the structured fraction would have been 6%. This is the same as the expected fraction of structured events at South Pole, and more than at Sondre Stromfjord. Since the fractions at the higher latitudes are at least two standard deviations below the expected value at Siple, there is probably a physical reason for it, not just random variation. As suggested above, the reason could be that Siple has better contact with the plasmopause than the higher latitude stations.

Diurnal Patterns for Waves Above 0.4 Hz

The diurnal plots for all events above 0.4 Hz are shown in Figure 7-5. All such events, structured or not, are in Figure 7-5a. The unstructured events are in 7-5b, and the structured in 7-5c. There is a clear difference between the unstructured events above and below 0.4 Hz (compare Figure 7-5 to 7-1). This suggests a different source region for the two bands as seen on the ground. Structured events above 0.4 Hz span a wide range of mostly prenoon magnetic local times: approximately 0300-1300 MLT at Siple, with a

peak near 1000 MLT and 0.6 Hz. At Sondre Stromfjord, they peak at approximately 0600 MLT and 0.6 Hz.

At South Pole however, the structured events are spread more uniformly than at the other two stations, from 0200 to 1430 MLT (Figure 7-5c). This pattern is partly due to the source location and partly to the efficiency of the ionospheric waveguide. South Pole may observe Pc1 more uniformly throughout the day than Sondre Stromfjord because it has more seasonal darkness without daily variation. Darkness aids wave ducting by reducing losses to the E region (Manchester, 1968; Greifinger & Greifinger, 1968). During Fall and Spring, the lack of a solar day may expose South Pole to the source region for structured waves above 0.4 Hz without the daily attenuation suffered by Sondre Stromfjord.

The larger quantity of structured events at Siple compared to the higher latitude stations is apparent in Figure 7-5. This indicates that the general location for their production is closer to Siple, the plasmopause station, than the two auroral zone stations. This is consistent with other work that has associated the structured ("pearl") events with the plasmopause region (for example Roth & Orr, 1975; Heacock, 1971 and Kozyra et al., 1984).

Event Length and Bandwidth

Event length is another characteristic that distinguishes the waves above from those below 0.4 Hz. The waves below 0.4 Hz tend to be longer than those above, and the following plots also suggest that events at Siple in the Pc1/2 band come from two sources. One is the high-latitude region seen by South Pole and Sondre Stromfjord, and the other is the plasmopause region. Event length analysis on a large scale has been rare

in the past. There is a significant time expense in recording the beginning and end of each event, but the database approach has made some new insights possible. The results will be presented in this section.

Figure 7-6 is a scatterplot of all Pc1/2 events. It illustrates the afternoon clustering, and shows how the number and length of events are distributed. A dot represents the event length and the mid-event time for a Pc1/2. The data are plotted in UT, so the occurrence peaks do not line up among the stations. Most of the events are less than 200 minutes long and are clustered in the local magnetic afternoon. The longest events at South Pole and Siple are 10-11 hours, and the longest at Sondre Stromfjord is over 17 hours. This indicates the stability of which the Pc1/2 source is capable.

One of the two 17 hour Sondre Stromfjord Pc1/2 events is plotted in a spectrogram (Figure 7-7). Although other waves are detected during this long interval, one extends throughout the spectrogram. It happens to be a good example of what was concluded from the association studies, described below. The Pc1/2 seem to occur under a variety of solar wind conditions and magnetospheric activity levels. The 17 hour Pc1/2 begins near 0645 UT and runs to about 2330 UT. The values of solar wind pressure, IMF B_z , Dst, AE and Kp are noted throughout. Increased pressure can enhance cyclotron wave growth. Southward IMF facilitates energy transfer from the solar wind into the magnetosphere. Dst, AE and Kp are all measures of currents in the magnetosphere that are ultimately driven by solar wind energy. During this long event, Dst, AE and Kp values are all typical of a magnetically quiet time, and the event continues despite changing solar wind pressure and B_z polarity. The IMF B_z went from northward to southward and back twice. Dynamic solar wind pressure is as high as 6.2, and as low as 2.6×10^{-8} dynes/cm². Dst ranges from -2 to +10, which are values representative of either magnetically quiet times or pressure pulses. The Kp index varied from 0o to 2o, and AE from 54 to 133 nT, all typical of quiet times.

Note also that the bandwidth of the event is ≤ 0.2 Hz, and the upper frequency edge has a stable, sharp cutoff. This could be partly due to the discrete nature of the Fourier transform, but this is still a rapid dropoff of power with increasing frequency compared to other types of events. The reason could be that a limited ion-cyclotron resonance is taking place, where a narrow band of frequencies are being amplified. It would be a remarkable feat of nature to maintain such a resonance over 17 hours, when solar wind parameters change and substorms take place in about an hour or less. Alternatively, the narrow-band nature could be due to the heavy ion composition at the amplification site and along the path to ground. Fraser (1982) shows a spectrum from ATS-6, a geosynchronous ($L \approx 6.6 R_E$) satellite. The presence of O^+ and He^+ created a passband in the Pc1/2 range in which wave power was detected. The bandwidth of the Pc1/2 is typically very narrow. At Sondre Stromfjord and South Pole, 94% are ≤ 0.2 Hz in bandwidth, and at Siple, the fraction is 87%.

Comparison of Event Length for Waves Above and Below 0.4 Hz

At Sondre Stromfjord and South Pole, the longest events occurred in the local summer. Scatterplots of Pc1/2 length vs month are presented in Figure 7-8, and the seasonal length maxima are clear. This suggests that the two auroral zone stations are best connected to the Pc1/2 source during local summer.

The trend is not as clear at Siple. This might be due to events below 0.4 Hz that come from the plasmopause region, which is closer to Siple than the higher latitude stations. Some of the longest Siple events below 0.4 Hz are during June and July, which are winter months there. The plasmopause events would be more noticeable in winter, when Pc1/2 are less common (see the section on seasonal Pc1/2 patterns).

At all three stations, Pc1/2 are typically longer than waves above 0.4 Hz. Cumulative distributions are plotted in Figure 7-9. The length difference is most extreme at Sondre Stromfjord. Approximately 43% of the Pc1/2 are one hour or less, compared to 65% for waves above 0.4 Hz.

A Kolmogorov-Smirnov (KS) test (Press, 1987) compares cumulative distributions of unbinned data. It was applied to the cumulative length distributions and it indicates a significant difference between the length of events above and below 0.4 Hz at both high-latitude stations. The KS significance level is less than 0.01% in both cases. This is the significance level of the null hypothesis that the two distributions are randomly drawn from the same parent. A large value of this number means that the difference in event lengths above and below 0.4 Hz is just due to random selection. Press (1987) considers a level of 1% or less to be a strong rejection of the null hypothesis.

The two bands are not as clearly distinguished at Siple. Events above 0.4 Hz are longer at Siple than at the other stations, and the Pc1/2 are shorter. The KS significance level in this case is 1.4%. This means they are significantly different, but not as much as at the high latitude stations.

Since 44-57% of the Pc1/2 at the three stations are longer than one hour, hourly-averaged values of magnetic indices and solar wind parameters could be used to look for possible associations with the occurrence of Pc1/2. IMP8 solar wind speeds and interplanetary magnetic field (IMF) measurements are available from the National Space Science Data Center in hourly-averaged values, as are the Dst and AE indices from the World Data Center C2 in Kyoto, Japan. These results will be discussed in a separate section.

Pc1/2 Global Event Onset

In 29 cases, segments of the same Pc1/2 event were observed at more than one station simultaneously. For these events, onset times at each station were studied for patterns consistent with a spatially localized, fixed-position source, such as the cusp, as suggested by Bolshakova et al. (1980). In the simplest case, such a source would be seen by each station, in order of station longitude, as the source came within view. However, only 4 of 29 events began in the order of station longitude. Moreover, none of the events that started in order of station longitude ended in that order. The start times at Sondre Stromfjord, the lead station in longitude, ranged from six hours before noon to two hours after noon. The source position seems to wander, and local ionospheric conditions may add to the variety in onset times at the stations.

The differences in onset times at each station for the 29 global Pc1/2 are shown graphically in Figure 7-10a. Figure 7-10b shows relative onset times for Pc1/2 seen at the two Antarctic stations. Most of the events observed at South Pole and Siple together were not seen by Sondre Stromfjord. South Pole is as likely to see a Pc1/2 before Siple as the reverse, which again suggests a variability in source position.

The source region seems to be mostly in the afternoon, but it can expand to the morning sector. These morning-onset events are plotted in the scatterplot of all Pc1/2 occurrence and duration in Figure 7-6. The longest simultaneously-observed Pc1/2 was 10.3 hours, beginning four hours before Sondre Stromfjord local noon. The events that start before noon have the same narrow-band spectra of the more common afternoon Pc1/2. The range in global onsets suggests that the Pc1/2 source region can extend over several hours of local time. Although the cusp and cleft can be approximately 3 and 8 hours wide, respectively (Newell & Meng, 1989), the spread in local time for the global events is even wider, so the source region may not be localized in either the cusp or cleft.

Seasonal Occurrence

Another difference between the waves above and below 0.4 Hz is the seasonal occurrence pattern. It clearly indicates a different production or propagation environment for waves above and below 0.4 Hz, because these two bands have the *opposite* seasonal pattern. Figure 7-11a shows all the events above 0.4 Hz observed in both hemispheres at Sondre Stromfjord and South Pole, the two auroral zone stations. The horizontal axis is time in months, and the height of a column represents 100% of the events that occurred at one or both of the two stations in any given month. The dark portion is the fraction of the events that were only seen at Sondre Stromfjord, the white for those only at South Pole, and the gray for events simultaneously at both.

Comparing the white and dark sections, it is clear that the local winter station sees more events above 0.4 Hz than the local summer station. However, the Pc1/2 band has the *opposite* seasonal behavior. The local summer station sees more than the local winter station. The winter maximum for the higher frequency waves is consistent with the notion that they are ducted up to these high latitude stations from a remote injection point, because the wave guide is expected to be lossy in the daytime hours due to enhanced absorption in the E-region (Manchester, 1968). The same seasonal pattern is shown in actual event counts in Figure 7-12.

Latitude Dependence of Pc1/2 and Pc1 Occurrence

Observations of events common to South Pole and Siple (auroral zone and plasmopause) suggest that the Pc1/2 source may be located between the L-shells of the two stations. In the top panel of Figure 7-13, the observations of waves above 0.4 Hz are shown for all of 1986. The horizontal axis is the month of the year, and the height of the each column represents 100% of the events that occurred during each month. The dark gray section of each column is the fraction that were seen at Siple, but not at South Pole. The white section is the opposite case. The light gray is the fraction seen in common at both stations. The waves above 0.4 Hz are rarely seen at the auroral zone station alone. They are generally at Siple alone, or Siple and South Pole together, as though appearance at Siple is a prerequisite for detection at South Pole. The source for waves above 0.4 Hz seems to have better independent access (i.e., seen only at one or the other) to the lower latitude station. The same data is shown in event counts in Figure 7-14.

On the other hand, AMPTE/CCE satellite observations have shown that the outer magnetosphere, beyond $L=5$, is a stronger source for Pc1 above the local He^+ gyrofrequency (approximately 0.4 Hz at $L=7$) than the plasmopause region (Anderson, 1989). If this is the case, one would expect the opposite pattern for South Pole-Siple observations of waves above 0.4 Hz. This is an indication that the presence of He^+ may be important to the propagation of these waves from outer magnetospheric sources down to the ground. If one were not aware of the Pc1 above 0.4 Hz at high L-shells, it would appear that there are two separate source regions: one for waves above 0.4 Hz, near the plasmopause, and one for 0.1-0.4 Hz waves between the plasmopause and the auroral zone.

The waves in the Pc1/2 band are more evenly distributed between the two stations (Figure 7-13b). The source for these waves clearly has better independent access to either

latitude, and may be located between their L-shells. To be more specific, for waves *above 0.4 Hz*, a monthly average of 37% ($\pm 11\%$) are at Siple alone, which is more than two standard deviations higher than the fraction at South Pole alone: 12% (± 3). On the other hand, the monthly averages for *Pc1/2* are: 28% (± 8) at South Pole alone, which, with the uncertainty, is equivalent to the fraction at at Siple alone: 39% (± 8). Note that the designation of "South Pole only" is not meant to imply that South Pole is the only station to see the event; just that Siple does not.

The events in Figure 7-13 marked "all SP-Siple" include both events known to be seen simultaneously at both, plus those that might be common sightings. The uncertainty arises because their bandwidths overlap, or they start at one station before stopping at the other. The uncertain events cannot be ignored when studying these common-observation patterns. It is necessary to know the maximum fraction that could be common to both in order to expose the trend for events observed at either station alone. However, they would not be suitable for studies of conditions during simultaneous observations.

The waves above 0.4 Hz in Figure 7-13 include structured events, which have periodically spaced elements, and are thought to be associated with the plasmapause region. However, the unstructured waves may not necessarily be from the same place, nor have the same latitude dependence as events above 0.4 Hz overall. The *Pc1/2* class does not include structured events, although some have minor quantities of structured elements. These "some str" *Pc1/2* are a small fraction of all *Pc1/2* (compare Figure 7-1 with Figure 7-4b).

To examine the latitude dependence of unstructured wave types, the structured events were removed from the waves above 0.4 Hz, along with events containing structured elements as a minor part. The South Pole-Siple comparisons were repeated as described above. Once again, the waves above 0.4 Hz were associated with Siple, the plasmapause

station. The monthly fraction at Siple alone was 35% ($\pm 8\%$); which is more than two standard deviations higher than the fraction at South Pole alone: 13% ($\pm 3\%$).

Possible Significance of the 0.4 Hz Frequency

The diurnal pattern for all unstructured waves (Figure 7-1) is organized by a frequency of approximately 0.4 Hz. The diurnal variation is different below this frequency than above. This first indication that 0.4 Hz is important is supported by the latitudinal, seasonal and event length patterns for waves above and below this frequency.

The He⁺ gyrofrequency at the magnetic equator, beyond a distance of 6 R_E is near 0.4 Hz. Figure 7-15 shows the He⁺ gyrofrequency at the magnetic equator, as calculated with the T89 model (D. Larson, p.c.). It approaches 0.4 Hz near L=7, and then decreases more slowly with L-shell beyond L=7. Near L=3, the O⁺ gyrofrequency approaches 0.4 Hz at the equator, but the Pc1/2 seem to come from a higher L-shell, as indicated by the latitude dependence. Finally, spacecraft spectra discussed below show signs of He⁺ ion cyclotron resonance. This means it is reasonable to suggest that the 0.4 Hz division in the data is due to an ion cyclotron resonance.

Another indication that He⁺ ions have an effect on wave propagation in the outer magnetosphere is the appearance of notches at the local He⁺ gyrofrequency in wave spectra as seen on spacecraft. Perraut, et al. (1984), Roux, et al. (1982) and Young, et al. (1981) show notches in data from GEOS 1 (with an orbit of 1.3 R_E perigee, 7.0 R_E apogee, and a 26 inclination to the equatorial plane (Young, et al., 1981), and GEOS 2 (synchronous orbit, at 6.6 R_E, (Young, et al., 1981). At GEOS 2, the notches are at approximately 0.4 Hz. At GEOS 1, they are 0.4 Hz or above, since GEOS 1 comes in closer to the Earth. Fraser and McPherron (1982), and Fraser (1982) show the presence

of He⁺ ions in their ATS-6 (synchronous orbit) spectra as well. Finally, Anderson (1990) have AMPTE/CCE (8.8 RE apogee, 1000 km perigee) data that also show gaps at the He⁺ gyrofrequency.

Waves amplified below the He⁺ gyrofrequency at the equator will propagate in the left polarized mode down to the ionosphere. The local He⁺ gyrofrequency will rise above the wave frequency as the wave approaches regions of stronger magnetic field closer to the Earth. This means that waves *above* 0.4 Hz may easily reach the ground if they are amplified below the local equatorial He⁺ gyrofrequency. This could take place on L-shells lower than L=7.

Waves amplified above the local He⁺ gyrofrequency at the equator will be reflected by He⁺ ions along their field-line path to the ground if the He⁺ concentration is high enough (Rauch & Roux, 1982; Perraut, et al., 1984). This will occur at $\omega = \omega_{\text{bi-ion}}$ even if the wave-normal vector \mathbf{k} was initially parallel to the local magnetic field (Roux, et al., 1982). In the same way, a sufficient concentration of oxygen ions along the field line could prevent waves amplified between the local O⁺ and He⁺ gyrofrequencies at the equator from reaching the ground. This is apparently not the case when Pc1/2 are seen on the ground.

Notches in wave spectra have been observed at the O⁺ gyrofrequency at synchronous orbit (Fraser & McPherron, 1982; Fraser, 1982) near 0.16 Hz. However, the density of oxygen ions along the field line path seems to be insufficient to reflect the Pc1/2 before they reach the ionosphere.

The plasmopause region appears to be the source for most waves above 0.4 Hz that are seen on the ground, since those from higher L-shells cannot easily get past the He⁺ ions. The division in the data near 0.4 Hz suggests that the Pc1/2 are amplified most often in a region where the He⁺ gyrofrequency is approximately 0.4 Hz. Otherwise, the effect of

the He⁺ ions would be smeared out in the ground data, because the He⁺ gyrofrequency increases near the Earth (see Figure 7-15).

Possible Connection of Pc1/2 Occurrence with the Solar Wind and Magnetic Indices

A variety of energy sources for Pc1/2 have been discussed in literature. Previous work by Kaye & Kivelson (1979) suggested that dynamic solar wind pressure was responsible for Pc1/2 production and that the IMF B_z polarity was important. Heacock (1974) speculated that the plasma on the last closed field lines near the cleft, as well as detached plasma regions convecting sunward within the magnetosphere might be the energy source. Bolshakova, et al. (1980), considered the source to be in the magnetosheath region, on field lines that enter the cusp. All considered Pc1/2 to be ion-cyclotron waves. With so many explanations available, it was decided to use the large number of events in this 1986 survey, along with readily available solar wind measurements and magnetic indices, to test these ideas.

Associative studies were done between the occurrence of Pc1/2 and solar wind parameters and magnetic indices. Direct solar wind-magnetosphere interactions that might provide the energy were investigated through IMF orientation and dynamic solar wind pressure. Pressure pulses are known to cause Pc2-Pc5 waves (0.1 Hz-1.7mHz; Nishida, 1978). A southward component of the IMF is associated with magnetic activity within the magnetosphere, and energetic ions that could resonate with Pc1/2 are part of that activity. The dawn-dusk component of the IMF is known to affect convection in the magnetosphere, which could in turn decide where the principal wave growth region will be.

The solar wind data came from the National Space Science Data Center (NSSDC) database of IMP8 measurements, an on-line database available via the Space Physics Analysis Network (SPAN). This database, and network access procedures, are documented in the NSSDC Data Listing (Horowitz & King, 1990). A limited set of DMSP F7 measurements were used in conjunction with Pc1/2 occurrences, and these came from the online database described by Newell, et al. (1991).

Possible energy sources inside the magnetosphere were explored using the AE, Dst and Kp indices. These indices describe certain current systems within the magnetosphere by measuring the magnetic field at the surface of the Earth, in different places and for different lengths of time. One form of activity is the substorm, in which some energetic ions are injected into the ring current. Other ions are convected sunward, untrapped, on open drift paths within the magnetosphere. Either of these ion populations might ultimately resonate with and amplify Pc1/2 waves. The AE index is a measurement of part of the substorm process. It represents auroral electrojet intensity, which grows stronger during substorms. The AE index for this study was published in the World Data Center - C2 for Geomagnetism Data Book #19 (Kamei, Sugiura & Araki, 1990).

Geomagnetic storms are described by the Dst index. During storms, energetic particles are repeatedly injected into the ring current in a sequence of substorms. The calculation of the Dst index is an attempt to measure the magnetic field of this current at the surface of the Earth. Solar wind pressure pulses can also affect Dst measurements. Ring current ions are known to be an energy source for Pc1 (0.2-5.0 Hz) waves. The Dst index for 1986 was published by the same source as Provisional Values of Equatorial Dst (Sugiura & Kamei, 1986/87).

The Kp index is a general measure of variations in the magnetic field at the surface of the Earth. It describes the most extreme variation in a three-hour period, taking into account

measurements from 13 midlatitude stations around the world. Unlike the other two indices, it does not identify the source of the magnetic field disturbance. The Kp index is published monthly in the *Journal of Geophysical Research*. All data were either imported directly as files into the database software (solar wind parameters, DMSP data), or manually typed into files from paper documents (AE, Kp, Dst).

Except for the Kp index and DMSP measurements, the data were available in one-hour averages. Since the start and stop times for the Pc1/2 are known, events of less than 45 minutes duration were rejected in order to ensure comparison of similar timescales. Additionally, complete events, or segments of multiple-hour events, that overlapped an IMP8 or index data hour by less than 45 minutes were also discarded. For a given event, the solar wind or index values could either be averaged over the event duration, or treated as separate data points. Averaging over the event duration allows the event to be characterized by a single value. On the other hand, treating the values separately exposes extreme levels during the event, which could otherwise vanish due to averaging.

The timescale of the available index and solar wind data limits the scope of the associative studies. Statements made here about Pc1/2 associations strictly apply to Pc1/2 at least 45 minutes long. This represents 70.3% of the Pc1/2 at Sondre Stromfjord, 62.4% at South Pole and 60.7% at Siple. The shorter events may be produced in a different way, or in different places, but the available time resolution is not sufficient to address the question. The longer events should provide the best chance for insight from associative studies. The longer the physical mechanism producing the long Pc1/2 has to remain in operation, the easier it should be to identify. It is possible that none of the solar wind or index measurements in fact measure the key physical quantity, but they can narrow the range of possibilities through negative results.

Solar Wind Measurements: the IMP8 spacecraft

Approximately 40% of 1986 was covered for purposes of solar wind measurements (NSSDC1989), which were all from the IMP8 spacecraft. IMP8 had a $30 \times 40 R_E$ orbit with a 12.5 day period. It was in the solar wind for six to eight days per orbit (NSSDC, 1986). The maximum travel time of the solar wind from IMP8 to the magnetopause can be estimated, taking the modal solar wind speed for 1986 (350-400 km/s) and the maximum distance between IMP8 and the magnetopause. The magnetopause location moves in and out, depending on the solar wind pressure and IMF orientation. For example, it moves inward for either IMF B_z south or increased solar wind pressure (Sibeck et al., 1991).

Sibeck et al. (1991) show the radial dependence of the subsolar point of the magnetopause on pressure and B_z , from a data set of 1821 magnetopause crossings. The subsolar point is at $8.8 R_E$ for pressures in the range 4.9-9.0 nPa, which is higher than most of the pressures during Pc1/2 events (see Figure 7-17). For B_z in the range -6 to -4 nT, it is at $9.6 R_E$, which is again an extreme value for Pc1/2 (see Figure 7-20).

A scatterplot of magnetopause crossings during 1963-68 IMP measurements (Fairfield, 1971) shows a typical value of $10-11 R_E$ and a minimum of approximately $7 R_E$ along the Earth-Sun line at the equator. This gives a maximum travel time of $(40-7) \times 6400 \text{ km} / 350 \text{ km/s} = 603 \text{ sec}$, or 10 minutes. The IMP8 data are hourly-averaged values, and the segments of Pc1/2 used were at least 45 minutes long, so this maximum delay between IMP8 and the magnetopause is small compared to the time periods of the data.

Sibeck and Croley (1991) compare solar wind pressure and IMF measurements on IMP8 to ISEE 2 and cast doubt upon IMP8 solar wind pressures measured over periods of two minutes or less. They suggest this may be due in part to the time resolution of IMP8

plasma measurements. This does not create a problem for the IMP8 data used here, however.

Figure 7-16 shows the monthly distribution of IMP8 IMF hourly-averaged measurements during 1986. The measurements are not uniform throughout the year, and in fact are lowest in February, March and December, which are summer months in the southern hemisphere. Since Pc1/2 occur most often in local summer, the South Pole Pc1/2 would have fewer coincident IMP8 measurements than Sondre Stromfjord Pc1/2.

Dynamic Solar Wind Pressure During Pc1/2

Solar wind dynamic pressure depends on the mass of the solar wind particles, their number density and speed as: $P = mnV_{sw}^2$ (for example, Kaye & Kivelson, 1979). Increased solar wind pressure aids the amplification of Alfvén waves by 'compressing' the magnetosphere. Greater pressure means a greater charged particle speed or number density, and either one increases the magnetopause current (for example, Nishida, 1982). This increases the magnetic field inside, which in turn increases the anisotropy (pitch angles) of energetic ions, which may then more effectively supply energy to waves (Nishida, 1978). Nishida (1978) says that compression tends to increase the average frequency and bandwidth of a wave.

The solar wind pressure distribution for all Pc1/2 is shown in Figure 7-17. All three stations are presented, and the 1986 IMP8 solar wind pressure distribution is shown for comparison. There is a weak trend for the solar wind pressures during Pc1/2 at Sondre Stromfjord and Siple to be higher than the 1986 IMP8 reference. If the two distributions were offset from one another, the peak offset would be toward higher pressures by approximately $0.5-1.0 \times 10^{-8}$ dynes/cm². It would be surprising if Sondre Stromfjord and

Siple Pc1/2 occurred during higher solar wind pressures than Pc1/2 at South Pole, because of the latitude similarity for South Pole and Sondre Stromfjord, compared to Siple.

It is possible that pressure variations on a timescale that is short compared to the one hour average could be the source. If there are pressure pulses which are short compared to one hour, they must be present in a train that can be several hours long. Kaye & Kivelson (1979) suggested a relation between solar wind pressure and the occurrence of Pc1/2, from OGO-5 observations. However, the increases in pressure lasted approximately one hour for the events shown in their paper.

Note that approximately 8% of the pressures are below 2.5×10^{-8} dyn/cm². This is below Kaye & Kivelson's (1979) threshold defining "enhanced" solar wind pressure. They saw no pressures associated with Pc1-2 below this value, a point which suggested that Pc1/2 required elevated levels of pressure.

A χ^2 comparison of each station's pressure distribution to the 1986 reference shows that all three are similar to the reference. If one randomly draws a subset from a parent distribution, such as from the 1986 IMP8 solar wind pressures, the subset should have the same shape as the parent. This means that the solar wind pressures for Pc1/2 occurrence are consistent with a random selection from the 1986 IMP8 distribution. If there is a relation between solar wind pressure and Pc1/2 occurrence, then the complete range of all 1986 solar wind pressures satisfied it. Some other element of such a relation is still unidentified, because if solar wind pressure is both necessary and sufficient, one would expect to see Pc1/2 every day at each station, and this is not the case.

All three stations consistently have a lower count in the $2.0-2.5 \times 10^{-8}$ dyn/cm² pressure bin, compared to the 1986 reference. However, the weak trend and the count deficiency are not sufficient to distinguish the distributions from the 1986 solar wind pressure

distribution. Assuming that Poisson statistics apply, the probability of exceeding χ^2 is greater than 5% for pressures during Pc1/2, at any station, compared to the 1986 IMP8 reference.

As a check for consistency, the pressures for the first hour of those Pc1/2 which were long enough to overlap at least one hour of IMP8 data were selected. No averages were taken in this approach. These Pc1/2 had to be at least two hours long to ensure complete overlap. Their pressure distribution is plotted in Figure 7-18. For South Pole and Sondre Stromfjord, the distributions are similar to the 1986 IMP8 reference.

Siple shows some departure toward higher pressures. A comparison over the range of 1.5-6.0, with bins 5.0, 5.5 and 6.0 $\times 10^{-8}$ dynes/cm² gathered into one, gives a 1.4% probability of exceeding χ^2 , a borderline level of significance. This is similar to the trend for event-averaged solar wind pressures there. It could suggest that Pc1/2 may be associated with higher solar wind pressures when seen at Siple than at the higher latitudes. If there is an association, it may be that the increased pressure is part of a larger mechanism for Pc1/2 amplification, but is not directly responsible for wave growth.

Solar Wind Pressure: Discussion

The long Pc1/2 in Figure 7-7 rises no more than 0.1 Hz over a 2.5×10^{-8} dyne/cm² rise in average pressure. The initial segment does rise more than that in frequency, but the difference in average pressure is less than half of what is seen during the long, stable part. Apparently, a pressure change of more than 2.5×10^{-8} dyne/cm² is necessary to affect wave growth in the Pc1/2 band.

This study tested an association of Pc1/2 occurrence with average pressure. There is a possible threshold at approximately 2.0×10^{-8} dyne/cm², but overall, there is no general

preference for a particular value. Possibly the what is important is a *change* in pressure over some time, instead of some large absolute value. A sufficiently large change might increase anisotropy and temporarily add ions to the population that can promote wave growth. It may be that if the pressure remains at an arbitrary level, the drift paths of the ions and the wave growth rates may return to a state similar to the one before the change.

If a change in average pressure is important, it must be greater than 2.5×10^{-8} dyne/cm², because a change of this much made no difference in the character of the event in Figure 7-7. In addition, for most of the events in Figure 7-17, the pressures during Pc1/2, appear in a pressure range from 2.0 to 4.5×10^{-8} dyne/cm². This does not leave much room for a change in pressure greater than the change in Figure 7-7. It may be tentatively concluded that neither absolute values of, or changes in solar wind pressure are associated with the occurrence of Pc1/2. Since this study recorded the occurrence of micropulsations, not their amplitudes, the possibility of a pressure-amplitude relation is left open.

Sondre Stromfjord events show a variety of pressure patterns. One event lasted 5^h30^m (SS ser_no 258.0, 10/30/86), during which the hourly-averaged pressure went down, then up, in the following sequence: 4.8, 3.5, 3.9, 2.6, 1.9 and 3.0 ($\times 10^{-8}$ dynes/cm²). Another lasted for 2^h10^m, beginning during relatively low pressure and turning off during high pressure (SS ser_no 478.0, 9/11/86): 2.1, 2.2 and 6.1 ($\times 10^{-8}$ dynes/cm²). If pressure acts to produce Pc1/2, sometimes up to 17 hours long, it is not a simple mechanism.

IMF Orientations During Pc1/2

The possibility of an association of Pc1/2 occurrence with the IMF was also examined. IMF orientations during Pc1/2 were compared to the IMF orientations during 1986, as measured by IMP8. When the IMF has a southward component, it is directed oppositely to the Earth's field, and reconnection may occur. Field lines that led from the south to the north pole of the Earth connect to the IMF. The result is a field line that extends from the Sun through the polar caps and interior of the Earth, back to the Sun. This line is carried tailward by the solar wind, until it re-reconnects to a state of two separate field lines again: one looping through the Earth's poles, the other through the Sun's.

While the connection of the solar wind and Earth field exists, however, solar wind plasma may enter the magnetosphere along the field line (Nishida, 1978). Much of this plasma travels tailward, just inside the magnetopause, in the mantle (also called the high latitude boundary layer (see Lundin, 1988). This plasma flow is believed to be responsible for the dawn-dusk electric field over the polar cap, which drives convection inside the magnetosphere (for example, Lundin, 1988). Other solar wind plasma goes down to the cusp region through the entry layer (see Figure 2 in Lundin, 1988).

The fact that a southward IMF is associated with energy input to the magnetosphere has been shown in many past studies. Fairfield & Cahill (1966), using Explorer 12; Rostoker & Falthammar (1967), using IMP1; and Schatten & Wilcox (1967), using IMP3 all found that southward IMF was associated with increased magnetic activity on the ground. Arnoldy (1971) showed that the time-integrated southward IMF was related to the input of solar wind energy to the magnetosphere. Integrated over one hour intervals, the integrated southward IMF component was correlated with hourly averages of AE, with AE lagging by approximately one hour. Meng, et al. (1973) performed a similar study with 5.5 minute time resolution, and found a delay of approximately 40 minutes.

Other associative studies were done by Rostoker, et al. (1972), between the rate of southward flux arrival at the magnetosphere and AE; by Akasofu (1979) between the polar angle of the IMF and AE; and by Reif, et al. (1981), between the polar cap convection potential and parameters involving IMF orientation.

An example of the magnetospheric response to a southward-turning of the IMF is shown in Figure 7-22. The IMF B_z component, as measured by IMP8, is plotted, along with the AE index. Both are hourly-averaged values from the same databases used in this work. In Figure 7-22, B_z remains positive for about seven hours, during which the AE index remains relatively low. Low AE indicates a quiet auroral electrojet condition. After B_z turns south, the AE index rises, indicating an intensified electrojet and a substorm in progress. There is a brief northward-turning near 0 UT, which is followed by a slight reduction in the AE index. Near the end of the plot, B_z nears zero and then turns north, at which time the AE index decreases to its original level.

To summarize, a period of southward IMF is important for wave generation for two reasons. First, it can supply solar wind ions directly to the magnetosphere via the Sun-Earth magnetic field line connection ("reconnection"). Second, it enhances the dawn-dusk electric field, which convects ions into the afternoon sector. Convection time depends on the starting point of the ions, their pitch angles and energies (for example, see Ejiri, 1978). Once ions are present, wave growth may occur. Consequently, the B_z component at the time of Pc1/2 occurrence was selected, as well as from one and two hours before. The delay of two hours was suggested by observations by Kaye & Kivelson (1979).

The Geocentric Solar Magnetospheric (GSM) coordinate system was chosen for IMF data because it moves with the magnetic dipole of the Earth. The X axis is in the direction of the sun from the center of the Earth, and positive toward the Sun; the Y axis is perpendicular to the dipole axis, lies in the magnetic equatorial plane and is positive

toward dusk; and the Z axis is in the plane of the X axis and the Earth's magnetic dipole and is positive North. The Z axis is not always perpendicular to the ecliptic; it rotates (oscillates) about the X axis daily .

The X and Y components of the IMF are important to solar wind-magnetosphere coupling, so their values during Pc1/2 events were plotted and compared to the IMP8 reference. The Y component of the IMF (dawn to dusk) has an influence on the symmetry of convection in the magnetosphere (Kelley, 1989), so an association of Pc1/2 with the polarity of B_y could explain the postnoon occurrence. Small cone angles of the IMF to the X axis (Earth to Sun) have been associated with Pc3 and Pc4 waves directly transmitted into the magnetosphere (Nishida, 1978; Engebretson, et al., 1991) from the solar wind. Engebretson, et al. (1991) found broadband wave power up to at least 0.5 Hz in the magnetosheath during times of small IMF cone angles and Pc 3-4 activity, but no narrow-band waves are seen. Earthward-pointing IMF has also been associated with increased magnetic activity in the magnetosphere, particularly when accompanied by a southward component (Schatten & Wilcox, 1967).

B_x and B_y Dependence

The angles the IMF made with the X_{gsm} and Y_{gsm} axes during Pc1/2 events are plotted in Figure 7-19. Data for all three stations are presented, along with the 1986 IMF angles to X and Y as measured by IMP8. At all three stations, the angles of the IMF to the X and Y axes during Pc1/2 follow the distribution of the 1986 IMF angles. For the IMF-to-Y angles, a chi-square test that assumes Poisson statistics puts the probability of exceeding chi-square at greater than 4% for Sondre Stromfjord, and more than that at the other two stations. For the angles to the X axis, the probability is at least 5% for any station. This

indicates a similarity between all three station distributions and the 1986 IMP8 measurements.

In addition, there are some single-bin departures from the 1986 reference, such as the excess in the 50°-60° bin for Siple. Since they are confined to one 10° bin, and there are no similarities in these departures between South Pole and Sondre Stromfjord, they are probably not meaningful. Once again, this suggests that if the IMF orientation to the X and Y axes is involved in the production of Pc1/2, it may be necessary, but is not sufficient to do so.

B_z Dependence

The distribution of IMF B_z values during Pc1/2 events is presented in Figure 7-20. B_z values for every hour of each event were treated as separate counts, because the magnetic activity within the magnetosphere is higher during southward IMF than northward. Averaging IMF values over the event duration could mask the presence of B_z south during Pc1/2.

The hourly-averaged IMP8 IMF B_z peak for 1986 is in the range 0-2 nT; it is not symmetric about zero. Chi-square tests assuming Poisson statistics suggest a difference for all three stations, but this is due to differences of 5-10 counts between the reference and the station distributions, usually in one bin with 21 counts or less. Compared to the number of counts in the peak bins, which range from 84 at Siple to 177 at Sondre Stromfjord, 5-10 is a small number. Each bin is 2 nT wide.

Nevertheless, if there is a significant difference in the B_z distributions for Pc1/2 vs the IMP8 B_z values, it would be useful to calculate the peak centroids to quantify any

preference for positive or negative B_z during Pc1/2. The centroids were calculated for each peak as:

$$B_{z\text{peak}} = P = \frac{\sum X_i N_i}{\sum N_i}$$

where X_i is the center value of the B_z bin, N_i is the quantity in the bin and the sum runs over all bins that contain at least 15% of the peak bin quantity. The uncertainty in the peak value was calculated following Bevington (1969):

$$\text{For } P = \frac{\sum XN}{\sum N}, \quad \sigma_p^2 = \left(\frac{\sigma_{\sum XN}^2}{(\sum XN)^2} + \frac{\sigma_{\sum N}^2}{(\sum N)^2} \right) \left(\frac{\sum XN}{\sum N} \right)^2$$

where

$$\sigma_{\sum XN}^2 = \sum \sigma_{N_i}^2 \left\{ \frac{\partial \sum XN}{\partial N_i} \right\}^2 + \sigma_{X_i}^2 \left\{ \frac{\partial \sum XN}{\partial X_i} \right\}^2 = N_1 X_1^2 + N_1^2 + \dots$$

and

$$\sigma_{\sum N}^2 = \sum \sigma_{N_i}^2 \left\{ \frac{\partial \sum N}{\partial N_i} \right\}^2 = N_1 + N_2 + \dots$$

The IMF B_z peak positions for the three stations are : Siple 0.9 ± 0.5 nT; Sondre Stromfjord 0.4 ± 0.5 nT; and South Pole 0.9 ± 0.6 nT.

The 1986 IMP8 IMF B_z peak using this method is 0.5 ± 0.5 nT. This centroid value was calculated from a distribution with bins that are 2 nT wide. To check the quality of this centroid value, the average of all IMP8 hourly-averaged B_z values was calculated from the IMP8 database. Based on 3618 measurements, the mean B_z value from 1986 was 0.3 nT, which agrees with the centroid calculation.

All of the Pc1/2 centroids are within one standard deviation of each other and the 1986 IMF B_z reference. Evidently, the differences detected by the chi-square test are not collectively arranged to create a preference for positive or negative B_z during Pc1/2 events, compared to the 1986 B_z distribution.

Since a southward-turning of B_z is associated with enhanced energy input to the magnetosphere, and since this turning precedes the appearance of energetic ions inside the magnetosphere which could amplify Pc1/2, it is necessary to look for B_z values prior to the Pc1/2 occurrence. Such a relation was suggested by Kaye & Kivelson (1979). The process of finding B_z values for Pc1/2 and segments of Pc1/2 was repeated, but B_z for the hour preceding the Pc1/2 hour was taken from the IMP8 database instead. B_z values were also taken for the hour that was two hours before the Pc1/2. The centroids of all three stations' B_z distributions remained consistent with each other. In addition, at any given station, there were no significant changes in the B_z distribution due to the hour offsets.

It may only be necessary for the IMF to turn southward for a short time to supply the energy for the Pc1/2, then it may be northward again. During the longer events, inclusion of B_z values for every hour might explain the lack of association with negative B_z . Consequently, another approach was used, in which B_z was selected for the hour preceding every Pc1/2 that was at least 45 minutes long and began within 10 minutes after the hour.

No evidence of a preference for southward B_z was found in the hour preceding these selected Pc1/2. If there is any trend, it is toward positive B_z instead. Table 7-1 shows the number of Pc1/2 that were preceded by positive or negative hourly-averaged B_z . If they are described by binomial statistics, then the fraction of hours with B_z positive is assumed to be the probability of seeing B_z positive on all other samples. One standard deviation

($\sigma = [n\pi(1-\pi)]^{1/2}$) is the uncertainty in that assumption. The standard deviation is listed for each station in Table 7-1.

Siple and Sondre Stromfjord each have as many positive as negative B_z , within two standard deviations. The opposite is true for South Pole; there is a preference for B_z positive in the hour preceding Pc1/2. This pattern is repeated for all stations for B_z values two hours before Pc1/2.

Also shown in Table 7-1 are the number of Pc1/2 that were preceded by $|B_z| \geq 2$ nT to show how the more extreme B_z values were distributed. Again, if there is a relation, it seems to be toward positive B_z .

Table 7-1. B_z Values in the Hour Preceding Pc1/2 Events

Station	Qty $B_z \geq 0$	Qty $B_z < 0$	Qty $B_z \geq 2$ nT	Qty $B_z < 2$ nT
Siple	14 (± 3)	13 (± 3)	2	5
SP	23 (± 3)	15 (± 3)	12	5
SS	32 (± 4)	28 (± 4)	14	5

The possibility of a seasonal association of Pc1/2 occurrence with the IMF projection in the XY GSM plane was also checked. Figure 7-21 is a scatterplot showing the angles of the hourly-averaged IMF to the X and Y axes for Pc1/2 events at Sondre Stromfjord. The events are from June and December solstice, ± 45 days each. There is no clear seasonal pattern. The Parker Spiral can be seen in this figure, since the IMF during most of the Pc1/2 events points westward and Sunward or eastward and Earthward.

IMF Relation to Pc1/2: Discussion

No direct association of Pc1/2 occurrence with the IMF has been found. The B_z component during and at fixed offsets prior to the Pc1/2 shows no preference for negative values. This is consistent with Troitskaya, et al., (1980) found "no clear relationship" between B_z and Pc1/2 observations, although they did not discuss this point in any detail. The lack of a southward IMF just before, or during Pc1/2 indicates that the ions that enter the magnetosphere through reconnection do not immediately amplify the Pc1/2.

The solar wind ions that enter the magnetosphere may amplify the Pc1/2 after convecting sunward from the tail, however. A complication for this study is that convection times for ions to go from the plasma sheet to the postnoon sector might be irregular because the enhancements in the electric field occur when the IMF turns south. In fact, sudden enhancements and decreases in the convection electric field can create plasma "clouds", whose sunward drift from the plasma sheet is affected by later enhancements of the electric field (DeForest & McIlwain, 1971). If the irregularities in drift times are more than one hour, the technique of looking a fixed number of hours before an event may not reveal the southward IMF connection to the Pc1/2. The association of southward B_z two hours before Pc1/2 noted by Kaye & Kivelson (1979) may be a coincidence due to small sample size (11 events).

There is no association of Pc1/2 occurrence with the polarity of the IMF X or Y components either. Apparently IMF Y component does not explain the postnoon occurrence maximum. The lack of X association is consistent with the B_z case, since the negative sense for both is connected to higher levels of activity within the magnetosphere (Rostoker, 1968; Schatten & Wilcox, 1967). Since the energy in the magnetosphere comes primarily from the solar wind, the solar wind is ultimately the energy source for

Pc1/2. However, the link is not prompt, and the Pc1/2 do not seem directly related to either pressure or IMF orientation.

Possible Association of Pc1/2 with Magnetospheric Sources

The possibility that the Pc1/2 may have a source inside the magnetosphere that is associated with substorms was tested by selecting Dst, AE and Kp values during the Pc1/2. Substorms are an energy source for Pc1 because the energetic ions injected into the ring current may lose their energy in part via the ion-cyclotron instability (Bossen & McPherron 1976, Kozyra 1984,). The production of Pc1 by this process occurs during the recovery phase of a storm, which can be observed 2-5 days after the main phase, depending on the latitude of the station (Kuwashima et al., 1981; see also Mullen & Heacock 1972, Heacock & Kivenin 1972, Heacock & Akasofu 1973).

The Dst, AE and Kp indexes are designed to provide an indication of substorm activity. All three are simply measurements of the magnetic field at the surface of the Earth. However, the location and time resolution of the measurement are chosen in order to follow variations in certain current systems. Inevitably, other current systems will be present as well, and will somewhat degrade the fidelity to the system of interest, so the various indices are not exact measurements. Dst is a measure of the ring current, AE describes the auroral electrojet intensity and Kp provides a planetary-scale estimate of extremes in magnetic disturbances. Each of these will be further described below..

Dst During Pc1/2

The ring current builds after a series of substorms inject energetic ions into drift paths that encircle the Earth. The magnetic moment of these trapped charged particles is opposite to that of the Earth. The ring current field reduces the net field tangent to the Earth's surface near the equator, often by 30-40 nT. This is illustrated in Figure 7-24 by the December solstice ± 45 day Dst distribution. Storms, composed of many energetic substorms and repeated particle injections, can reduce the field by up to 300 nT or more (see Dst February 9, 1986), or 1% of the steady field at the Earth's equator (Kelley, 1989).

The Dst index, "Disturbance Amplitude, storm-time", is an index intended to measure the ring current magnitude. It is an hourly average of the *disturbance* in the horizontal component of the Earth's magnetic field (not the magnitude of the component itself), as measured at four stations near the equator. The stations are not located at the equator in order to avoid the E-region equatorial electrojet (Kelley, 1989).

Although storms can cause dramatic reductions in the magnetic field at the Earth's surface, an estimate of typical storm levels was made by surveying Dst values on the most "disturbed days" of May, June and July 1986 (see the "Geomagnetic and Solar Data" listing in the *Journal of Geophysical Research*). The mean hourly Dst value over disturbed days from all three months was -29 nT, with daily averages ranging from -10 to -78 nT. The same average over the quietest days was -7 nT. The figure of -29 nT is simply an estimate of a disturbed level of Dst; the storm threshold of Dst is not well defined.

Compressions of the magnetosphere can produce an effect opposite to that of the ring current. This magnetic field change is a consequence of increased currents at the magnetopause due to increased solar wind dynamic pressure. Their fields add to the magnetic field of the Earth (Nishida, 1982). A compressional change is typically 20 nT or

less (Figure 7-24). Since storms and compressions affect the Dst measurement in opposite ways, there is no way to tell from the Dst index alone which one is changing.

Figure 7-23 illustrates the 1986 Dst and solar wind pressures for those hours during which both were available. The effect of pressure on the Dst index is apparent at Dst values near and greater than zero. Increasing pressure and increasingly positive Dst are associated. At negative values of Dst, however, the effect of pressure vanishes; a range of pressures can occur for any negative Dst value.

A scatterplot of Dst and pressure during Sondre Stromfjord Pc1/2 is shown in the same figure, and it is clear that a range of solar wind pressures of $2-5 \times 10^{-8}$ dyn/cm² exists for all Dst values less than zero. The extent of negative Dst values for Sondre Stromfjord is limited to approximately -40 nT for the bulk of the Pc1/2, while the 1986 Dst distribution extends to approximately -85 nT.

Using the 45 minute criteria, Dst values were selected for each hour of Pc1/2. These hourly Dst values are plotted for each station in Figure 7-24, for Pc1/2 during the June and December solstice (± 45 days). Also plotted in that figure are all Dst values for the same time periods, as a reference. Dst during December solstice Pc1/2 have a distribution similar to the seasonal reference. On the other hand, Dst during June solstice Pc1/2 are in fact skewed to more positive values (Figure 7-24). In neither season is there a preference for large-magnitude negative values during Pc1/2 events.

If the Dst values are averaged over the Pc1/2 events, instead of plotting Dst for each hour of a Pc1/2 separately, the same trend appears. Some of the differences between the South Pole December solstice distributions and the seasonal reference are less distinct as a result of averaging.

Kaye & Kivelson (1979) found no Dst relation to the occurrence of Pc1/2, although their sample size was small (11 events). In this study, the trend for Pc1/2 to occur during quiet-time Dst suggests that the ring current is not usually very intense at the time. Enhanced solar wind pressure could give the same Dst pattern, but this is not a likely explanation because there is no evidence of enhanced pressure during Pc1/2

Possibility of Pc1/2 Occurrence during the Recovery Phase of Storms

Quiet-time values of Dst during Pc1/2 could also suggest that Pc1/2 are produced during the recovery phase of a storm. This is an accepted mechanism for Pc1 production, in which the energetic ions of the ring current provide the energy for wave amplification (Heacock, 1974; Roth & Orr, 1975; Kuwashima, 1981). The wave growth then maximizes near the contact surface between the plasmasphere and the ring current as the plasmasphere expands after a storm. As the plasmasphere expands, the wave growth will then be observed on increasingly higher latitude field lines on the ground. Kuwashima (1981) shows delays of approximately 2 and 5 days for Pc1 detected at about 30° and 70° magnetic latitude, respectively.

Dst values up to 7.5 days before Pc1/2 event hours were selected in a search for storm activity before the Pc1/2 at Sondre Stromfjord (74.1°). The June solstice events were used for this study because they are the most different from their seasonal reference toward quiet time values. If Pc1/2 tended to occur in the recovery phase of storms, the Dst values at some time prior to the Pc1/2 should be at storm levels. In fact, Dst at that time could be skewed enough toward storm levels to be significantly different from some standard reference. The reference used here was the seasonal Dst distribution, because it has values ranging from quiet to storm levels. In addition, if a Dst distribution is similar to the seasonal reference, it is consistent with a random selection from the reference.

It is possible to estimate what will happen if one looks at Dst values from very far before a Pc1/2 event. If the Dst are selected from far enough before, perhaps even before the storms that may produce the event, those Dst values will have no physical relation to the Pc1/2. One can guess what those Dst values be. The most likely would be the value most likely to occur in that season. This means that the distribution of Dst from very far before the Pc1/2 should be similar to the seasonal Dst distribution.

The Dst at the time of the Pc1/2, as well as those in the hours before, were selected. At each time before the Pc1/2, the distribution of Dst values were compared to the June solstice Dst reference. The similarity was characterized by the chi-square statistic. Small values of chi-square indicate close similarity, and this means there is no association of Pc1/2 with storm time Dst, since most Dst values during the June solstice were not at storm levels (estimated above at approximately -30 nT or less).

Large chi-square values indicate significant differences between the distributions. This happens at 0, 8 and 40 hours before the Pc1/2, because the Dst values at those times were even more positive than those of the June solstice (see the previous figure). The 99% confidence level in Figure 7-25 occurs at a chi-square value so large that the two distributions are significantly different. The "confidence" is in the rejection of the null hypothesis that the two distributions are randomly drawn from the same parent. Except for 136 hours before, there were no large chi-square values due to *storm levels* of Dst prior to Pc1/2. However, even at 136 hours before (see Figure 7-25), there is no convincing evidence that Pc1/2 were systematically preceded by storm-time Dst levels. This means most Pc1/2 do not appear in the recovery phase of storms.

In addition, it is often the case that Pc1/2 are produced during long periods without storm activity. For example, from May 18 to June 26, 1986, there were no Dst values less than -34 nT, yet Pc1/2 were observed.

AE During Pc1/2

The AE index was also examined for an association with Pc1/2 occurrence. This index is intended to monitor the auroral electrojet, a current system that intensifies in the westward direction during a substorm. Kamide et al., (1982) diagram the equivalent ionospheric current systems for different values of AE.

AE comes from a measurement of the horizontal component of the magnetic field by 12 stations located in the auroral zone between 63.0° and 71.2° magnetic latitude (Kamei, 1990), in the northern hemisphere. It was introduced by Davis and Sugiura (1966).

When two axes of measurement (X,Y) are used in the plane that is tangent to the Earth's surface at the station (Hess, 1965), the horizontal component (H) is their magnitude ($H = \sqrt{X^2 + Y^2}$).

The index is compiled every month by first calculating a "quiet" baseline for each station. This is done by averaging the station's data from the five "international quietest days" of that month. Johnston (1943 as referenced by Mayaud, 1980) discussed the selection process for these days. The quiet base value is then subtracted from each minute's data. All the stations are compared for each minute, and the largest and smallest values are identified as AU and AL, respectively. The AU index is an indication of the largest current intensity of the eastward auroral electrojet (Kamei, 1990), not the total electrojet current (Akasofu, 1983, Kamide,1982). The AL index describes the maximum westward electrojet intensity. Another index, AO, is the average of AU and AL ($AO = (AU + AL)/2$). The AE index is defined as the difference ($AE = AU - AL$). Since AU is generally greater than zero, and AL is generally less, AE becomes the sum of their magnitudes and is an estimate of overall electrojet activity (Kamei, 1990). Hourly-

averaged values of AE for January-June 1986 from WDC C-2 (Kamei, 1990) were used for this study.

A reference for what might be considered a quiet level of AE is provided by the average hourly AE value from the five international quietest days of each month. For January-June, 1986 the average hourly AE values for the quietest days are: 46, 61, 52, 77, 88, and 106 nT (WDC C2 Data Book #19, 1990). The mean of all five is 72 ± 23 nT. For comparison, in distributions of AE during Pc1/2, the bin that typically has the most counts is 50-100 nT.

During relatively quiet times between substorms, the auroral oval contracts poleward (Akasofu 1973, Lui 1976), beyond many of the AE stations (Akasofu, 1983). The consequence is that some substorm activity may take place without detection by the AE network. To quantify the effect this would have on the standard AE index, Akasofu (1983) and Kamide (1982) compiled an AE index from a 71-station network and compared it to the standard 12 station index. The 71 stations were spread over a broader latitudinal range, up to 86° geomagnetic. The 71 and 12 station AE indexes had a high correlation (0.93 correlation coefficient), but the 12 station AE value was generally lower than the 71 station AE by approximately 100 nT (Kamide et al., 1982). The high correlation and the constant 100 nT offset suggest that both versions are equally reliable above a threshold of the weakest or most poleward electrojet activity.

Heacock (1974) found a "moderate" correlation (cross-correlation coefficient of approximately 0.45) between AE and Pc1/2 occurrence. This was attributed to the approach of subcleft lines to the station as the cleft moved equatorward with increasing AE. The possibility of 'detached' plasma regions (Barfield & McPherron 1972) that could enhance the growth rate of Pc1/2 beyond the plasmopause was also raised. However, Heacock pointed out that the distribution of such regions (Chappell, 1974) is

not consistent with the narrow diurnal peak of the Pc1/2. Kaye & Kivelson (1979) found no relation between AE and the occurrence of their Pc1/2 events.

The AE values during June solstice Pc1/2 hours were selected according to the 45 minute criteria and are plotted in Figure 7-26. Since the AE index can increase substantially in one hour (for example, 508 nT on 3/21/86), the hourly values were treated as separate counts to expose high, substorm values.

Note in Figure 7-26 that South Pole and Siple show excesses at or below 100 nT compared to the June solstice pattern, although their overall distributions are not significantly different. The same is true for South Pole, compared to the December solstice AE distribution. In both seasons, Sondre Stromfjord AE values were well-matched to the seasonal reference. The December solstice comparison did not include Siple because no data were available there until Feb 12, 1986. Actually, neither solstice data set had 90 days of data because AE was only available for January-June 1986.

In this study, no significant difference was found between the AE distribution for Pc1/2 events and the respective seasonal AE distribution. The probability of exceeding chi-square was never less than 2%, which is not low enough to be significant. Any departures from the seasonal models were toward lower AE values, particularly 100 nT or less. Pc1/2 do occur during substorm AE levels, but no more often than is consistent with a random selection from the seasonal AE distribution.

The AE distributions illustrate the need for caution when using statistical tests on micropulsation data. A very conservative statistical significance was required due to physical reasoning. Waves observed by stations at the same magnetic latitude should behave the same way, unless there are differences due to solar exposure, dipole tilt, or some other reason. Positive statistical results should be required for both stations if they are to be believed. The following is an example where a statistical relation appears to be

significant for one station, but not at the other. It sets a conservative standard for the level of significance that should generally be required

The South Pole December solstice AE distribution showed the most difference from the seasonal model for any station for any season. There was a 2% chance of exceeding χ^2 . However, in the opposite season there is an approximately 90% chance of exceeding χ^2 for South Pole. This could be interpreted as a real seasonal phenomenon, except that it doesn't occur at the nearly conjugate station. Sondre Stromfjord AE distributions are both similar to their seasonal references. This is true even though the shape of the AE distribution for the December solstice is different from that of the June solstice, in that the December reference peaks in the 0-50 nT bin.

This difference probably cannot be attributed to the fact that AE is calculated only from Northern hemisphere stations (McLennan, et al., 1991), and that ionospheric conductivities change seasonally (de la Beaujardiere, 1991), because South Pole Pc1/2 AE values show an excess in the lowest bin in both seasons. The result is that the 2% confidence level for the South Pole Pc1/2 AE distribution is insufficient to conclude that it is different from the December solstice reference.

Substorms identified by AE may provide energy to ULF waves through energetic ions injected from the plasma sheet into the magnetosphere. These ions will drift sunward due to the enhanced convection electric field associated with the substorm (DeForest & McIlwain, 1971). The drift paths will depend on energy, charge and pitch angle of the ions. Some of these ions will be on trapped orbits when the substorm ends, and others will drift toward the sunward magnetopause on 'open' paths. The trapped ions add to the ring current and may amplify Pc1 or be lost via charge exchange (the dominant loss mechanism; see Nishida, 1978). The open drift times may last from approximately one to perhaps twenty hours before the particle is lost at the magnetopause, depending on the

initial energy and pitch angle (Ejiri 1978; Ejiri et al., 1980; McIlwain 1972 ; DeForest & McIlwain, 1971).

Hence, it is reasonable to look at AE values prior to the Pc1/2 event for indications of substorms. The AE values for 1-51 hours before each Pc1/2 segment were selected, and distributions were formed for each hourly offset. These distributions were compared to the respective seasonal AE distribution with a χ^2 test, and the value of chi-square was plotted vs. offset before the Pc1/2 segments. AE values about 16 hours before the Pc1/2 segments were distributed differently from the December seasonal reference. However, the reason was an excess of Pc1/2 segments during AE in the 0-50 nT range, compared to the number one would expect from the December reference. For either season, it was generally true that differences detected by the chi-square test were due to excesses in the number of Pc1/2 hours during AE values of 150 nT or less.

AE of 150 nT represents a relatively quiet level and also indicates that the auroral zone has retreated poleward (Akasofu 1973, Lui 1976). Possibly the convection electric field during these low AE values is appropriate for convection of ions that can resonate with Pc1/2. Otherwise there is no clear relation of substorm activity to the production of Pc1/2 as there is for Pc1, since Pc1/2 may be produced during a variety of AE values, with no preference relative to the seasonal AE pattern.

The method of selecting AE values the same number of hours before each event is a good first step because Pc1/2 amplification by ion-cyclotron resonance requires ions of similar energy and pitch angle distributions every time. However, if the Pc1/2 are amplified by substorm-injected ions, there may be a range of delay times between the substorm and the beginning of the Pc1/2. The time it takes for the ions to drift sunward into the postnoon sector depends on the convection electric field, which may increase and decrease

irregularly, depending on the level of solar wind-magnetosphere coupling; and the ion pitch angles and energies.

Other complications are ignored by this method. For example, the substorms might not last the same time as the events they may ultimately produce. That could hide a substorm-Pc1/2 relation from the method used here, because a range of AE values, from substorm to quiet time, could occur over the timespan of one event.

The fact that Pc1/2 can occur in the absence of substorms demonstrates the importance of ion convection during magnetically quiet times. The ions may be injected from the plasma sheet into a sunward drift inside the magnetosphere during substorms. However, some of the convection toward the postnoon sector may take place under quieter conditions (Kamide, 1988).

It might be possible to keep track of the convection electric field using the work of Reiff et al. (1981), who found a correlation of the polar cap potential with IMF parameters in the expression: $V_{sw}B^2\sin^4(\theta/2)$. If it is assumed that most of the ions are injected by substorm, it might be possible to identify the plasma sheet as the source by following the magnitude of the convection electric field between a substorm and the beginning of an event.

The latitude dependence of the Pc1/2 (Figure 7-13) that suggests a source region between the auroral zone and the plasmapause L-shells, plus the lack of a direct energy input in the form of solar wind pressure or IMF orientation (reconnection), all indicate that the waves are amplified within the magnetosphere. Although AE and Dst studies show no direct link between Pc1/2 and magnetospheric ion convection, the possibility is by no means eliminated.

Kp During Pc1/2

A third indication of magnetic activity is the Kp index. This is a planetary-scale index that is sensitive to auroral zone electrojets, field-aligned currents and the ring current (Kelley, 1989) because it is calculated from mid-latitude stations. There are 13 stations between 46°-63° north and south geomagnetic latitude. Eleven of those are in the northern hemisphere (Monthly Summary of Geomagnetic Activity, Jan., 1986).

Kp comes from a compilation of K indices at each station. The K value at a given station is the largest excursion in the H component from maximum to minimum amplitude during a three hour period (Mayaud 1980, Rostoker 1972, Kelley, 1989), after first eliminating the S_R daily variation. S_R magnetic variations are due to tidal motions of neutral wind that produce currents by $\mathbf{v} \times \mathbf{B}$ dynamo action in the dayside ionosphere (Nishida, 1978). These current systems are stably localized with respect to the Sun (Mayaud 1980) and produce a regular magnetic variation best observed in quiet times. Rostoker (1972) describes the method used to remove their contribution.

The K range at each station has nine steps. The excursion at the ninth step is chosen to be 100 times as much as for the zeroth step (Rostoker, 1972). Since the activity varies with latitude, a K step at one latitude can be different range in nanoTesla than the same K step at another latitude (Mayaud 1980). Moreover, the K steps themselves are not uniform at a given station. Mayaud (1980) points out that the K steps are ordinal, and they could be represented equally well by non-numerical characters. The K indices are converted to Ks, a process that removes seasonal and diurnal variations, and divides each K step into three parts (Rostoker 1972, Mayaud 1980). The Ks indices from all stations are then averaged to give the Kp index for the three hour period.

Some characteristics of Kp are worth noting. The fact that Kp is a measure of the most extreme variation in the H component in a three hour period means that three hours of

great activity can be equivalent to a single large variation during the period. This makes it difficult to estimate the timescale of the K_p index for purposes of comparison to $Pc1/2$ events. Also, the K_p index has limited sensitivity to substorms above the auroral zone (Rostoker 1972). When K_p does increase, it may be due to increased auroral electrojet magnitude, or to the approach of the electrojet as the auroral oval expands equatorward during the substorm (Akasofu & Chapman, 1963).

An association of K_p and the occurrence of $Pc1/2$ was noted by OV Bolshakova et al. (1980). The K_p values at the time of the events were the lowest for $Pc1/2$ at the highest latitude stations, and vice versa. They concluded that the $Pc1/2$ were produced in the magnetosheath on field lines crossing the sheath and the dayside cusp. The K_p relation was consistent with the idea that equatorward movement of the auroral oval during magnetic activity would bring the $Pc1/2$ source closer to the low-latitude stations. They expected no conjugate events because these field lines are not conjugate to both hemispheres.

The K_p distributions for the $Pc1/2$ used in these associative studies are similar for all three stations. K_p values for the start times of the $Pc1/2$ that satisfy the 45 minute criteria are plotted in Figure 7-27a. Only one value of K_p was selected for each event, regardless of event length. The distributions are the same for all three stations, with approximately 40% chance of exceeding chi-square.

If *all* $Pc1/2$ are used for K_p selection, however, including those <45 minutes long, the inverse K_p vs. latitude relation reported by Bolshakova (1980) seems to be reproduced here (Figure 7-27b). There are more $Pc1/2$ during active times ($K_p > 2$), and fewer during quiet times, at Siple than at the high latitude stations. A comparison of either high latitude station to Siple results in a difference so great that there is less than a 0.5% chance of exceeding chi-square. This development is mostly due to changes in the K_p distribution

at Siple, the low-latitude station, after the length criterion is applied. This suggests that event length is an important part of such a relation, not the polar cusp latitude.

Although Bolshakova et al. (1980) anticipated no conjugacy for Pc1/2, this study shows that up to 18% of Pc1/2 at South Pole and Sondre Stromfjord are seen in any month at both simultaneously (see Figure 7-11*b*). Of course, if the Pc1/2 source is near the cusp, this could be simply due to ion-cyclotron interactions in the magnetosheath, near both cusps simultaneously. The longest common-station event was seen near an equinox (3/30/86) at all three for 10 hours and 20 minutes, so this might be possible. However, the post-noon occurrence peak, without a B_y dependence, makes a cusp source unlikely. This suggests the source is on closed field lines, and that simultaneous observations in both hemispheres are of waves from one source region.

DMSP F7 Coincident Measurements of the Auroral Oval

To examine the possibility that the cusp/cleft region moves equatorward when a lower latitude station observes Pc1/2, DMSP data for selected events was reviewed. This provided an identification of the plasma mantle and low-latitude boundary layer latitudinal boundaries.

The DMSP F7 satellite was in a sun-synchronous orbit (1030-2230 MLT plane) with an orbital inclination of 98.3° (Brautigam et al., 1991). Electrons and ions from 32 eV to 30 keV are measured by electrostatic analyzers in the SSJ/4 package on the spacecraft (Newell & Meng, 1989). The orbit is nearly circular; always within 15 km of 835 km (Newell et al., 1991).

On each orbit, the cusp, cleft, low latitude boundary layer, plasma sheet boundary layer and central plasma sheet have been identified with a neural network. The identification is

estimated to be most reliable near noon and midnight (Newell 1990 , and 1991). Distinctions between the cusp and cleft are described in Newell & Meng (1989). The mantle features are described in Newell et al. (1991). All these identifications are available in a public database, which is accessible via SPAN, as described in Newell et al. (1991). Information with each identification includes: average energy flux ($\text{ergs/cm}^2\text{s}$), averaged over an assumed π radians (online help file), average ion and electron energies (all averaged over the time spent in a region), magnetic local times of the detections of each region and magnetic latitudes of the region boundaries.

The best cusp-observing times for DMSP F7 were 10-14 UT (Newell, p.c., 1991). DMSP overflights of Sondre Stromfjord were the most likely of all three stations; mostly near 1000 MLT. Table 7-2 presents selected Pc1/2 events for which DMSP coincident measurements were available and the average energies for the LLBL agreed with Newell & Meng's (1989) definition. Pc1/2 events that began before 1400 UT and lasted more than three hours were chosen for possible DMSP conjugate measurements. Note that six out of the 10 turned out to be on international quiet days, and one on an international disturbed day. This is an example of the variety of conditions in which Pc1/2 may occur. All three events with LLBL measurements put Sondre Stromfjord (gm lat 74.1°) below the equatorward edge of the LLBL, well below the cleft.

Table 7-2 DMSP F7 Measurements During Pc1/2 Events

Date	SS (UT)	SP (UT)	Siple (UT)	LLBL Eq Edge (deg)	Mantle Eq-Edge (deg)	"Plasma Sheet BL" Eq-Edge	Approx UT (±1min)	DMSP MLT (hours)	SS MLT (hours)	SP MLT (hours)
3/20	0955- 2130	0950- 1900	1005- 1930	79.1	79.6	76.9	1045	10.0	9.2	
7/15	0750- 2120	0915- 1825	1005- 1400		81.2	79.1	1134	9.6	10.0	
9/22	1220- 2235	1250- 2230	1250- 2235		80.6	77.8	1145	9.9	10.2	
10/7	1015- 1530	1025- 1515	1015- 1510		79.0	77.2	1142	10.1	10.2	
10/8	0945- 1900	1605- 2055	1635- 2105		78.7	75.7	1122	10.2	9.8	
4/12	1050- 2200		p1645- 2245		-79.0		1036	8.8		7.1
					79.3	74.9	1123	10.0	9.8	
5/5	1105- 1800				76.7	75.3	1200	9.8	10.5	
6/27	1320- 1610			-75.8			1331	11.7		10.0
10/30	1140- 1710	p1250- 1410		75.8	77.1	74.5	1218	10.2	10.8	

11/21	1120-	p1215-	79.4	77.3	1136	10.3	10.1
	1515	1440					

A comparison of some cases in Table 7-2 shows that the Pc1/2 source may not be associated with the cusp/cleft position. The first case was on a disturbed day (6/27/86), where K_p was 5+ and 5- during the event. The LLBL location is from a southern hemisphere measurement, so this case has no reliable northern hemisphere LLBL position. Also, there is a 1.7 hour difference between the DMSP and South Pole longitudes. However, it is not surprising that the auroral zone was at a low latitude (-75.8°) on a disturbed day. The Pc1/2 event was not seen at either southern hemisphere station, despite the relatively low latitude of the auroral oval in the southern hemisphere. Since this was during local winter for South Pole and Siple, the seasonal blocking mechanism may be in operation.

Another case in Table 7-2 shows a near-equinox event (10/30/86) during a low latitude oval. This was seen at Sondre Stromfjord, possibly at South Pole, but not at Siple. The seasonal mechanism is less likely to be in operation here than in the disturbed case. In addition, the K_p value was 2 \circ for this event, although the LLBL location in the northern hemisphere for this event is the same as in the southern hemisphere before (75.8°). This suggests that K_p is not always a good indicator of the auroral zone location.

In neither of these two cases were the Pc1/2 seen at Siple, even though DMSP indicated a low auroral zone. In the third example from Table 7-2, the Pc1/2 was on 3/20/86, again near an equinox. It was seen at all three stations, but the LLBL equatorward edge was at 79.1° , well above Sondre Stromfjord (74.1°).

Four other events in Table 7-2 have no LLBL determination. However, they do show three-station commonality when the mantle's equatorward edge is within 0.9° of where it was during the 3/20 event, in which the LLBL was well above Sondre Stromfjord at 79.1° . There are not enough cases in Table 7-2 to do a convincing statistical study, but there are enough to doubt a simple link between the latitude of the auroral oval and the observation of Pc1/2 on the ground.

Discussion

The Pc1/2 appear to be amplified within the magnetosphere. South Pole-Siple common observations suggest the region is at L-shells between the plasmopause and the auroral zone. The clear division in the data at approximately 0.4 Hz (Figure 7-1), and the different qualities of waves above and below this frequency suggest that the two populations originate from a different source. Waves above and below 0.4 Hz are distinguished from each other by event length, diurnal and seasonal occurrence. The South Pole-Siple observations suggest that the waves above 0.4 Hz come from plasmopause region L-shells, while the Pc1/2 come from a region between the plasmopause and the boundary layer. If the clear frequency division in the ground data, plus the sharp frequency bounds of the Pc1/2 spectra, are due to the presence of He^+ at the equator, then the region near $L=7$ is favored for Pc1/2 wave growth. A small DMSP study also indicates a source region inside the magnetosphere, since Sondre Stromfjord was placed well below the cleft as determined by the authors of the DMSP F7 database. Additionally, the lack of a direct connection between the occurrence of Pc1/2 and solar wind pressure or IMF orientation suggest that the source of wave amplification is the ion population that convects sunward within the magnetosphere to the afternoon sector.

The postnoon sector of the magnetosphere might be a source for Pc1/2 because ions of suitable pitch angles are there, along with cold He that can affect wave growth in this band. These ions convect into that region from the plasma sheet. Sibeck, et al.(1987) discussed convection patterns in the magnetosphere in the following way. If the magnetospheric field were a dipole, all particles would follow circular paths at constant radial distances from the Earth. However, the magnetopause currents, induced by solar wind flow past the magnetosphere, and cross-tail plasma sheet currents distort the field so that the dayside magnetic field strength is greater than on the nightside at the same radial distance. Particles trapped at the equator follow contours of constant equatorial magnetic field strength to maintain the first adiabatic invariant ($mv_{\perp}^2/2B_0$). This moves them radially outward when drifting from midnight to noon. Particles of lower pitch angles drift around Earth in more nearly circular orbits, and do not follow contours of constant equatorial B. This is drift shell splitting (see also Roederer, 1970). In the dayside magnetosphere, particles at large L with 90° degree pitch angles are more likely to intercept the magnetopause than particles with lower pitch angles. The ions would be lost to the magnetosheath at the postnoon magnetopause, and electrons go out at the prenoon magnetopause.

Ejiri (1978) shows calculated particle trajectories in the equatorial plane. For a given energy in one example, the ions with larger magnetic moments ($mv_{\perp}^2/2B_0$) generally drifted toward the duskside as they convected from the plasma sheet sunward on open drift paths. In another example, ions with 90° pitch angles and large energy (and magnetic moment) generally drifted to the duskside. Even if they start from the same place, the exact paths depend on the energy and pitch angle of the ions (Ejiri, 1978).

Takahashi & Iyemori (1989) simulated particle drifts for $K_p=4$ in the magnetosphere. They showed the convection flow for 30° and 90° pitch angle, 10 keV ions as they drifted from the nightside, at $13 R_E$, sunward past the Earth on the dusk side. The flow of the 90°

(initial) pitch angle particles converged farther from the Earth than the flow of the 30° particles. A simulation of particles with initial pitch angles of 60°, and two energies, 5 and 10 keV, showed a flow convergence of the lower energy particles closer to the Earth than the more energetic particles.

One might conclude that the tendency for ions with large pitch angles to separate outward from those with small pitch angles in the post-noon sector would lead to anisotropic pitch angle distributions, suitable for wavegrowth, at large distances from the Earth.

Moreover, beyond 3 R_E , gradient and curvature drift velocities are higher on the nightside than the dayside. (Roederer, 1970; see also Takahashi & Iyemori, 1989). This would suggest that energetic, large pitch angle ions, ideal for wavegrowth, would spend the most time in the outer afternoon sector.

Roux et al., (1982), using GEOS 1 and 2, found that cold He^+ (<110 eV) is concentrated in the postnoon sector, along with the maximum occurrence of waves below the He^+ gyrofrequency. This cold He^+ may come from the ionosphere, drawn out by the postnoon aurora. Evans (1985), using the TIROS/NOAA satellites, reported a region of persistent energy flux of electrons of less than 3 keV in the 75-80° invariant latitude range, particularly for 14-16 MLT during low magnetic activity.

Anderson et al. (1990) calculated the logarithmic derivatives ($\partial \ln S_m / \partial X$) of the maximum convective growth rate S_m with respect to X : the magnetic field magnitude, hot and cold proton density, hot proton perpendicular temperature and anisotropy ($A = T_{\perp} / T_{\parallel} - 1$). This was done using the expression from Kozyra et al. (1984) for a pure proton plasma. They show that the growth rate is more sensitive to magnetic field magnitude (inversely) and anisotropy than hot or cold plasma density, or even T_{\perp} . This means that equatorial regions and regions far from the Earth are favored as wavegrowth sites. It may be

necessary to include cold He^+ in such a calculation, however, since satellite and this ground-based study indicate that it is clearly present.

The seasonal occurrence pattern of the Pc1/2 may be due to the distortion in the Earth's magnetic field as the rotation axis inclines toward the Sun. An asymmetric pattern of hot proton anisotropy relative to the magnetic equator might develop. This could favor wavegrowth in the summer hemisphere below the He^+ gyrofrequency. The cold He^+ may play a role in blocking the Pc1/2 from the winter hemisphere, either by reflecting or absorbing the Pc1/2, depending on the magnetic field magnitude in the wavegrowth region compared to the region of cold He^+ concentration.

The presence of He^+ in the magnetosphere can block Pc1 from high latitudes and distant parts of the magnetosphere from reaching the ground. This study strongly suggests the role of He^+ by the clear division at 0.4 Hz in the wave data. No previous study has shown this clear division, nor the fact that the strong diurnal pattern is in the waves below this frequency. The waves above this division come from latitudes near the plasmapause, while the Pc1/2 come from further out in the magnetosphere⁺.

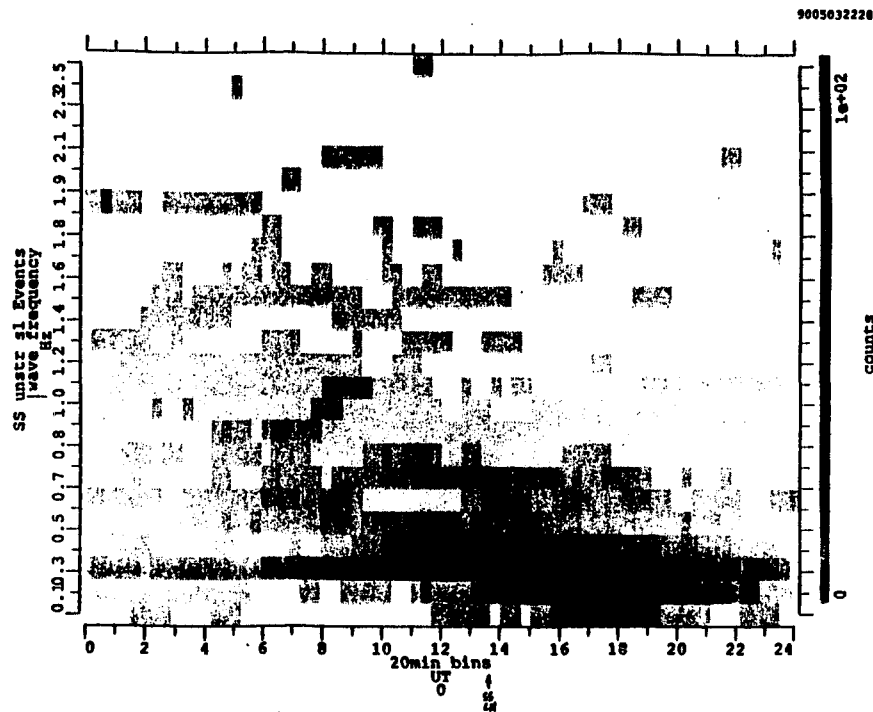
For ground observations, He^+ prevents the use of Pc1 micropulsations as a reliable diagnostic tool for the outer magnetosphere. Pc1/2 waves seem to be the best probe of that region, because of their low frequency compared to the He^+ gyrofrequency. This study shows that as a diagnostic, Pc1/2 waves signal the presence of energetic ions in the afternoon sector, between the plasmapause and the boundary layer. These ions are at least as far away as $L=6$, and may spread over the entire dayside. They have probably drifted sunward from the plasmashet, since no direct solar wind connection to Pc1/2 waves has been found in this large sample study.

Conclusions

1. A natural frequency division at approximately 0.4 Hz exists in the ground data from three high latitude stations. Below this frequency, in the Pc1/2 band, the diurnal distribution, the event length distribution, and seasonal occurrence is considerably different from the Pc1 band above.
2. The Pc1/2 source region is centered in the postnoon sector of the magnetosphere. The diurnal occurrence pattern is not a consequence of sunlight effects on the ionosphere.
3. South Pole (auroral zone) and Siple (plasmopause) observations of Pc1/2 indicate a source region at radial distances between the plasmopause and the auroral zone. They also indicate that the Pc1 observed on the ground, above 0.4 Hz, comes primarily from plasmopause latitudes.
4. He⁺ ions appear to keep waves from the distant dayside magnetosphere from reaching the ground if they were amplified above the local He⁺ gyrofrequency there. Anderson, et al. (1990) found that Pc1 are about four times more common beyond L=7 than for L≤6, and occur primarily in the afternoon. In the outer region, waves above the local He⁺ gyrofrequency are the most common (Anderson, 1989). If He⁺ ions along the magnetic field path to the ground were not blocking these waves, the South Pole-Siple Pc1 (0.4 Hz) observation pattern would be reversed. Pc1 would be seen at South Pole alone more often than at Siple alone, since South Pole is closer to the L=7-9 region than Siple.
5. The characteristic narrow-band spectrum of the Pc1/2 events, with a typical upper frequency of 0.3 - 0.4 Hz, suggests the presence of He⁺ ions at the wavegrowth site. Heavy ion-modulated wavegrowth is also suggested by the persistence of the narrow-band spectrum for up to 17 hours, through changing magnetospheric and solar wind

conditions. Such narrow band resonance in a pure proton plasma with monochromatic waves seems unlikely for such long periods of time, under such changing conditions. If He^+ ions are present, and wavegrowth occurs below the He^+ gyrofrequency, as suggested by Kozyra (1984), the wavegrowth region is at least as far away as $L=6$. This agrees with the simple radial estimate from the South Pole-Siple observations above.

6. There is no direct solar wind connection to Pc1/2 occurrence that may be expressed by hourly averaged values of solar wind parameters. This suggests an energy source inside the magnetosphere. It has been found that Pc1/2 may occur in quiet times, as described by the AE, Kp and Dst indices. This, plus the afternoon sector wavegrowth region, is consistent with sunward-convecting plasma sheet ions as the energy source (as suggested by Kaye & Kivelson, 1979, and Anderson et al., 1990).



Pc1/2 in Local Magnetic Time

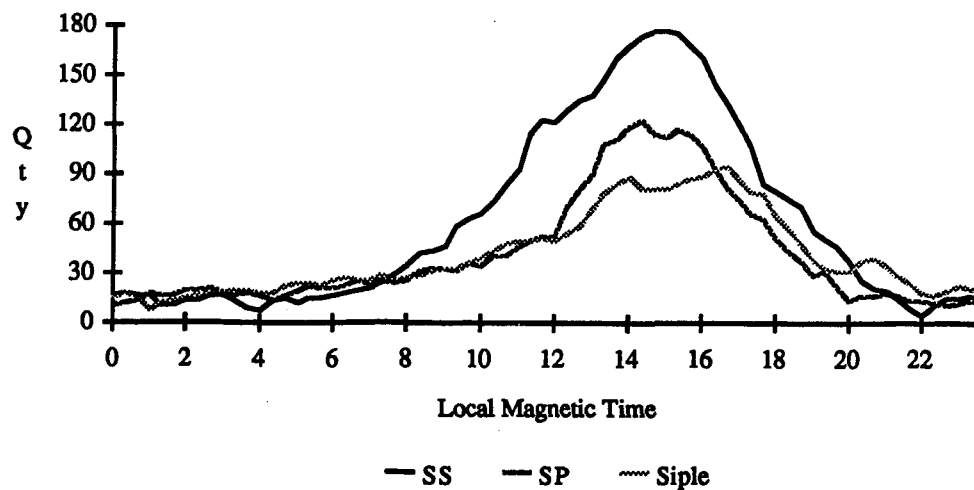


Figure 7-1. (Top) The waves above and below 0.4 Hz display different diurnal patterns. All the events in this survey from Sondre Stromfjord have been superimposed in a wave-frequency vs. time of day plot. The frequency steps are increments of 0.1 Hz. Magnetic noon for Sondre Stromfjord is 1330 UT. Note the post-magnetic noon occurrence peak below 0.4 Hz.

(Bottom) The 0.1-0.4 Hz band (Pc1/2) are plotted in local magnetic time for all three stations in the study. The presence of the diurnal pattern at South Pole, which has no solar day, indicates a magnetospheric afternoon source region. It rules out propagation effects due to sunlight on the ionosphere as the cause of the diurnal pattern.

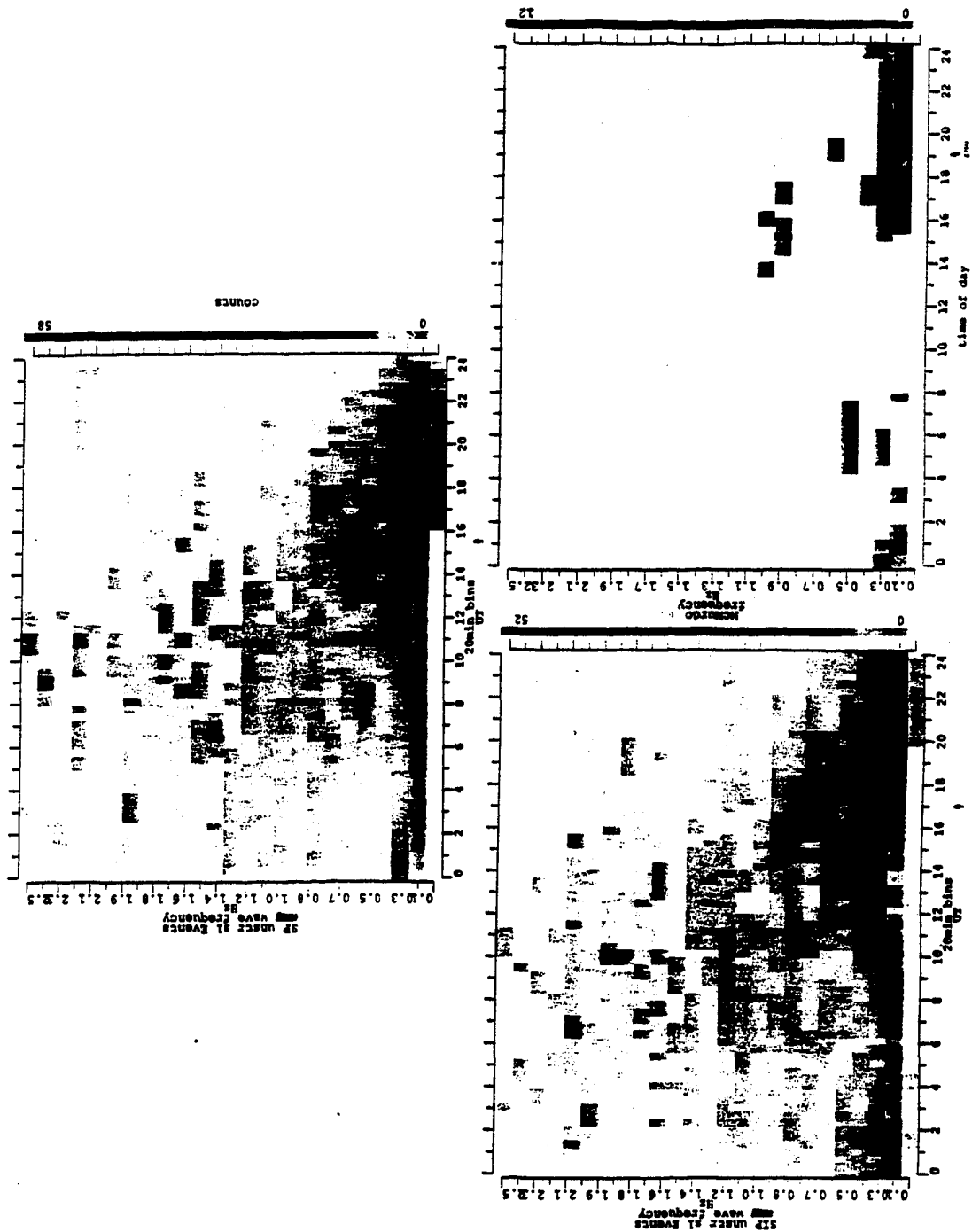


Figure 7-2 (top) The unstructured events at South Pole are displayed by frequency and time of day as in Figure 1a. Note the different maximum grayscale values for each plot. Local magnetic noon at South Pole is 1530 UT.

(left) Siple unstructured events; the 0.1-0.4 Hz band again has a strong postnoon peak. Local magnetic noon is 1700 UT.

(right) McMurdo also displays the diurnal pattern. Local magnetic noon is approximately 1900 UT. McMurdo has a geomagnetic latitude of -80° , well within the polar cap (open field lines).

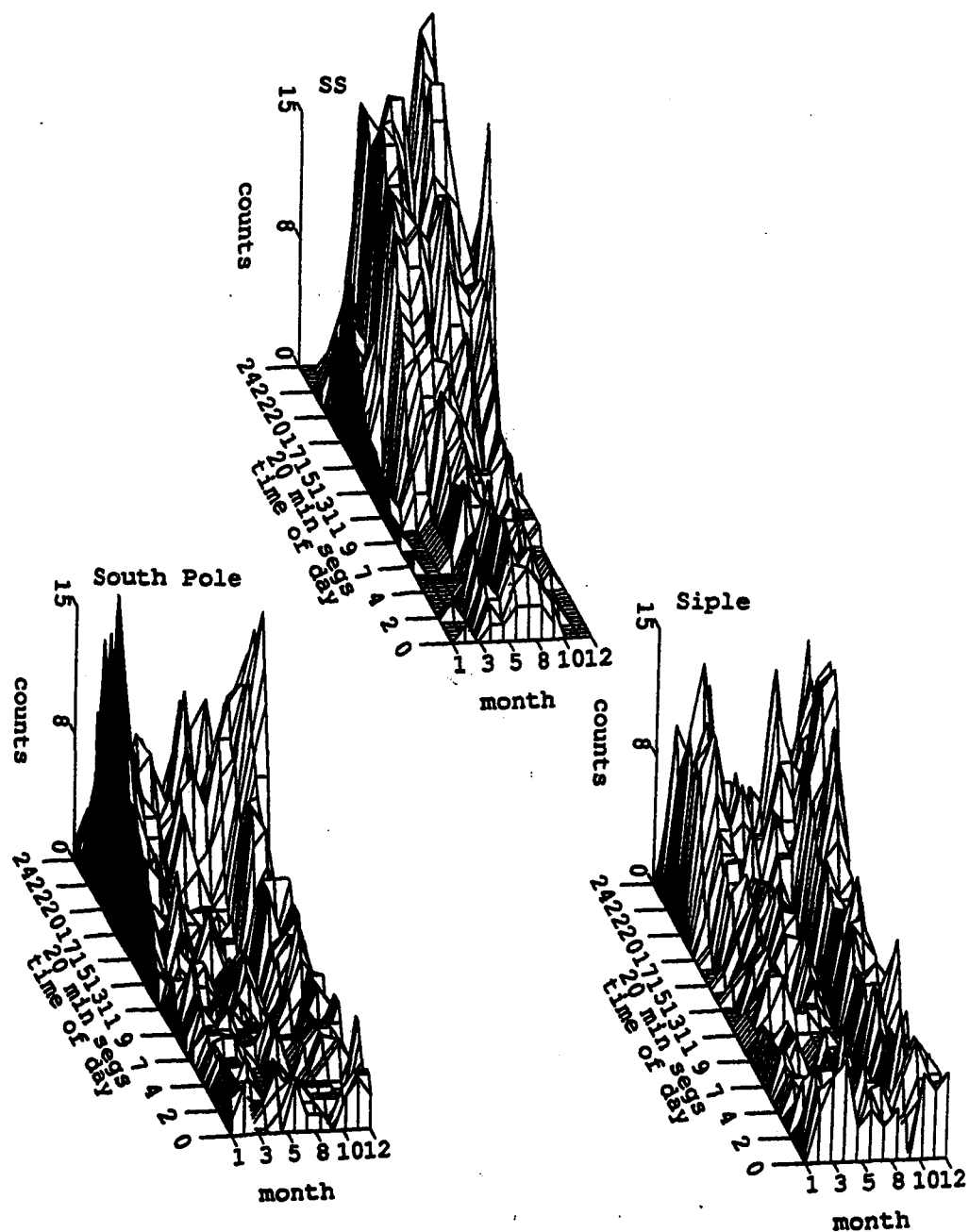
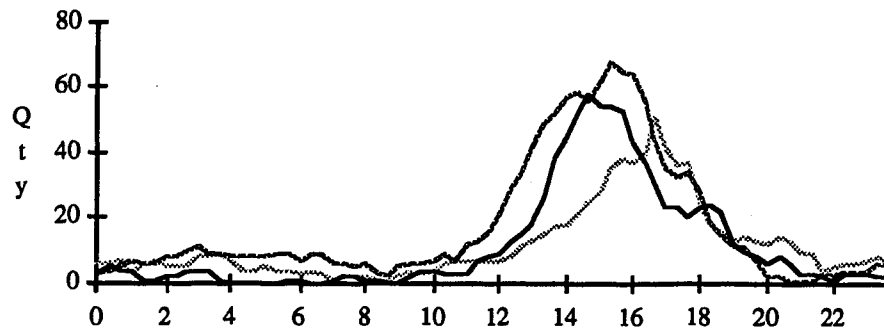


Figure 7-3. (top) The diurnal occurrence of Pc1/2 at Sondre Stromfjord is shown for each month of 1986. The time scale is UT, and local magnetic noon at Sondre Stromfjord is 1330 UT. The post-magnetic noon peak persists throughout the year, but most Pc1/2 appear in local summer.

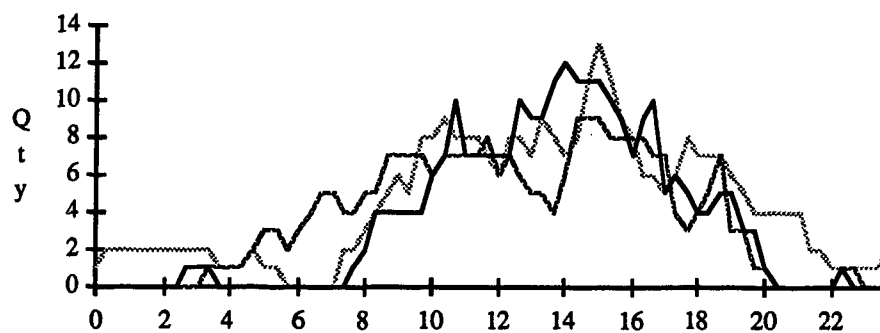
(middle) The South Pole Pc1/2 are shown. Local magnetic noon is 1530 UT, and an afternoon peak appears at this station with no solar day.

(bottom) Siple Pc1/2 also have a peak occurrence in the afternoon. Local magnetic noon is 1700 UT. No data were available at Siple until after 2/12/86.

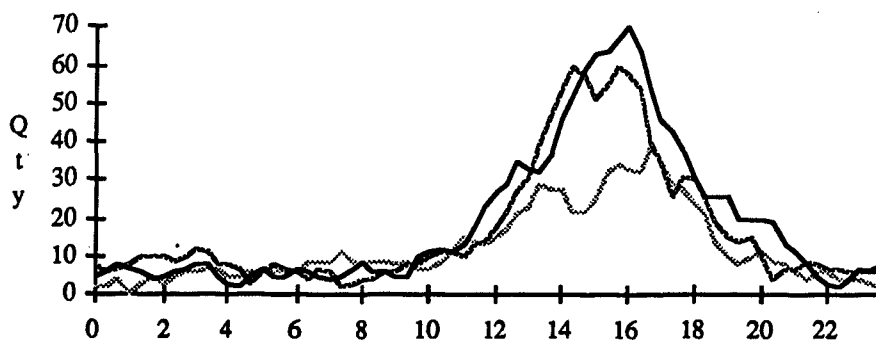
Pc2 Events in Local Magnetic Time



Pc1/2 "Some Str" Events in Local Magnetic Time



Narrow-Band (0.1 Hz) Pc1/2 in Local Magnetic Time



Local Magnetic Time (bin 1.1. shown)

..... Siple - - - SP — SS

Figure 7-4. a) (top) Unstructured Pc2 diurnal occurrence at all three stations, in local magnetic time. The horizontal axis is divided into 20 minute segments, and the vertical axis is the number of times Pc2 were seen during 1986 at any given time. Their peaks have narrower local time spans than Pc1/2 overall. *b) (middle)* Diurnal pattern of events in the Pc1/2 band that have some structured elements as a minor part of the event. These occur somewhat more in noon and prenoon hours than the Pc1/2 band as a whole. *c) (bottom)* Diurnal pattern of the narrow-band (0.1 Hz wide) subset of the Pc1/2 band. Their afternoon spread is less than for Pc1/2 overall.

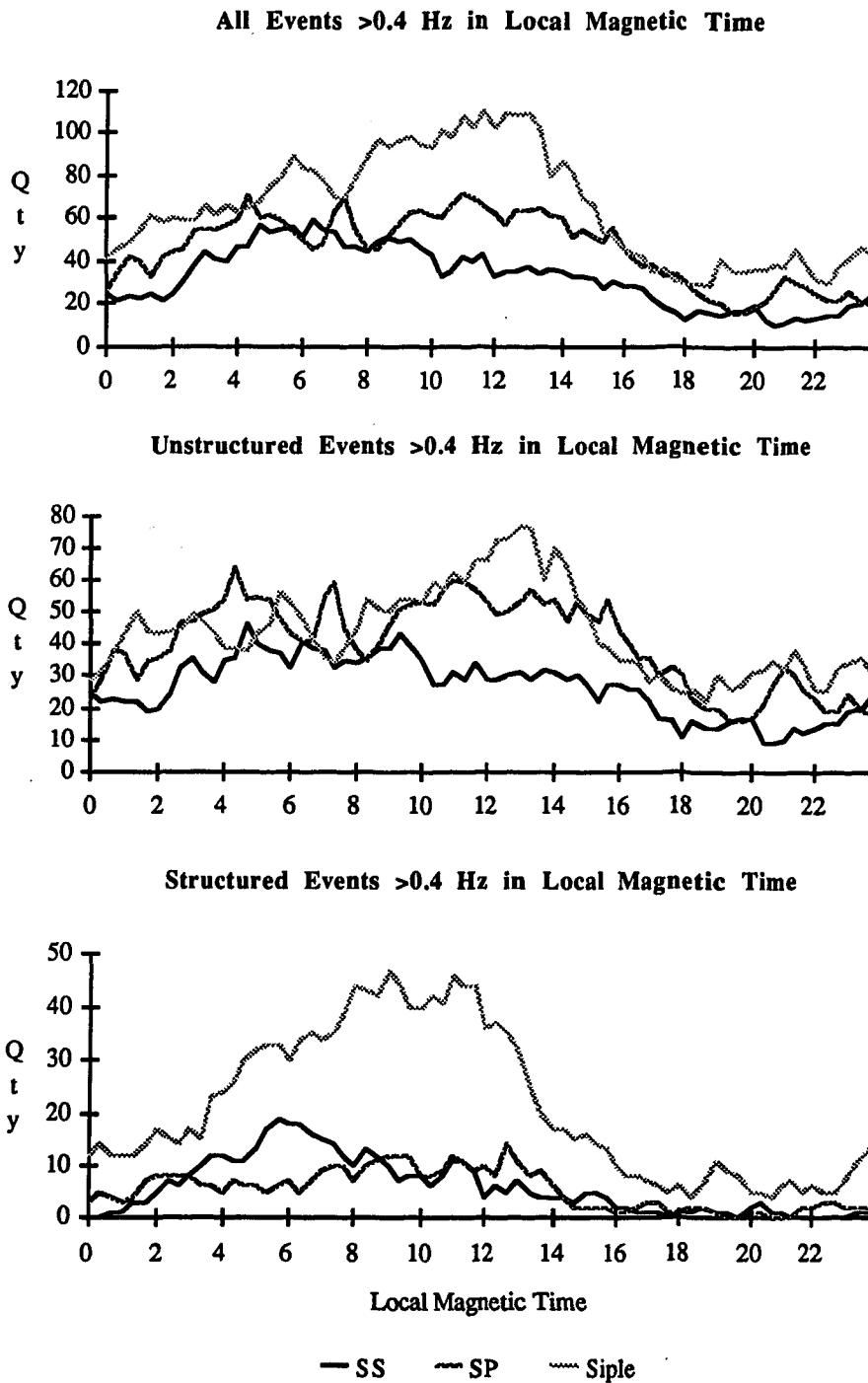


Figure 7-5. a) (top) All events above 0.4 Hz, structured or not, are presented in local magnetic time as in Figure 4. The diurnal pattern is quite different from that of the Pc1/2 band
b) (middle) The diurnal pattern of unstructured events shows a noon and prenoon peak occurrence.
c) (bottom) Note the larger number of structured events at the low-latitude station (Siple), relative to either higher latitude station.

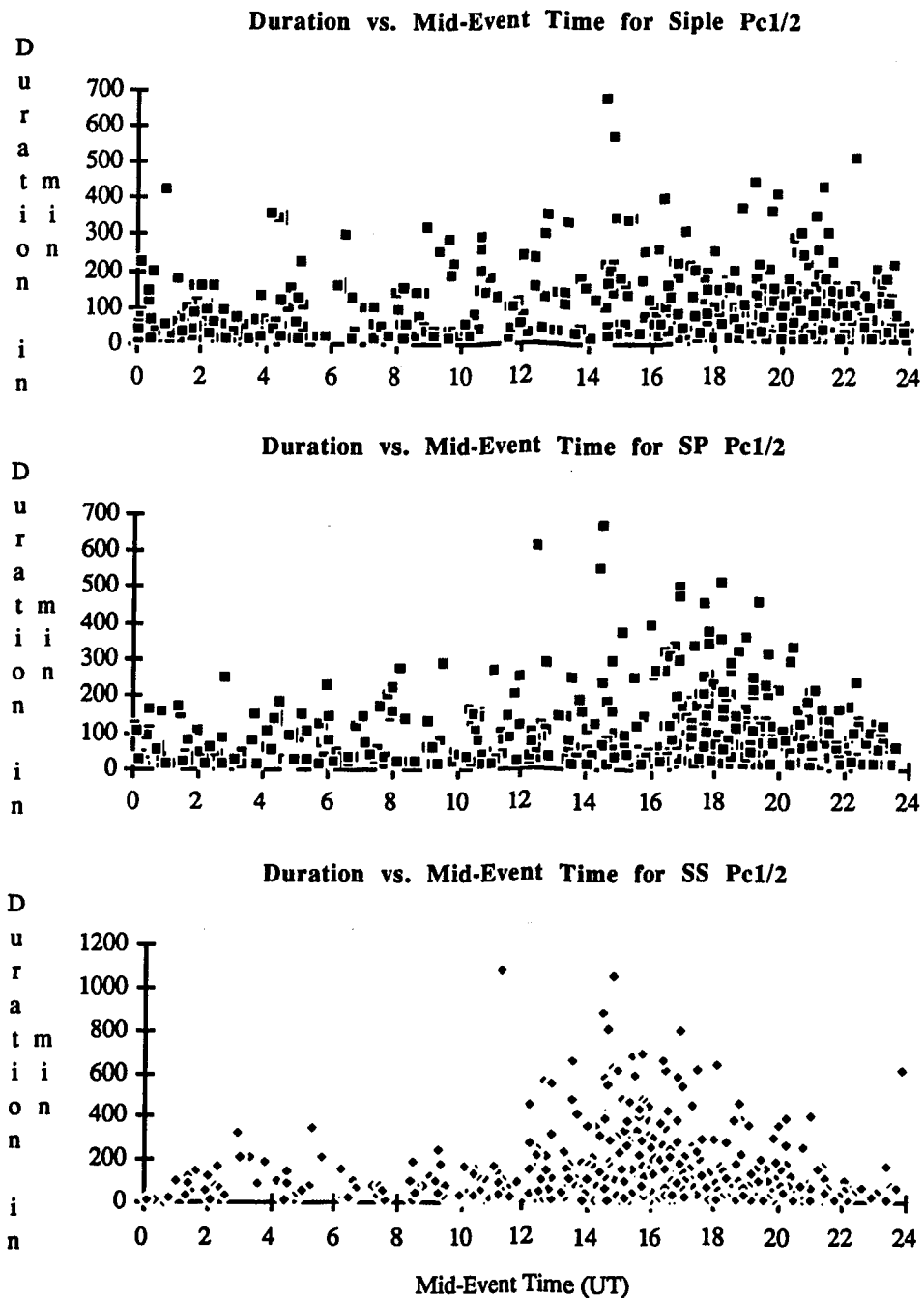


Figure 7-6. *a) (top)* Each Pc1/2 (unstructured events in the 0.1-0.4 Hz band) event is plotted by mid-event time (horizontal axis, in UT) and length in minutes (vertical axis). Local magnetic noon at Siple is 1700 UT, and most events cluster in the region after that time.

b) (middle) South Pole Pc1/2 have a somewhat more distinct postnoon peak occurrence than Siple. Local magnetic noon is 1530 UT at South Pole. There is no solar day at South Pole to account for this pattern.

c) (bottom) Pc1/2 at Sondre Stromfjord are the longest at any of the three stations. Note the vertical axis length scale difference in the plots. The longest Sondre Stromfjord event was approximately 17 hours.

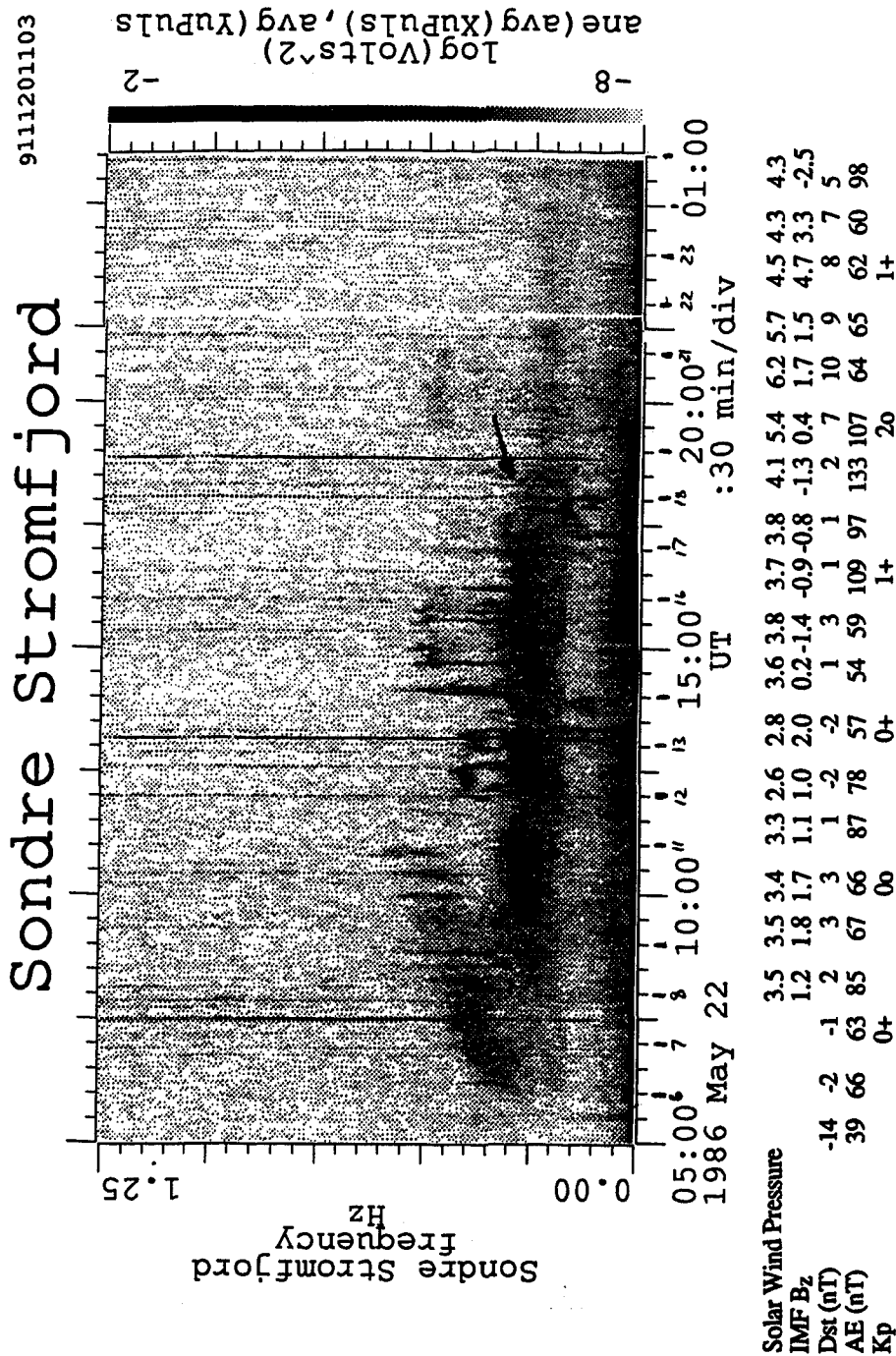
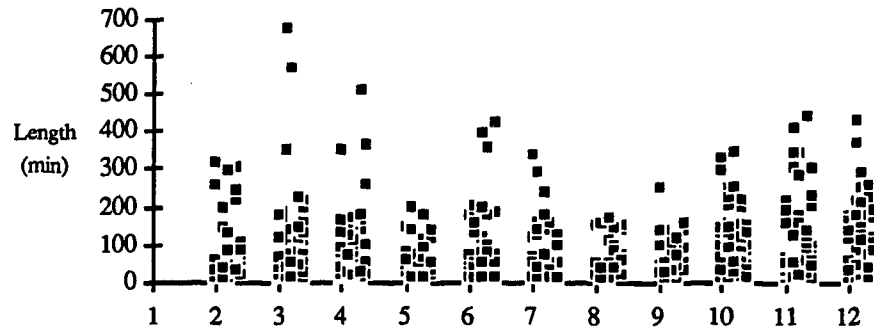
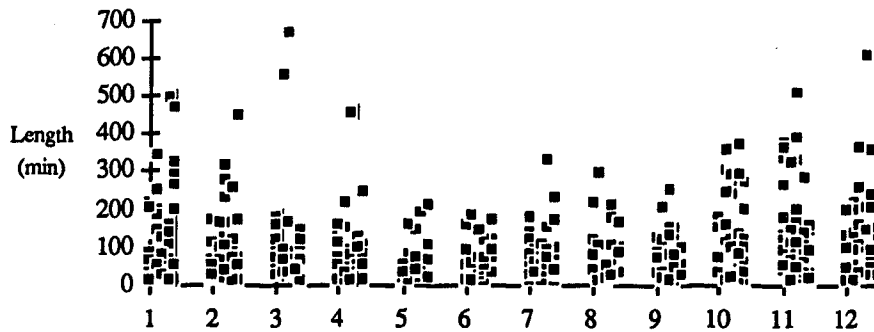


Figure 7-7. This Sondre Stromfjord Pc1/2 (indicated by an arrow) is one of the longest observed during 1986 at any of the three stations. The panels are each six hours long. The event runs from 0700 to 2400 UT at approximately 0.25 Hz. Note the narrow-band (≤ 0.2 Hz) nature throughout. The solar wind pressure went from 2.6 to 6.2×10^{-8} dynes/cm². The IMF Bz component turned southward, then northward, twice. Magnetic indices Kp, AE and Dst are all consistent with magnetically quiet times. Another Pc1/2 extends from 0600 to 1100 UT, rising in frequency. This could indicate an earthward motion of the cyclotron resonance region.

Siple Pc1/2 Events: Length vs. Month



South Pole Pc1/2 Events: Length vs. Month



Sondre Stromfjord Pc1/2 Events: Length vs. Month

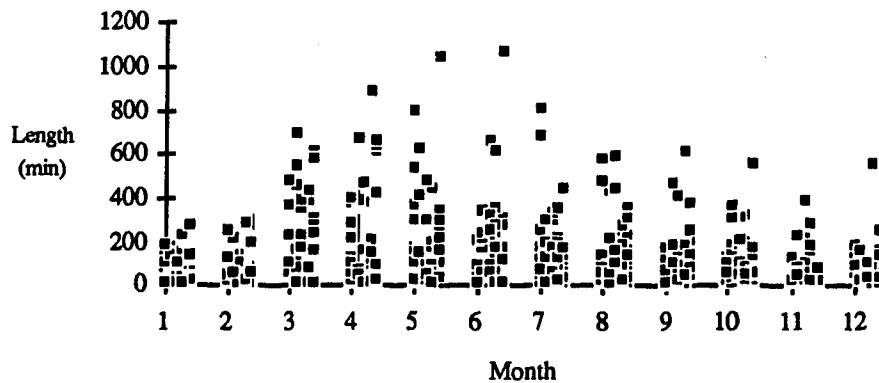
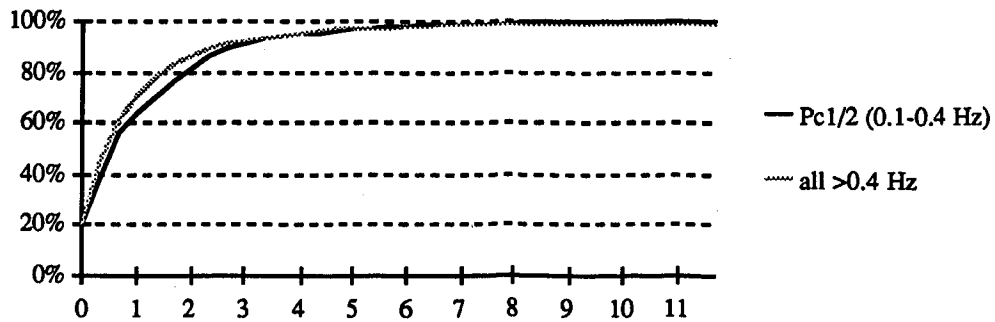
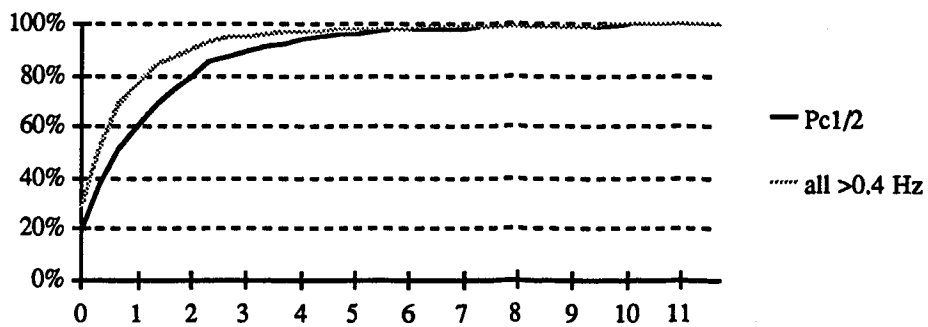


Figure 7-8. *a) (top)* Event length by month of 1986 is shown for Siple. None of January and only half of February was available for Siple, but the local summer months generally have the longest Pc1/2. *b) (middle)* The seasonal maximum length pattern is clearer at South Pole. *c) (bottom)* The Sondre Stromfjord Pc1/2 are the longest in the summer as well. Note the scale difference for event length in this plot.

Siple Cumulative Event Length Distribution



SP Cumulative Event Length Distribution



SS Cumulative Event Length Distribution

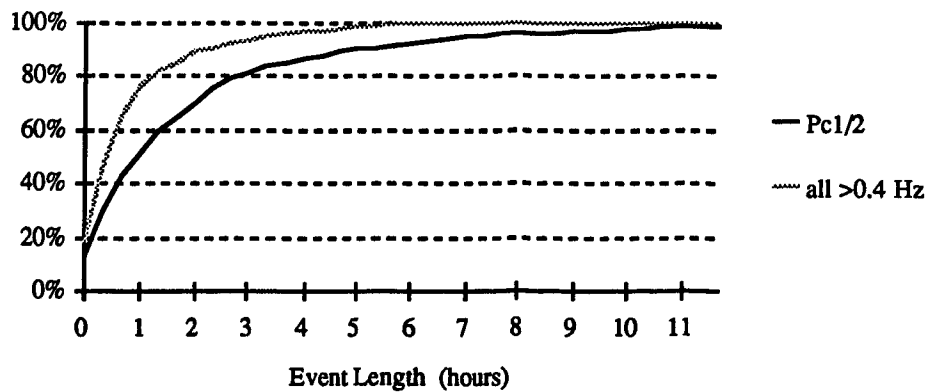


Figure 7-9. a) (top) Cumulative length distributions are shown for waves above and below 0.4 Hz. All those below 0.4 Hz are unstructured (Pc1/2). The vertical axis is the fraction of events that are up to or equal to the length on the horizontal axis.

b) (middle) South Pole events below 0.4 Hz are similar in length distribution to Siple, but the higher frequency events are shorter than those at Siple.

c) (bottom) Sondre Stromfjord length distributions are the most extreme of any station. Event lengths for waves above 0.4 Hz are similar to those at South Pole, but those below 0.4 Hz are longer than at any station.

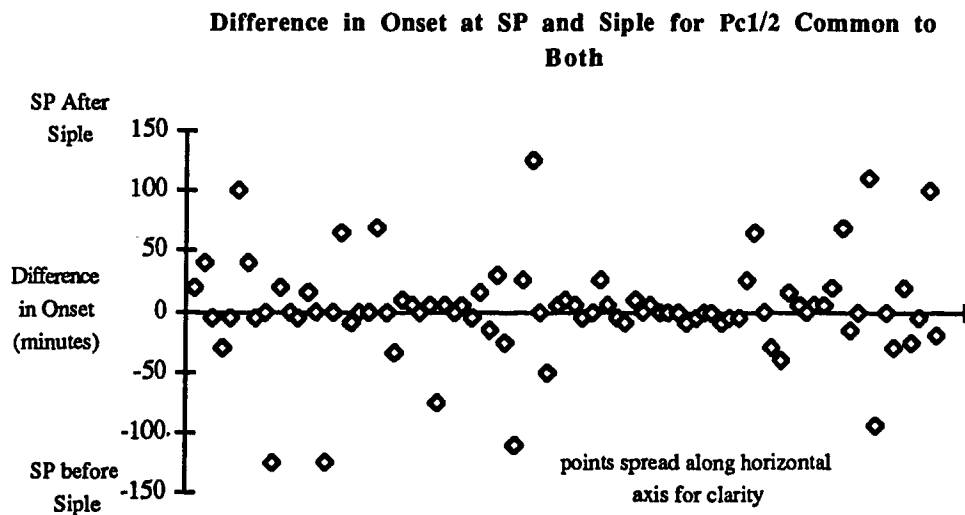
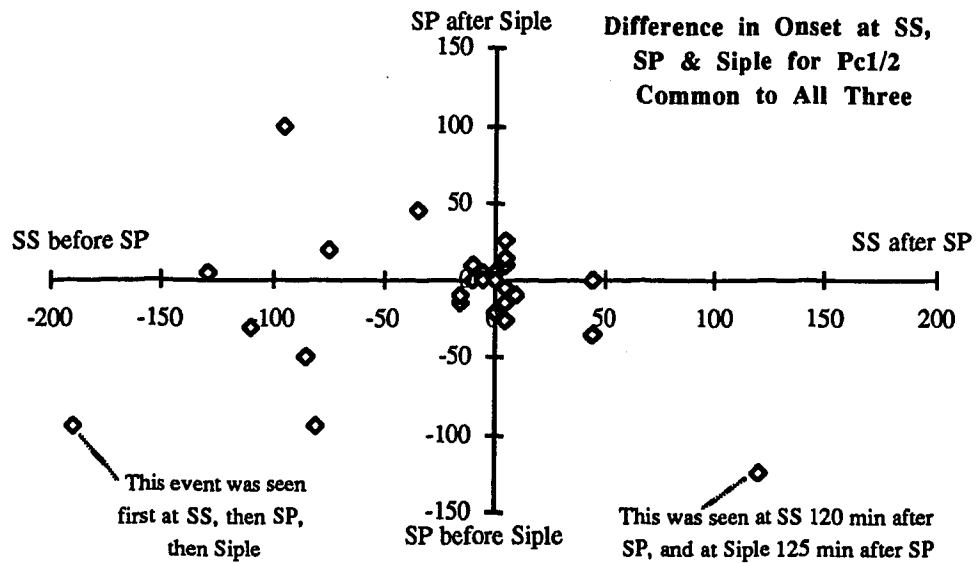
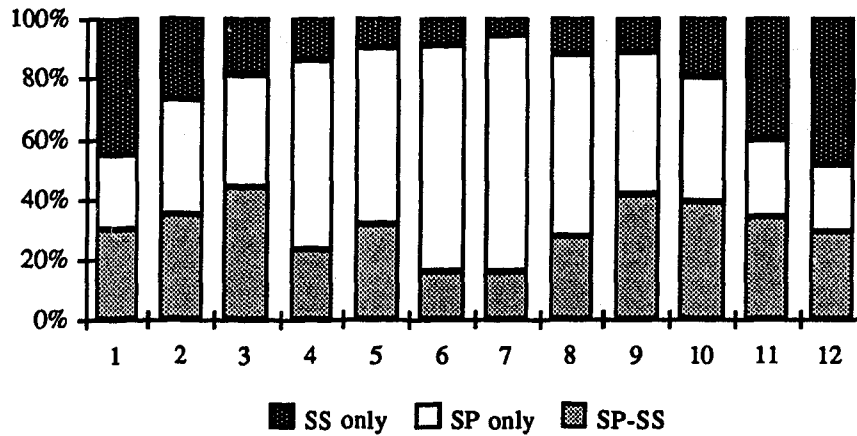


Figure 7-10. a) (top) The time delays between pairs of stations during Pc1/2 common to all three stations is shown. The vertical axis compares South Pole to Siple onset times, and the horizontal axis compares Sondre Stromfjord to South Pole. Most events occur with less than 40 minutes between any pair of stations. No systematic pattern exists that would suggest a localized cusp region source, as suggested by Bolshakova et al. (1980).

b) (bottom) Differences in onset times for Pc1/2 seen at both Antarctic stations indicate that there is no preference for the station that leads in longitude (South Pole) to see the events first.

Monthly SP-SS >0.4 Hz Distribution



Monthly SP-SS Pc1/2 Distribution

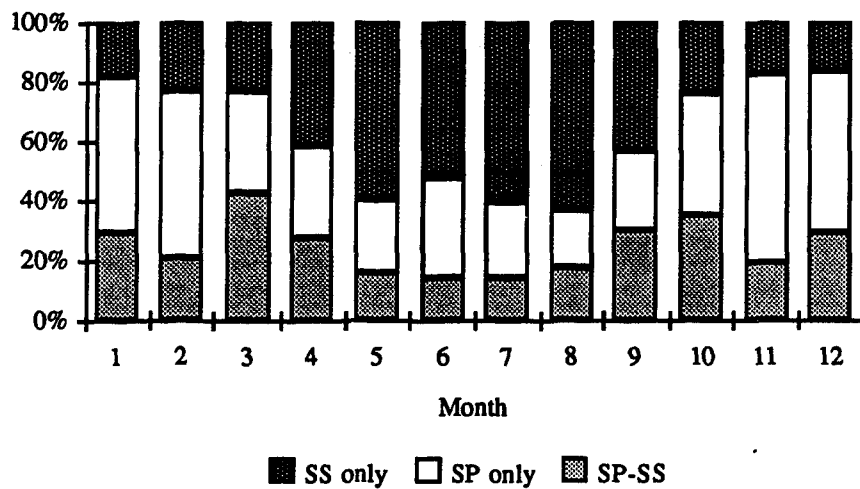
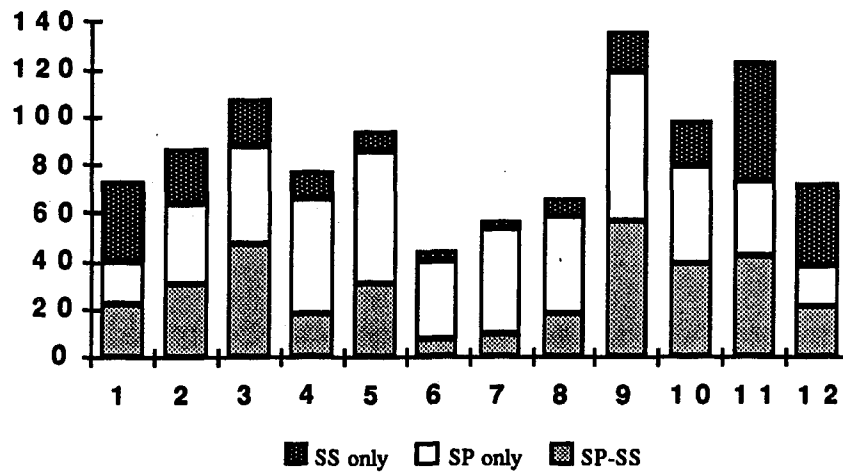


Figure 7-11. a) (top) The fraction of events above 0.4 Hz seen in each month at South Pole alone, Sondre Stromfjord alone, or at both simultaneously. The waves above 0.4 Hz are more common at the local winter station.

b) (bottom) The same as above, but for the Pc1/2 band (0.1-0.4 Hz). These waves are more common at the local summer station; the opposite seasonal pattern from those above 0.4 Hz. This suggests that the presence of He⁺ at high latitudes.

Monthly SP-SS >0.4 Hz Distribution



Monthly SP-SS Pc1/2 Distribution

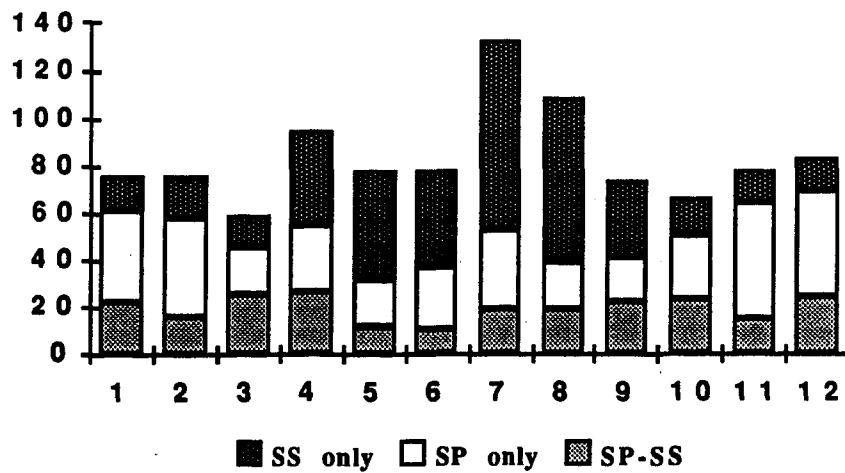
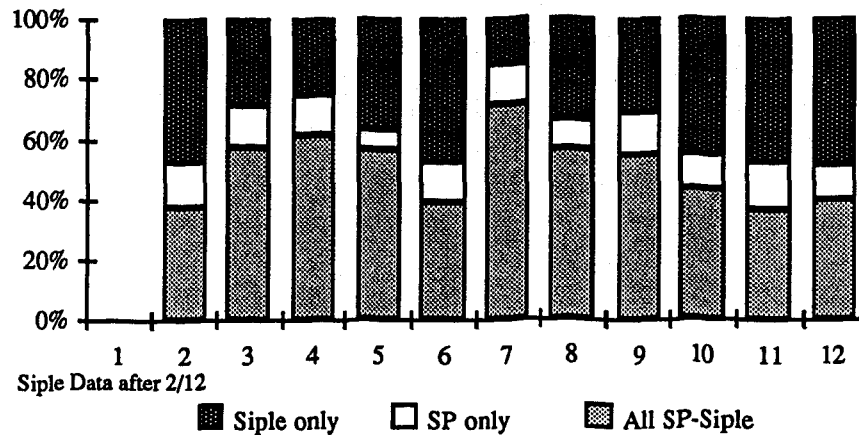


Figure 7-12. Events at South Pole and Sondre Stromfjord are presented by month, as in Figure 11, but in terms of event counts instead of fractions.

Monthly SP-Siple >0.4 Hz Distribution



Monthly SP-Siple Pc1/2 Distribution

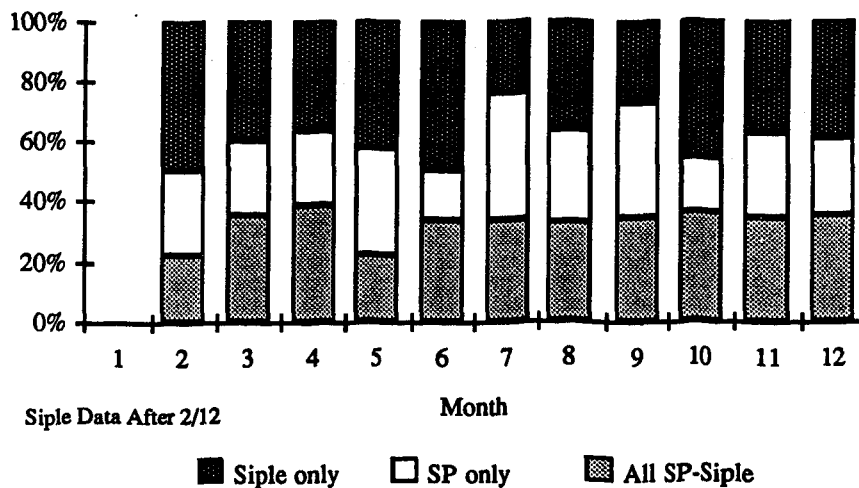
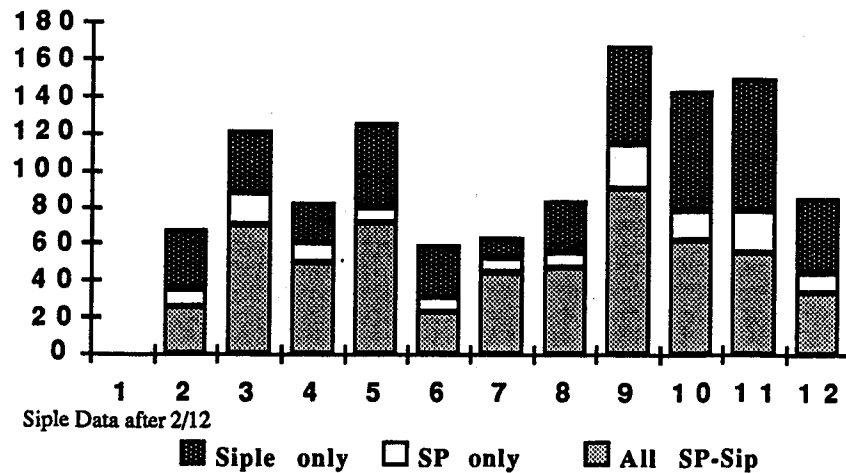


Figure 7-13a. a) (top): The fraction of events above 0.4 Hz seen in each month at South Pole alone, Siple alone, or at both simultaneously. These events are mostly at Siple alone or with South Pole, suggesting a source closer to Siple. At $L=4.3$, Siple is near the plasmapause. South Pole is near the auroral zone on the dayside. The Pc1 at high latitudes (Anderson, 1989, 1990; Erlandson 1990) seem to be blocked from reaching the ground, probably by the presence of He^+ , which has a gyrofrequency of 0.4 Hz near geosynchronous orbit (see also Perraut 1984).

b) (bottom) The same as above, but for waves in the Pc1/2 (0.1-0.4 Hz) band. The source for these clearly has better independent access to both stations and may be located between their L shells.

Monthly SP-Siple >0.4 Hz Distribution



Monthly SP-Siple Pc1/2 Distribution

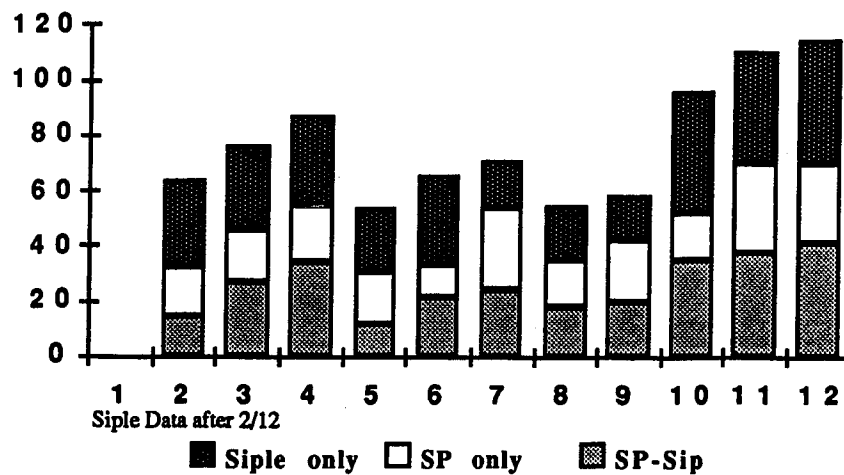


Figure 7-14. Events at South Pole and Siple are presented by month, as in Figure 7-13, but in terms of event counts instead of fractions.

He⁺ Gyrofrequency vs. L (T89)

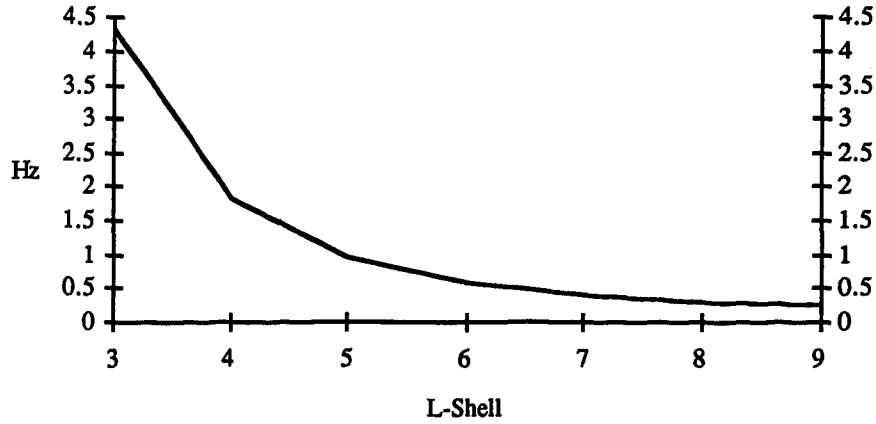


Figure 7-15. The He⁺ gyrofrequency at the magnetic equator was calculated with the T89 Tsyganenko magnetic field model and plotted vs. L-shell. The gyrofrequency approaches the 0.3-0.5 Hz range at L=6-9, and the slope flattens there. The presence of He⁺ at the equator, near the amplification site, may provide the sharp upper frequency bound that is typical of Pc1/2 events. He⁺ along field lines may also reflect waves above 0.4 Hz that were amplified near the equator at these high L-shells.

IMP8 IMF & Pressure Measurements by Month

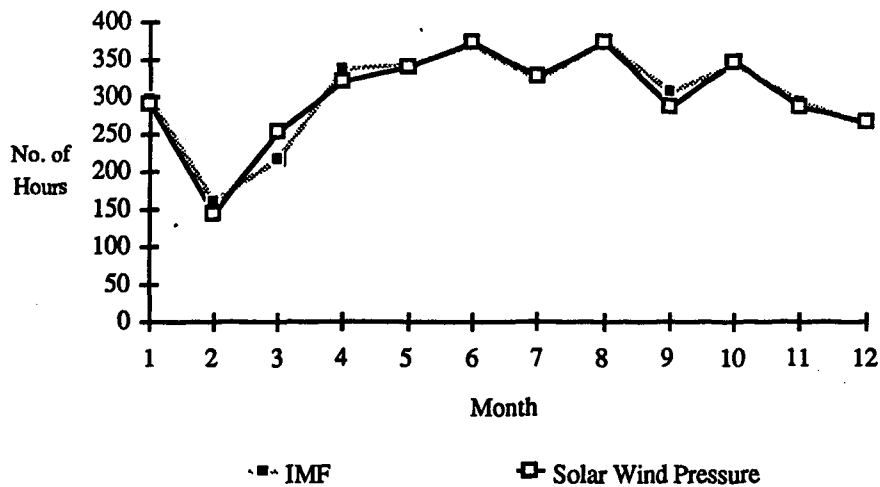


Figure 7-16. The number of hourly IMF and solar wind dynamic pressure measurements by IMP8 are plotted by month for 1986. Southern summer months, when Pc1/2 are most common there, are somewhat underrepresented.

Solar Wind Pressure Averaged Over Pc1/2 Events

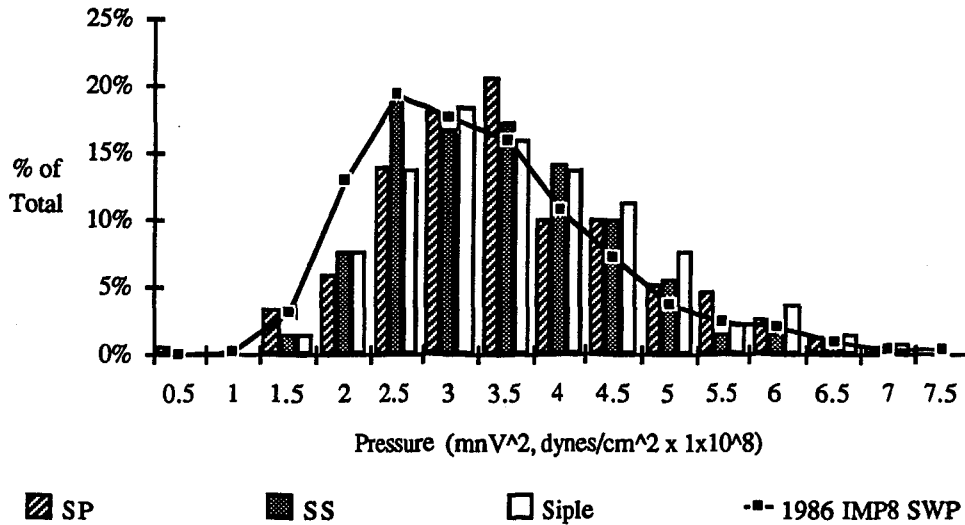


Figure 7-17. The dynamic solar wind pressure, averaged over Pc1/2 events, is similar to the distribution of 1986 IMP8 measurements. The relatively small number of Pc1/2 with pressures in the range $1.5\text{-}2.0 \times 10^{-8}$ dynes/cm² is not enough to create a significant departure from the IMP8 reference. This suggests that solar wind pressure is not a sufficient condition for Pc1/2 amplification.

Pressure During the First Full Hour of Pc1/2 Events

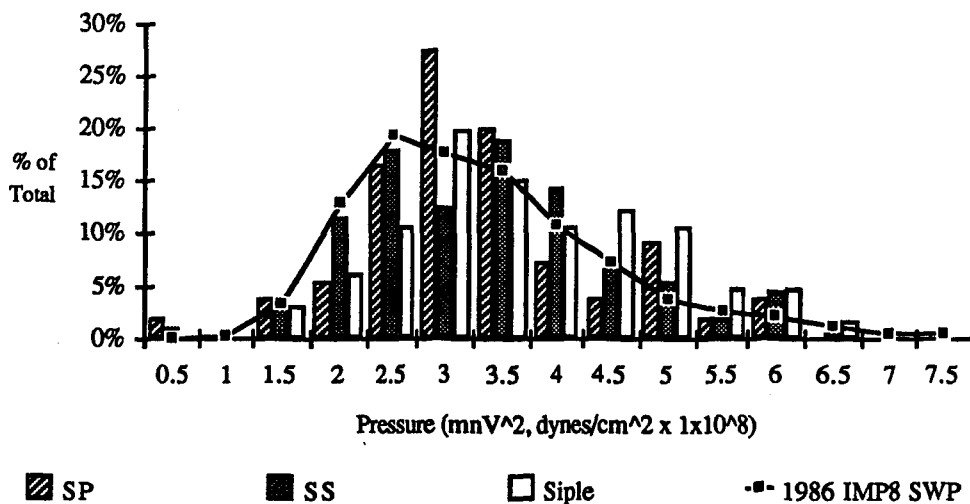
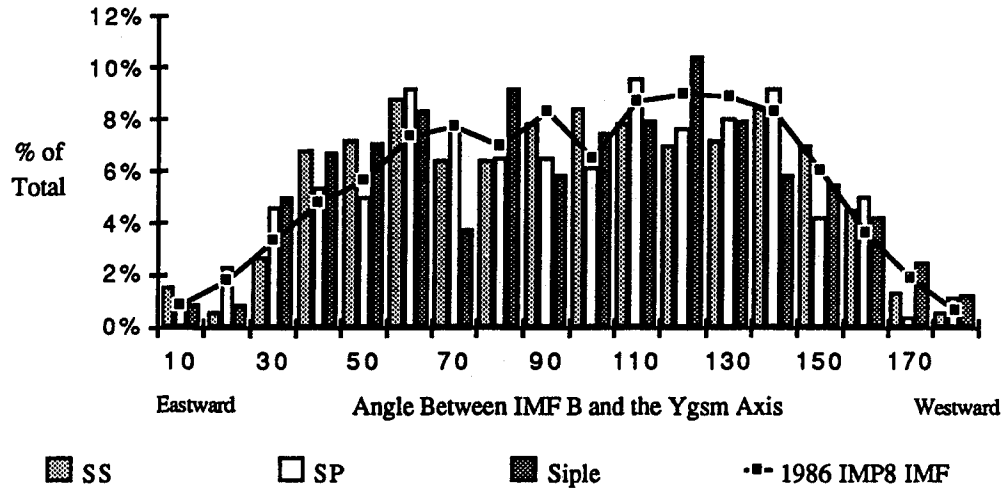


Figure 7-18. The solar wind pressures during the first full hour of Pc1/2 at the three stations are also similar to the 1986 IMP8 distribution. More Siple Pc1/2 occurred during pressures of 4.0 to 5.0 than the IMP8 distribution would have predicted. This makes the Siple first hour pressure distribution different from IMP8 with borderline significance.

Cone Half-Angles Between the IMF and Y_{gsm} for Pc1/2



Cone Half-Angles Between the IMF and X_{gsm} for Pc1/2

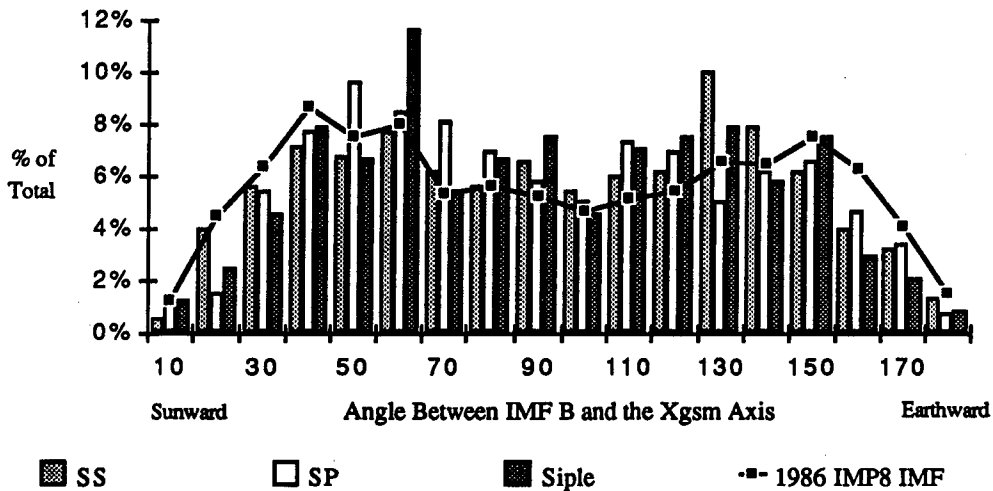


Figure 7-19. (top) The cone angles between the IMF and the Y_{gsm} axis during Pc1/2 at the three stations are plotted, together with the IMP8 IMF-to-Y measurements during 1986. The distributions from all the stations are similar to that of IMP8, with at least a 4% chance of exceeding chi-square. The Y component of the IMF has an influence on the symmetry of convection in the magnetosphere, so an association of Pc1/2 with a polarity of B_y could have explained the postnoon occurrence.

(bottom) The cone angles between the IMF and the X axis also follow the 1986 IMP8 cone angle distribution. Small cone angles have been associated with Pc3 and Pc4 waves directly transmitted into the magnetosphere (Nishida, 1978; Engebretson et al., 1991), and earthward-pointing IMF with increased magnetic activity in the magnetosphere, particularly when accompanied by a southward component (Schatten & Wilcox, 1967).

IMF Bz for Pc1/2 Event Hours

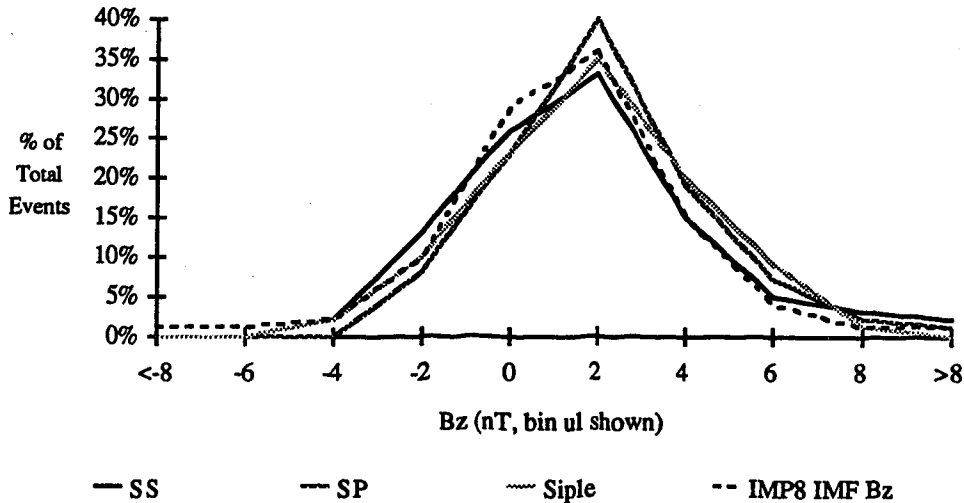


Figure 7-20. The Bz values during Pc1/2 are distinct from the 1986 IMP8 measurements by a chi-square test, but centroids of all these peaks agree within one standard deviation (1 nT). There is no preference for negative or positive Bz compared to the IMP8 average for 1986. The 1986 IMP8 average Bz is +0.3 nT over 3618 hourly measurements.

IMF Half-Cone Angles to X and Y Axes for SS Pc12 Hours

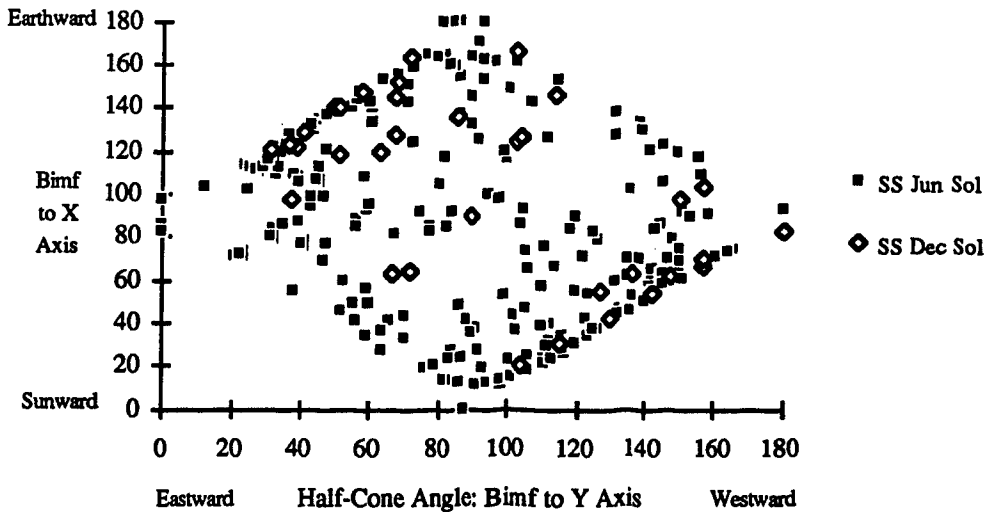


Figure 7-21. The cone angles between the IMF and the X and Y axes are plotted seasonally for Sondre Stromfjord Pc1/2 event hours. The IMF scatter in the XY plane covers the same angle space in both seasons, so the X and Y components of the IMF do not explain the seasonal occurrence of the Pc1/2. Note the Parker Spiral in this Figure, where most IMF directions in the XY plane are Westward-Sunward or Eastward-Earthward.

AE Response to IMF Bz
(1/17/86 hr 9 - 1/18/86 hr 4, including hr 0)

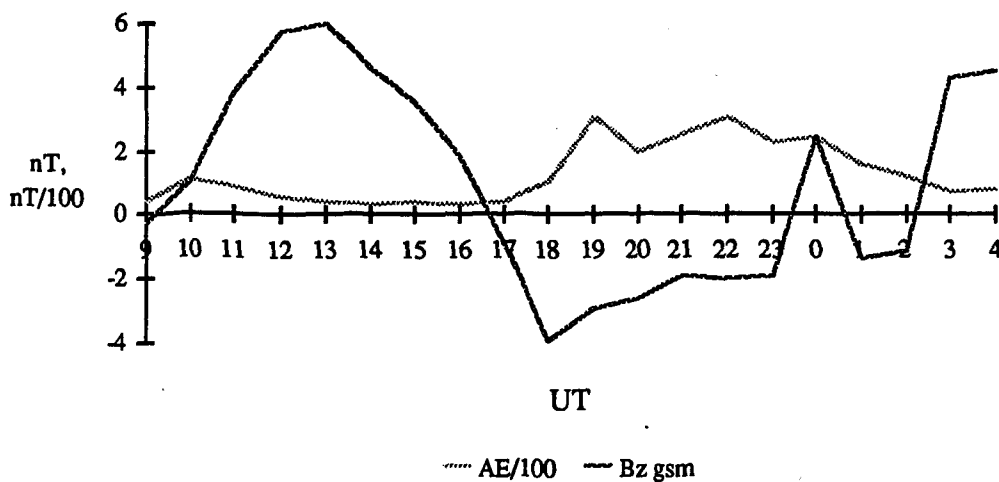
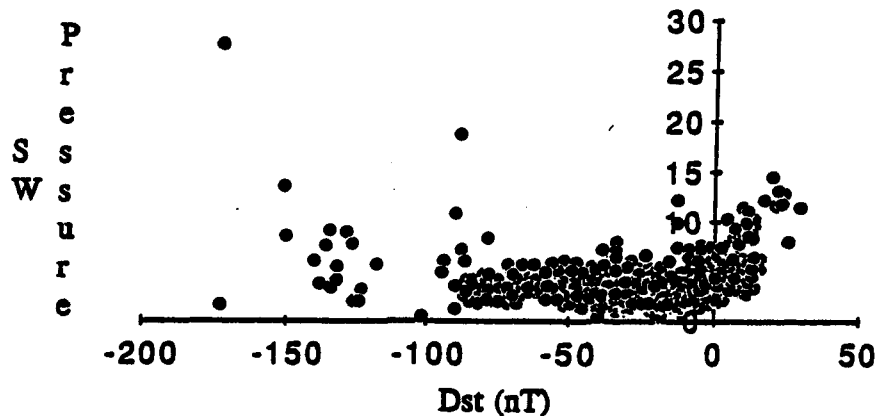


Figure 7-22. This is an example of how the magnetosphere responds to a southward-turning of the IMF. The AE index follows the auroral electrojet intensity, which increases during substorm activity. It is divided by 100 for scaling purposes. The z component of the IMF as measured by IMP8 is also plotted. Both quantities are hourly averaged values from the same databases as the AE and IMF used elsewhere in this work. The extended period of northward IMF (10-16 UT) is accompanied by a relatively quiet electrojet. After the southward-turning of the IMF near 17 UT, the electrojet intensity increases, indicating substorm activity in progress. The typical lag of AE response behind the southward-turning of the IMF is approximately one hour (see text).

SW Pressure and Dst Simultaneously Measured in 1986



SW Pressure and Dst for SS up to 4 Hours of Events ≥ 45 min Long

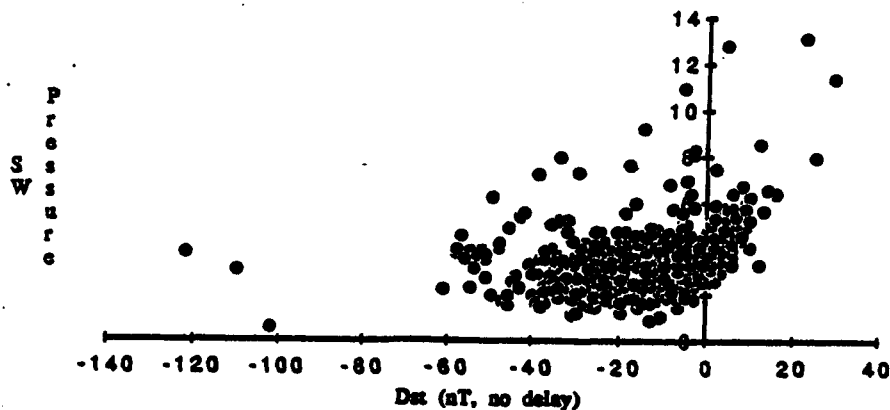
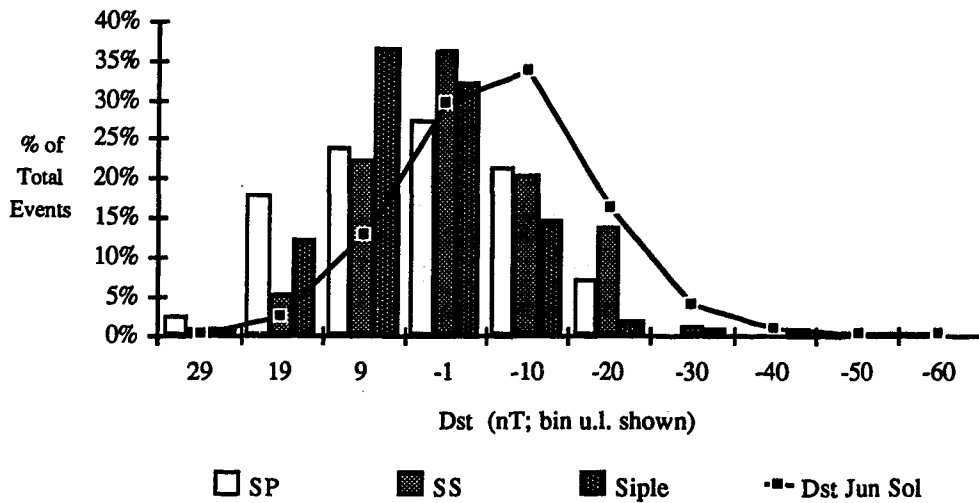


Figure 7-23. (top) The solar wind pressure and Dst values are plotted for 1986 whenever both were available. Above $Dst=0$, increased pressure is associated with more positive Dst. 'Compression' of the magnetosphere, or increased magnetopause currents due to enhanced solar wind pressure, adds to the field of the Earth, producing positive Dst. Negative values are from an enhanced ring current, whose magnetic field subtracts from that of the Earth at its surface.

(bottom) Dst and solar wind pressures during Pc1/2 observed at Sondre Stromfjord appear to be similar to the 1986 distribution. The Dst values during Pc1/2 do not extend to the extremes of the 1986 Dst and have no preference for large negative storm values. There is also no indication that Pc1/2 are being amplified during the storm recovery phase.

Dst for Pc1/2 Hours During June Solst +-45 Days



Dst for Pc1/2 Hours During Dec Solst +-45 Days

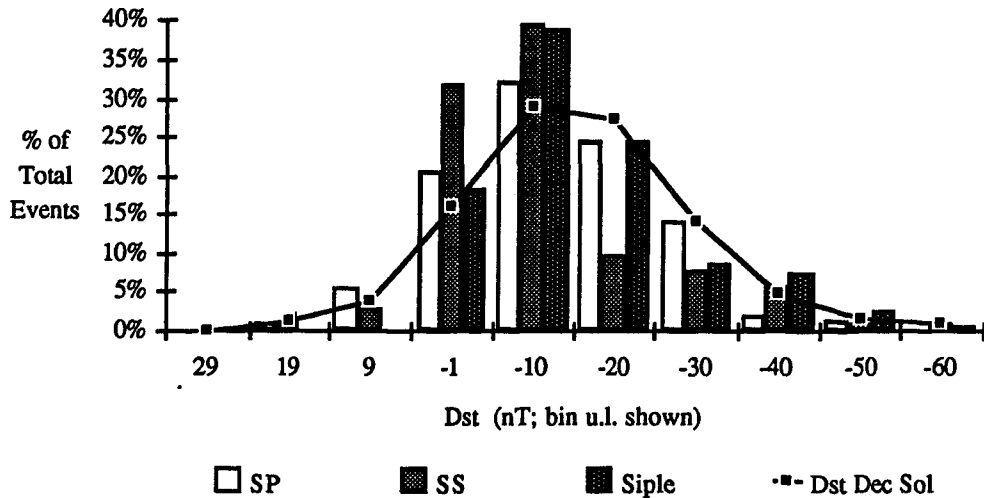
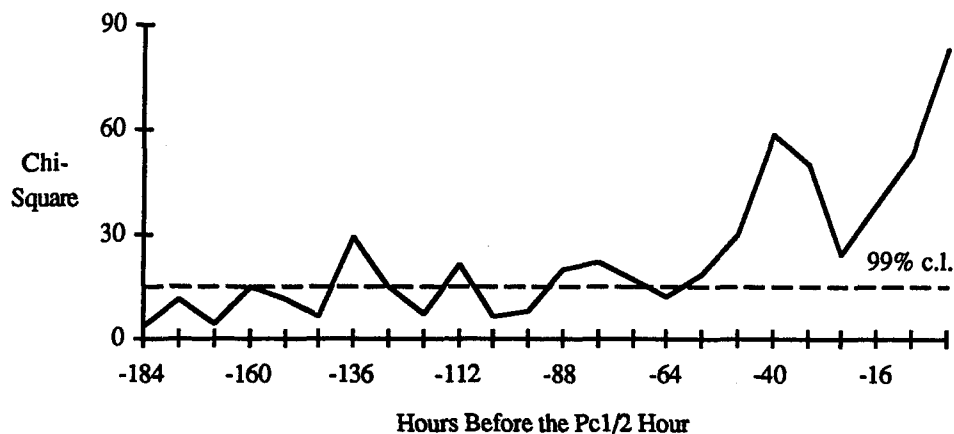


Figure 7-24. (top) Dst values during Pc1/2 hours in the June solstice season are typical of magnetically quiet times, or high solar wind pressures. They are significantly different from the seasonal Dst reference. High pressure is an unlikely explanation, though, because the Dst distributions for Pc1/2 shift toward negative values in the December solstice, yet there was no seasonal difference in solar wind pressures.

(bottom) Dst during the December solstice season Pc1/2 are consistent with the seasonal Dst reference, and no preference exists for storm-time conditions.

Chi-Square for Offset-Dst vs June Sol Dst Model for Hours Before SS Pc1/2



Dst for June Sol and 136 Hours Before SS Jun Sol Pc1/2

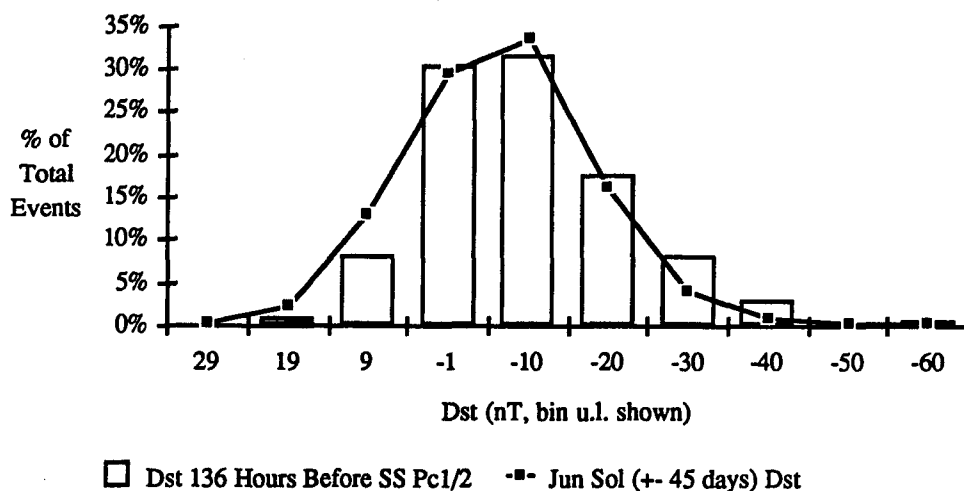
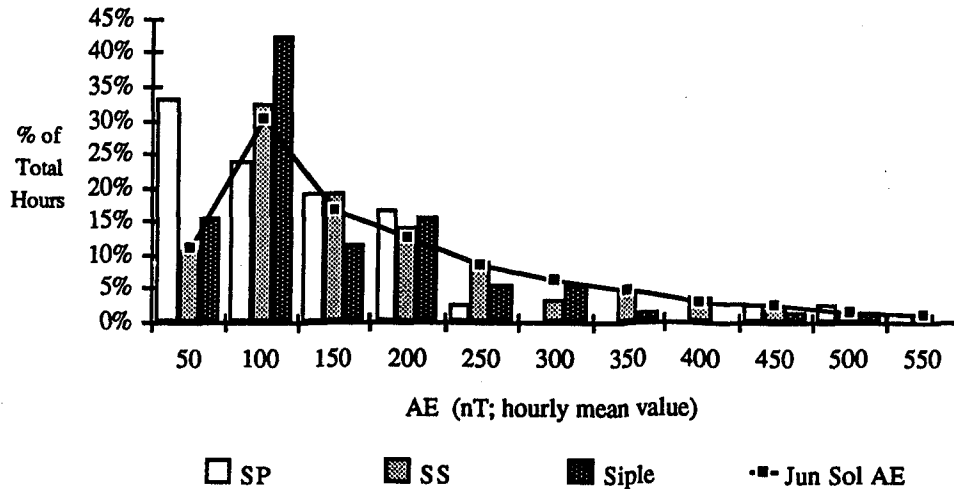


Figure 7-25. (top) To see if Pc1/2 occurred during the recovery phase of storms, the Dst at the time of the Pc1/2, as well as those in the hours before, were selected. At each time before the Pc1/2, the distribution of Dst values were compared to the June solstice Dst reference. The similarity was characterized by the chi-square statistic. Small values indicate close similarity, and this means there is no association of Pc1/2 with storm time Dst, since most Dst values during the June solstice were not at storm levels.

Large chi-square values indicate significant differences between the distributions. This happens at 0, 8 and 40 hours before the Pc1/2, because the Dst values at those times were even more positive than those of the June solstice (see the previous figure). Chi-square values above the 99% confidence level indicate a significant difference between the two distributions under comparison. Except for 136 hours before, there were no large chi-square values due to storm levels of Dst prior to Pc1/2. The distribution for 136 hours before is shown below, and it shows no convincing preference for storm-time Dst levels. This means most Pc1/2 do not appear in the recovery phase.

(bottom) The Dst distribution for 136 hours before the Pc1/2 shows a slight excess in storm levels, near -20 nT and below, compared to the June solstice reference.

AE for Pc1/2 Hours During June Sol ± 45 Days



AE for Pc1/2 Hours During Dec Sol ± 45 Days

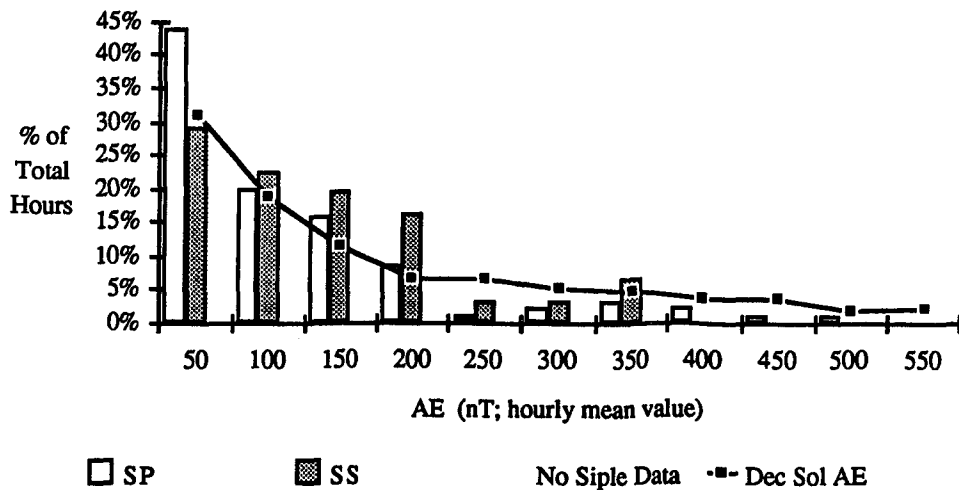
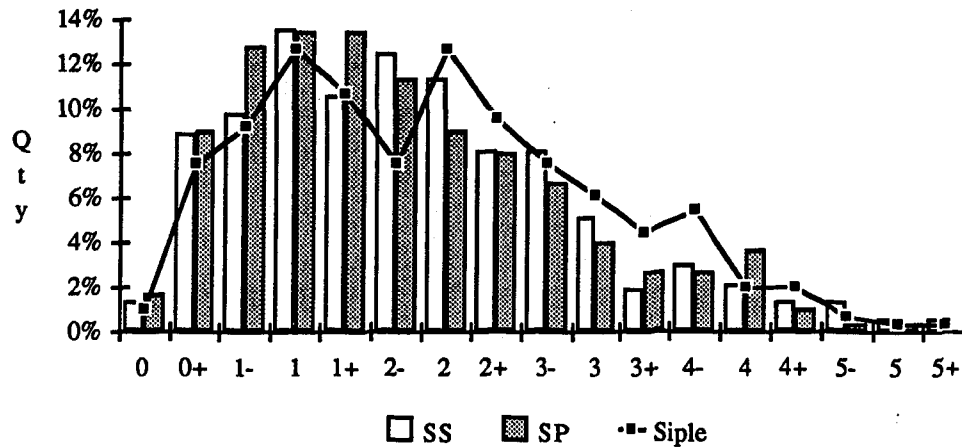


Figure 7-26. (top) AE values during June solstice (± 45 days) Pc1/2 hours have a distribution similar to that of the seasonal AE reference. The average AE during the "international quietest days" of January-June 1986 was 72 nT. It serves as a quiet time standard. Some Pc1/2 occur during substorm AE levels, but no more than random selection from the reference distribution would predict.

(bottom) The seasonal AE distribution during the December solstice peaks in the 0-50 nT bin, somewhat lower than the June solstice case. Note that Sondre Stromfjord follows the seasonal peak from June to December, but South Pole does not. Both are at about the same magnetic latitude, however, so the difference between South Pole and the June reference may not be significant.

**Kp at Start of Pc1/2 >45 Min Long
(with ≥ 45 min Data Hour Overlap)**



Kp at Start of All Pc1/2

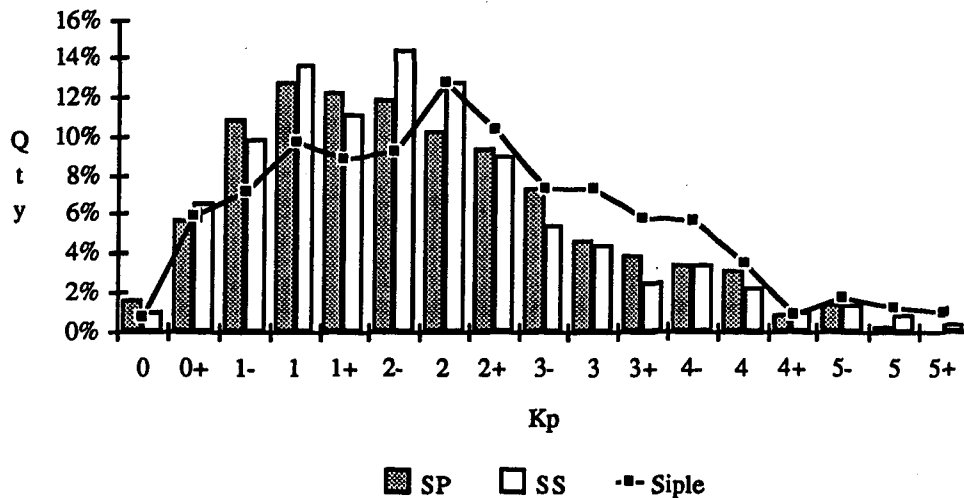


Figure 7-27 (a) (top) The Kp values at the start of Pc1/2 are compared to the Kp distribution for 1986. These Pc1/2 are the set used for the IMF, solar wind pressure, AE and Dst studies. They are at least 45 minutes long, and they are required to overlap a data or index hour by at least 45 minutes. Kp values were selected for them to provide another view of the same events. There is no significant difference among the three stations, although there is a weak trend for the low-latitude station to observe Pc1/2 when Kp is high.

(b) (bottom) If all Pc1/2 are used for Kp selection, regardless of length, an inverse Kp-latitude relation becomes apparent. This was noted by Bolshakova et al (1980). The higher latitude stations see more Pc1/2 during low Kp than low-latitude stations, and vice versa. Event length is the only difference between the two Figures, and this suggests that short events are associated with higher Kp and lower latitudes.

References

- Akasofu, S. -I., P. D. Perraut, F. Yasuhara, and C. -I. Meng, Auroral substorms and the interplanetary magnetic field, *J. Geophys. Res.*, **78**, 7490-7508, 1973.
- Akasofu, S. -I., Interplanetary energy flux associated with magnetospheric substorms, *Plan. Space Sci.*, **27**, 425, 1979.
- Akasofu, S.-I., Relationship between the growth of the ring current and the interplanetary quantity ϵ , *Planet. Sp. Sci.*, **27**, 1039, 1979.
- Akasofu, S. -I., B. -H. Ahn, Y. Kamide, and J. H. Allen, A note on the accuracy of the auroral electrojet indices, *J. Geophys. Res.*, **88**, 5769-5772, 1983.
- Akasofu, S.-I., The dynamic aurora, *Scientific American*, p 90, May, 1989.
- Anderson, B. J., R. E. Erlandson, L. J. Zanetti, and T. A. Potemra, Pc1 pulsations in the outer equatorial magnetosphere (abstract), *EOS Trans. American Geophysical Union*, **70**, 1266, 1989.
- Anderson, B. J., K. Takahashi, R. E. Erlandson, and L. J. Zanetti, Pc1 Pulsations observed by AMPTE/CCE in the Earth's outer magnetosphere, *Geophys. Res. Lett.*, **17**, 1853-1856, 1990.
- Arnoldy, R. L., M. J. Engebretson, and L. J. Cahill, Jr., Bursts of Pc 1-2 near the ionospheric footprint of the cusp and their relationship to flux transfer events, *J. Geophys. Res.*, **93**, 1007-1016, 1988.
- Arnoldy, R. L., Signature in the interplanetary medium for substorms, *J. Geophys. Res.*, **76**, 5189-5201, 1971.
- Ashour-Abdalla, M., and R. M. Thorne, The importance of electrostatic ion cyclotron instability for quiet time proton auroral precipitation, *Geophys. Res. Lett.*, **4**, 45, 1977.
- Baranskiy, L. N., Some characteristics of the polarization of Pc1 pulsations associated with their waveguide propagation, *Geomagnetism and Aeronomy*, **10**, 86-89, 1970.
- Barfield, J. N., and R. L. McPherron, Investigation of interactions between Pc1 and 2 and Pc5 micropulsations at the synchronous orbit during magnetic storms, *J. Geophys. Res.*, **77**, 4707-4719, 1972.
- Baumjohann, W., Merits and limitations of the use of geomagnetic indices in solar wind-magnetosphere coupling studies, in *Solar Wind-Magnetosphere Coupling*, edited by Y. Kamide & J. A. Slavin, 3-15, Terra Publishing Co, Tokyo, 1986.

- Berthold, W. K., A. K. Harris, and H. J. Hope, Worldwide effects of hydrodynamic waves due to Argus, *J. Geophys. Res.*, *65*, 2233, 1960.
- Bevington, P. R., *Data Reduction and Error Analysis for the Physical Sciences*, McGraw-Hill, NY, NY, 1969.
- Bolshakova, O. V., V. A. Troitskaya, and K. G. Ivanov, High latitude Pc1-2 geomagnetic pulsations and their connection with location of the dayside polar cusp, *Plan. Space Sci.*, *28*, 1-7, 1980.
- Bossen, M., R. L. McPherron, and C. T. Russell, A statistical study of Pc1 magnetic pulsations at synchronous orbit, *J. Geophys. Res.*, *81*, 6083, 1976.
- Brice, N., Fundamentals of very low frequency emission generation mechanisms, *J. Geophys. Res.*, *69*, 4515-4522, 1964.
- Bythrow, P. F., R. A. Heelis, W. B. Hanson, R. A. Power, and R. Hoffman, Observational evidence for a boundary layer source of dayside region 1 field-aligned currents, *J. Geophys. Res.*, *86*, 5577-5589, 1981.
- Chappell, C. R., Thermal ions in the magnetosphere, in *The Earth's Magnetospheric Processes*, edited by B. M. McCormac, D. Reidel, Dordrecht, 280-290, 1972.
- Chappell, C. R., Detached plasma regions in the magnetosphere, *J. Geophys. Res.*, *79*, 1861-1870, 1974.
- Chen, F. F., *Introduction to Plasma Physics*, Plenum Press, NY, NY, 1974.
- Cornwall, J. M., On the role of charge exchange in generating unstable waves in the ring current, *J. Geophys. Res.*, *82*, 4699, 1977.
- Cowley, S. W. H., Pitch angle dependence of the charge exchange lifetime of ring current ions, *Planet. Space Sci.*, *25*, 385-393, 1977.
- Cowley, S. W. H., The causes of convection in the Earth's magnetosphere: a review of developments during the IMS, *Rev. Geophys. Space Phys.*, *20*, 531-565, 1982.
- Cross, R., *An Introduction to Alfvén Waves*, Adam Hilger, Philadelphia, PA, 1988.
- Davis, T. N., and M. Sugiura, Auroral electrojet activity index AE and its universal time variations, *J. Geophys. Res.*, *71*, 785-801, 1966.
- Dawson, J. A., *Technical Note 342*, National Bureau of Standards, June 30, 1966.
- de la Beaujardiere, O., D. Alcayade, J. Fontanari, and C. Leger, Seasonal dependence of high latitude electric fields, *J. Geophys. Res.*, *96*, 5723-5735, 1991.
- DeForest, S. E., and C. E. McIlwain, Plasma clouds in the magnetosphere, *J. Geophys. Res.*, *76*, pp. 3587-3611, 1971.
- Denisse, J. F., and DelCroix, J. L., *Plasma Waves*, Interscience Publishers, NY, NY, 1963.

- Dowdy, S., and S Wearden, *Statistics for Research*, John Wiley & Sons, NY, NY, 1983.
- Doyle, M. A., and W. J. Burke, S3-2 measurements of the polar cap potential, *J. Geophys. Res.*, **88**, 9125, 1983.
- Dungey, J. W., Interplanetary magnetic field and the auroral zone, *Phys. Rev. Lett.*, **6**, 47-48, 1961.
- Eastman, T. E., E. W. Hones, S. J. Bame, Jr., and J. R. Asbridge, The magnetospheric boundary layer: site of plasma, momentum and energy transfer from the magnetosheath into the magnetosphere, *Geophys. Res. Lett.*, **3**, 685-688, 1976.
- Ejiri, M., Trajectory traces of charged particles in the magnetosphere, *J. Geophys. Res.*, **83**, 4798-4810, 1978.
- Ejiri, M., R. A. Hoffman, and P. H. Smith, Energetic particle penetrations into the inner magnetosphere, *J. Geophys. Res.*, **85**, 653-663, 1980.
- Engebretson, M. J., N. Lin, W. Baumjohann, H. Luehr, B. J. Anderson, L. J. Zanetti, T. A. Potemra, R. L. McPherron, and M. G. Kivelson, A comparison of ULF fluctuations in the solar wind, magnetosheath, and dayside magnetosphere 1. Magnetosheath morphology, *J. Geophys. Res.*, **96**, 3441-3454, 1991.
- Evans, D. S., The characteristics of a persistent auroral arc at high latitude in the 1400 MLT sector, in *The Polar Cusp, NATO ASI Series*, edited by J. A. Holtet, and A. Egeland, D. Reidel Pub. Co., Dordrecht-Holland, 99-109, 1985.
- Fairfield, D. H., and Cahill, L. J. Jr., Transition region magnetic field and polar magnetic disturbances, *J. Geophys. Res.*, **71**, 155, 1966.
- Fairfield, D. H., Average and unusual locations of the Earth's magnetopause and bow shock, *J. Geophys. Res.*, **76**, 6700-6716, 1971.
- Frank, L. A., Relationship of the plasma sheet, ring current, trapping boundary and plasmopause near the magnetic equator and local midnight, *J. Geophys. Res.*, **76**, 2265-2275, 1971.
- Fraser, B. J., and R. L. McPherron, Pc1-2 magnetic pulsation spectra and heavy ion effects at synchronous orbit: ATS-6 results, *J. Geophys. Res.*, **87**, 4560, 1982.
- Fraser, B. J., and W. R. Summers, Simultaneous observations of Pc1 micropulsation polarization at four low latitude sites, *Ann. Geophys.*, **28**, 697-708, 1972.
- Fraser, B. J., Ionospheric duct propagation and Pc 1 pulsation sources, *J. Geophys. Res.*, **80**, 2790-2796, 1975.
- Fraser, B. J., Pc1-2 observations of heavy ion effects by synchronous satellite ATS-6, *Plan. Sp. Sci.*, **30**, 1229, 1982.
- Fujita, S., and T. Tamao, Duct propagation of hydromagnetic waves in the upper ionosphere, 1. Electromagnetic field disturbances in high latitudes associated with localized incidence of a shear Alfvén wave, *J. Geophys. Res.*, **93**, 14665-14673, 1988.

- Fujita, S., Duct propagation of hydromagnetic waves in the upper ionosphere, 2. Dispersion characteristics and loss mechanism, *J. Geophys. Res.*, *93*, 14674-14682, 1988.
- Fukunishi, H., Classification of hydromagnetic emissions based on frequency-time spectra, *J. Geophys. Res.*, *86*, 9029-9039, 1981.
- Gendrin, R., S. Lacourly, A. Roux, F. Z. Feigin, M. V. Gokhberg, V. A. Troitskaya, and V. L. Yakimenko, Wave packet propagation in an amplifying medium and its application to the dispersion characteristics and to the generation mechanisms of Pc 1 events, *Planet. Space Sci.*, *19*, 165-194, 1971.
- Greifinger, C., and Greifinger, P., Theory of hydromagnetic propagation in the ionospheric waveguide, *J. Geophys. Res.*, *73*, 7473-7490, 1968.
- Greifinger, P., Ionospheric propagation of oblique hydromagnetic plane waves at micropulsation frequencies, *J. Geophys. Res.*, *77*, 2377-2390, 1972a.
- Greifinger, P., Micropulsations from a finite source, *J. Geophys. Res.*, *77*, 2392-2396, 1972b.
- Greifinger, C., and Greifinger, P., Wave guide propagation of micropulsations out of the plane of the geomagnetic meridian, *J. Geophys. Res.*, *78*, 4611-4618, 1973.
- Haerendel, G., and G. Paschmann, Interaction of the solar wind with the dayside magnetosphere, in *Magnetospheric Plasma Physics*, edited by A. Nishida, pp. 49-142, D.Reidel Publishing Co., Boston, MA, and The Center for Academic Publications, Tokyo, Japan, 1982.
- Halliday, D., and R. Resnick, *Fundamentals of Physics*, third edition, John Wiley & Sons, NY, NY, 1988.
- Hayashi, K., S. Kokubun, T. Oguti, K. Tsuruda, S. Machida, T. Kitamura, O. Saka, and T. Watanabe, The extent of Pc1 source region in high latitudes, *Can. J. Phys.*, *59*, 1097-1105, 1981.
- Heacock, R. R., The 4-second summertime micropulsation band at College, *J. Geophys. Res.*, *71*, 2763-2775, 1966.
- Heacock, R. R., The relation of the Pc 1 micropulsation source region to the plasmasphere, *J. Geophys. Res.*, *76*, 100-08, 1971.
- Heacock, R. R., and M Kivinen, Relation of Pc 1 micropulsations to the ring current and geomagnetic storms, *J. Geophys. Res.*, *77*, 6746-6760, 1972.
- Heacock, R. R., and M. Kivinen, Relation of Pc1 micropulsations to the ring current and geomagnetic storms, *J. Geophys. Res.*, *77*, 6746-6760, 1972.
- Heacock, R. R., and S. -I., Akasofu, Periodically structured Pc1 micropulsations during the recovery phase of intense magnetic storms, *J. Geophys. Res.*, *78*, 5524-5536, 1973.
- Heacock, R. R., Midday Pc 1-2 pulsations observed at a subcleft location, *J. Geophys. Res.*, *79*, 4239-4245, 1974.

- Hess, W. N., *Introduction to Space Science*, Gordon and Breach Scientific Publishers, NY, NY, 1965.
- Horowitz, R., and King, J., *National Space Science Data Center Data Listing, catalog 90-06*, NASA/Goddard Space Flight Center, Greenbelt, MD, February, 1990.
- Hughes, W. J., and D. J. Southwood, The screening of micropulsation signals by the atmosphere and ionosphere, *J. Geophys. Res.*, *81*, 3234-3240, 1976a.
- Hughes, W. J., The effect of the atmosphere and ionosphere on long period magnetospheric micropulsations, *Planet. Space Sci.*, *22*, 1157-1172, 1974.
- Hujanen, A., *University of Minnesota Space Science Center Report*, June 5, 1987.
- Ichimaru, S., *Basic Principles of Plasma Physics, A Statistical Approach*, W. A. Benjamin, Inc., Reading, MA, 1973.
- Inan, U. S., T. F. Bell, and R. A. Helliwell, Nonlinear pitch angle scattering of energetic electrons by coherent VLF waves in the magnetosphere, *J. Geophys. Res.*, *83*, 3235-3253, 1978.
- Jackson, J. D., *Classical Electrodynamics*, John Wiley & Sons, NY, NY, 1975.
- Johnston, H. F., Mean K-indices from twenty one magnetic observatories and five quiet and five disturbed days for 1942, *Terr. Magn. Atmos. Elec.*, *47*, 219, 1943.
- Kamei, T., M. Sugiura, and T. Araki, *World Data Center C2 for Geomagnetism Data Book #19*, Faculty of Science, Kyoto University, Japan, 1990.
- Kamide, Y., B. -H. Ahn, S. -I. Akasofu, W. Baumjohann, E. Friis-Christensen, H. W. Kroehl, H. Maurer, A. D. Richmond, G. Rostoker, R. W. Spiro, J. K. Walker, and A. N. Zaitzev, Global distribution of ionospheric and field aligned currents during substorms as determined from six IMS meridian chains of magnetometers: Initial results, *J. Geophys. Res.*, *87*, 8228, 1982.
- Kamide, Y., *Electrodynamic Processes in the Earth's Ionosphere and Magnetosphere*, Kyoto Sangyo University Press, Kyoto, Japan, 1988.
- Kan, J. R., Developing a global model of magnetospheric substorms, *EOS Trans., American Geophysical Union*, *71*, 1083-1087, 1990.
- Kaye, S. M., and M.G. Kivelson, Observations of Pc 1-2 waves in the outer magnetosphere, *J. Geophys. Res.*, *84*, 4267-4276, 1979.
- Kelley, M. C., *The Earth's Ionosphere*, Academic Press, NY, NY, 1989.
- Kennel, C. F. and Petschek, H. E., Limit on stably trapped particle fluxes, *J. Geophys. Res.*, *71*, 1-28, 1966.
- Kozyra, J. U., T. E. Cravens, A. F. Nagy, E. G. Fontheim, and R. S. B. Ong, Effects of energetic heavy ions on electromagnetic ion cyclotron wave generation in the plasmapause region, *J. Geophys. Res.*, *89*, 2217-2233, 1984.

- Kuwashima, M., T Toya, M Kawamura, T Hirasawa, H Fukunishi, and M Ayukawa, Comparative study of magnetic Pc1 pulsations between low latitudes and high latitudes: statistical study, *Memoirs of the National Institute of Polar Research*, 18, 101, 1981.
- Lee, D. H., and R. Lysak, Magnetospheric ULF wave coupling in the dipole model: the impulsive excitation, *J. Geophys. Res.*, 94, 17097-17103, 1989.
- Lin, N. G. and J. Plombon, *Documentation: Search Coil and Preamplifier*, University of Minnesota, July, 1985.
- Lui, A. T. Y., S. -I. Akasofu, E. W. Hones, Jr., S. J. Bame, and C. E. McIlwain, Observation of the plasma sheet during a contracted oval substorm in a prolonged quiet period, *J. Geophys. Res.*, 81, 1415-1419, 1976.
- Lundin, R., and D. S. Evans, Boundary layer plasmas as a source for high-latitude, early afternoon, auroral arcs, *Planetary Space Sci.*, 33, 1389-1406, 1985.
- Lundin, R., On the magnetospheric boundary layer and solar wind energy transfer into the magnetosphere, *Sp. Sci. Rev.*, 48, 263-320, 1988.
- Manchester, R. N., Correction of Pc 1 micropulsations at spaced stations, *J. Geophys. Res.*, 73, 3549-3556, 1968.
- Mayaud, P. N., *Derivation, Meaning and Use of Geomagnetic Indices*, American Geophysical Union, Washington, DC, 1980.
- McIlwain, C. E., Plasma convection in the vicinity of the geosynchronous orbit, in *Earth's Magnetospheric Processes*, edited by B. M. McCormac, D. Reidel Pub. Co., Dordrecht-Holland, 268-279, 1972.
- McLennan, C. G., L. J. Lanzerotti, S. -I. Akasofu, A. N. Zaitzev, P. J. Wilkinson, A. Wolfe, and V. Popov, Comparison of "electrojet" indices from the northern and southern hemispheres, *J. Geophys. Res.*, 96, 267-274, 1991.
- Meng, C. -I., B. Tsurutani, K. Kawasaki, and S. -I. Akasofu, Cross-correlation analysis of the AE index and the interplanetary magnetic field B_z component, *J. Geophys. Res.*, 78, 617, 1973.
- Montbriand, L. E., A simple method for calculating the local time of corrected geomagnetic midnight, *J. Geophys. Res.*, 75, 5634-5636, 1970.
- Monthly Summary of Geomagnetic Activity, in *Geomagnetic Indices Bulletin*, National Geophysical Data Center, Boulder, CO, 1986.
- Mulholland, H., *Fundamentals of Statistics*, Plenum Press, NY, NY, 1968.
- Mullen, A. J., and R. R. Heacock, Correlation of ground-based measurements of structured Pc1 micropulsations with Ogo 5 plasmopause observations, *Ann. Geophys.*, 28, 519-525, 1972.
- National Space Science Data Center catalog 88-26*, NASA/Goddard Space Flight Center, Greenbelt, MD, January, 1989.

- National Space Science Data Center Interplanetary Data Book - Supplement 3, 1977-1985, April, 1986.*
- Newell, P. T., and Meng, C. -I., On quantifying the distinctions between the cusp and the cleft/LLBL, in *Electromagnetic Coupling in the Polar Clefts and Caps*, edited by P. E. Sandholt and A. Egeland, Kluwer Academic Publishers, 87-101, 1989.
- Newell, P. T., S. Wing, C. -I. Meng, V. Sigillito, The auroral oval position and structure 1984-1989: An automated online database, *EOS Trans. American Geophysical Union*, 71, 598, 1990.
- Newell, P. T., S. Wing, C. -I. Meng, and V. Sigillito, The auroral oval position, structure, and intensity of precipitation from 1984 onward: An automated on-line data base, *J. Geophys. Res.*, 96, 5877-5882, 1991.
- Nishida, A., Ionospheric screening effect and storm sudden commencement, *J. Geophys. Res.*, 69, 1861-1874, 1964.
- Nishida, A., *Geomagnetic Diagnosis of the Magnetosphere*, v. 9 in *Physics and Chemistry in Space*, Springer-Verlag, NY, NY, 1978.
- Nishida, A., Origin of magnetospheric plasma, in *Magnetospheric Plasma Physics*, edited by A. Nishida, pp. 1-47, D.Reidel Publishing Co., Boston, MA, and The Center for Academic Publications, Tokyo, Japan, 1982.
- Olson, J. V. and G Rostoker, Pi2 pulsations and the auroral electrojet, *Planet Sp Sci.*, 23, 1129-1139, 1975.
- Parady, B. K., *Measurement of Low Frequency Magnetic Fluctuations in the Magnetosphere*, Ph. D. Dissertation, University of Minnesota, 1974.
- Perraut, S., R Gendrin, A Roux, C de Villedary, Ion cyclotron waves: direct comparison between ground-based measurements and observations in the source region, *J. Geophys. Res.*, 89, 195-202, 1984.
- Press, W. H., B. P. Flannery, S. A. Teukolsky, and W. T. Vetterling, *Numerical Recipes, the Art of Scientific Computing*, Cambridge University Press, Cambridge, 1986.
- Rauch, J. L., and A. Roux, Ray tracing of ULF waves in a multicomponent plasma: Consequences for the generation mechanism of ion cyclotron waves, *J. Geophys. Res.*, 87, 8191-8198, 1982.
- Reiff, P. H., R. W. Spiro, and T. W. Hill, Dependence of polar cap potential drop on interplanetary parameters, *J. Geophys. Res.*, 86, 7639, 1981.
- Reiff, P. H., The use and misuse of correlation analyses, in *Solar-Terrestrial Physics*, edited by R. L. Caravillano and J. M. Forbes, D. Reidel Pub. Co., Dordrecht-Holland, 493, 1983.
- Reiff, P. H., and J. G. Luhmann, Solar wind control of the polar cap voltage, in *Solar Wind-Magnetosphere Coupling*, edited by Y. Kamide & J. A. Slavin, 453-476, Terra Publishing Co, Tokyo, 1986.

- Roederer, J. G., ed., *Dynamics of Geomagnetically Trapped Radiation*, in *Physics and Chemistry in Space*, vol. 2; Springer-Verlag, NY, NY, 1970.
- Rokityanskaya, D. A., Micropulsations with periods of 4-12 seconds, *Geomagnetism and Aeronomy*, 9, p.918 (English version), 1969
- Rostoker, G., and C. G. Falthammar, Relationship between changes in the interplanetary magnetic field and variations in the magnetic field at the Earth's surface, *J. Geophys. Res.*, 72, 5853, 1967.
- Rostoker, G., Relationship between the onset of a geomagnetic bay and the configuration of the interplanetary magnetic field, *J. Geophys. Res.*, 73, 4382, 1968.
- Rostoker, G., H. L. Lam, and W. D. Hume, Response time of the magnetosphere to the interplanetary electric field, *Can. J. Phys.*, 50, 544, 1972.
- Roth, B., and D. Orr, Locating the Pc 1 generation region by a statistical analysis of ground based observations, *Planet. Space Sci.*, 23, 993-1002, 1975.
- Roux, A., S. Perraut, J. L. Rauch, C de Villedary, G. Kremser, A. Korth, and D. T. Young, Wave particle interactions near Ω_{He^+} observed on board GEOS 1 and 2, 2. Generation of ion cyclotron waves and heating of He⁺ ions, *J. Geophys. Res.*, 87, 8174-8190, 1982.
- Russell, C. T., Geophysical coordinate transformations, *Cosmic Electrodynamics*, 2, 184-196, 1971.
- Saito, T., Geomagnetic pulsations, *Space Sci. Rev.*, 10, 318-412, 1969.
- Samson, J. C., Pi 2 pulsations: high latitude results, *Planet Sp Sci*, 30, pp. 1239-1247, 1982.
- Sato, N., and T. Saemundsson, Unstructured Pc 1-2 pulsations observed at geomagnetically conjugate stations in the auroral zone, submitted to *Research Note for the Journal of Geomagnetism and Geoelectricity*, 1989.
- Schatten, K. H., and J. M. Wilcox, Response of the geomagnetic activity index Kp to the interplanetary magnetic field, *J. Geophys. Res.*, 72, 5185, 1967.
- Sibeck, D. G., R. W. McIntire, A. T. Y. Lui, R. E. Lopez, S. M. Krimigis, Magnetic field drift shell splitting: Cause of unusual dayside particle pitch angle distributions during storm and substorms, *J. Geophys. Res.*, 92, 13485-13497, 1987.
- Sibeck, D. G., and Croley, Solar wind dynamic pressure variations and possible ground signatures of flux transfer events, *J. Geophys. Res.*, 96, 1669-1683, 1991.
- Sibeck, D. G., R. E. Lopez, and E. C. Roelof, Solar wind control of the magnetopause shape, location and motion, *J. Geophys. Res.*, 96, 5489-5495, 1991.
- Sims, W. E., and F. X. Bostick, Atmospheric parameters for four quiescent earth conditions, *Rept. No. 132, Electrical Engineering Research Lab, Univ. of Texas*, Sept. 1, 1963.

- Smith, R. L., and N Brice, Propagation in multicomponent plasmas, *J. Geophys. Res.*, **69**, 5029-5040.
- Stix, T. H., *The Theory of Plasma Waves*, McGraw-Hill, NY, NY, 1962.
- Sugiura, M., and T. Kamei, *Provisional Values of Equatorial Dst*, World Data Center C2 for Geomagnetism, Faculty of Science, Kyoto University, Japan, 1986, 1987.
- Swanson, D. G., *Plasma Waves*, Academic Press, NY, NY, 1989.
- Takahashi, K., ULF waves in the magnetosphere, in *Rev. of Geophys., Supplement, Contributions in Solar-Planetary Relationships/ US National Report to the International Union of Geodesy and Geophysics, 1987-1990*, 1066-1074, 1991.
- Takahashi, S., and T. Iyemori, Three dimensional tracing of charged particle trajectories in a realistic magnetospheric model, *J. Geophys. Res.*, **94**, 5505-5509, 1989.
- Tamao, T., The structure of three dimensional hydromagnetic waves in a uniform cold plasma, *J. Geomagn. Geoelectr.*, **16**, 89-114, 1964.
- Tamao, T., Direct contribution of oblique field-aligned currents to ground magnetic fields, *J. Geophys. Res.*, **91**, 183-189, 1986.
- Taylor, W. W. L., B. K. Parady, P. B. Lewis, R. L. Arnoldy, L. J. Cahill, Jr., Initial results from the search coil magnetometer at Siple, Antarctica, *J. Geophys. Res.*, **80**, 4762-4769, 1975.
- Tepley, L. R., R. Heacock, and B. J. Fraser, Hydromagnetic emissions (Pc1) observed simultaneously in the auroral zone and at low latitudes, *J. Geophys. Res.*, **70**, 2720, 1965.
- Troitskaya, V. A., O. V. Bolshakova, and E. T. Matveeva, Geomagnetic pulsations in the polar cap, *J. Geomagn. Geoelectr.*, **32**, 309, 1980.
- Whalen, J. A., The aurora: phenomenology, morphology and occurrence, in *Handbook of Geophysics and the Space Environment*, edited by AS Jursa, Air Force Geophysical Laboratory, p.12-2, 1985.
- Yamagishi, H., ELF emission in high latitudes; ray path calculation and ground-satellite observations, *Memoirs of National Institute of Polar Research, Ser. A*, **19**, 120, 1989.
- Young, D. T., S. Perraut, A. Roux, C. de Villedary, R. Gendrin, A. Korth, G. Kremser, and D. Jones, Wave particle interactions near Ω_{He^+} observed on GEOS 1 and 2, 1. Propagation of ion cyclotron waves in a He^+ -rich plasma, *J. Geophys. Res.*, **86**, 6755-6772, 1981.
- Young, H. D., *Statistical Treatment of Experimental Data*, McGraw-Hill, NY NY, 1962.

Appendix

The Chi-Square Test

When studying possible associations between the occurrence of Pc1/2 and a solar wind parameter or magnetic index, a chi-square test was often used to compare entire distributions to each other. One of these was usually some reference, or parent, such as all the measured IMF values during 1986. The other distribution was typically the same parameter, except during Pc1/2 events. The question to be answered in these cases was whether or not the distributions were different. If not, then one could say that the values during the Pc1/2 were consistent with a random selection from the parent, and had no special association with any values of the parent. This is of interest for testing the importance of high solar wind pressure or negative B_z to the occurrence of Pc1/2, for example.

The chi-square test is appropriate for binned data (Press et al., 1986), and binning was often employed to display solar wind and other distributions in an easily visualized fashion. For k terms in each distribution, the chi-square statistic is (Reiff, 1983):

$$\chi^2 = \sum_{i=1}^k \frac{(y_i - e_i)^2}{\sigma_i^2}. \quad (\text{A-1})$$

A data point is represented by y_i ; e_i is the corresponding expected value, and σ_i is the uncertainty associated with each data point. The data points would be parameter values during Pc1/2, and the expected values would be those of the parent, such as the 1986

IMF measurements. If the two distributions are similar, the chi-square statistic will have a small value.

When a sample distribution is randomly drawn from a parent distribution, it should have the same shape as the parent most of the time. If the parent is normalized by a factor of $N_{\text{sample}}/N_{\text{parent}}$, to have the same total as the sample, a chi-square comparison of the two should result in a small value of the statistic. Of course, the sample distribution will sometimes be so different that it will appear to be drawn from a different parent, and one might mistakenly conclude that it is. In these cases, the chi-square statistic will be large. The probability of having a large value, *assuming the difference is only due to random selection*, is estimated with the incomplete gamma function, which is (Press, 1986; or Mulholland, 1968), using the notation of Press:

$$Q(a,x) \equiv \frac{1}{\Gamma(a)} \int_x^{\infty} e^{-t} t^{a-1} dt \quad (a>0), \quad (\text{A-2})$$

where

$$\Gamma(a) = \int_0^{\infty} e^{-t} t^{a-1} dt \quad (\text{A-3})$$

and

$$Q(a,0) = 1$$

and $a = \nu/2$, where ν is the number of degrees of freedom; and $t = \chi^2/2$ (Mulholland, 1968). $Q(a,x)$ is the probability of calculating a chi-square value of x or more, given $2a$ degrees of freedom. In the case of binned data, such as a range of IMF B_z in bin steps of $2 nT$, the number of degrees of freedom is the number of bins, minus the number of

calculations performed with the data. For example, one degree is subtracted if the parent distribution is normalized, as described above, or if a mean value is calculated from the sample and then used as the expected value. Each such calculation "forces" some agreement between the two distributions under comparison (Young, 1962). The expected value of the chi-square statistic is equal to the number of degrees of freedom. This is true either if a sample is compared to a parent, or if both distributions under comparison are in fact drawn from the same parent (Dowdy & Wearden, 1983).

The integral $Q(a,x)$ can only describe how such distributions differ. The null hypothesis is that the two distributions are randomly drawn from the same parent; a large value of chi-square leads to the rejection of that hypothesis. In other words, if an observed distribution is compared to a model and the chi-square value is so large that there is less than a 1% chance of finding a larger one through random selection, one might conclude that the two distributions are *not* drawn from the same source. Of course, it is possible that they are, but by chance appear very different from each other. In a sense, the probability ($Q(a,x)$) of exceeding the calculated chi-square can be thought of as the probability that the two distributions are drawn from the same parent. This probability is small for large values of chi-square.

The probability of finding a chi-square value at least as large as the calculated value x is *estimated* with $Q(a,x)$, because $Q(a,x)$ does not strictly describe the probability distribution of the chi-square statistic. However, it is close for either a large number of bins ($\gg 1$) or a large number of counts in any bin ($\gg 1$, see Press, 1986). What $Q(a,x)$ really represents is the probability of finding a value of $2t$ (see equation 2) at least as large as a specified x , where $2t$ is (Mulholland, 1968, and Press, 1986):

$$2t = \sum_{i=1}^k \frac{(y_i - \mu)^2}{\sigma} \quad (\text{A-3})$$

The terms in the sum are samples from a *normal* distribution, which is described by the probability density:

$$f(y) = \frac{1}{\sigma(2\pi)^{1/2}} \exp \left[-\frac{1}{2} \left(\frac{(y - \mu)}{\sigma} \right)^2 \right]. \quad (\text{A-4})$$

Specific recommendations on sample sizes were taken from Dowdy & Wearden (1983; see also Mulholland, 1968). They note that the probability distribution of the chi-square statistic is well approximated by the integrand of $Q(a,x)$ if no expected value is less than one, and not more than 20% of the expected values are less than five. These conditions were used for all chi-square comparisons here.

The uncertainty of each data point is specified in the denominator of its chi-square term. If the data are described by Poisson statistics, then $\sigma_i = \min(\sqrt{y_i}, 1)$ (Reiff, 1983). If the uncertainties in the y_i are not known, or all known and are the same for all N terms in the sum, the chi-square statistic is (Reiff, 1983):

$$\chi^2 = \frac{1}{\sigma_y^2} \sum_{i=1}^N (y_i - e_i)^2 \quad (\text{A-5})$$

where σ_y is the uncertainty of the data. It is either the known constant, or else it is calculated from:

$$\sigma^2 = \sum_{i=1}^N \frac{(y_i - \bar{y})^2}{(N-1)}. \quad (\text{A-6})$$

If two sample distributions are being compared, instead of a sample and a model, the denominator becomes the sum of the individual sample variances (Press, 1986; Bevington, 1969), because the $(y_i - z_i)^2$ term in the chi-square statistic involves two quantities with uncertainties, instead of one. This comes from the uncertainty of a calculation, which is, for $f(y_i, z_i) = (y_i - z_i)$ (Bevington, 1969; Young, 1962):

$$\sigma_f^2 = \sigma_z^2 \left(\frac{\partial f}{\partial z} \right)^2 + \sigma_y^2 \left(\frac{\partial f}{\partial y} \right)^2 + 2\sigma_{zy}^2 \left(\frac{\partial f}{\partial z} \right) \left(\frac{\partial f}{\partial y} \right) + \dots \quad (\text{A-7})$$

so that for a comparison of two sample distributions, such as Kp for Sondre Stromfjord Pc1/2 vs. Kp for South Pole Pc1/2, the denominator for each term in the chi-square sum would be $\sigma_z^2 + \sigma_y^2$, assuming no correlation ($\sigma_{zy} = 0$). If Poisson statistics apply to the data in bin i , then the denominator would be $(y_i + z_i)$, since the measured number in a bin is assumed to be the average for that bin over repeated samples, and the standard deviation for a Poisson distribution with an average of z_i is $\sqrt{z_i} = \sqrt{Np_i}$. In this case, N is the sample size, and $p_i = z_i/N$. N could be the total number of IMF measurements during Pc1/2, and p_i the probability of finding Pc1/2 counts in the 2-4 nT bin, for example.

Poisson statistics were assumed for all chi-square comparisons. However, the strictly correct way to estimate the uncertainty for the counts in each bin is to use binomial statistics. There, the uncertainty (standard deviation) is $\sqrt{Np_iq_i}$, where p_i is the probability of finding counts in bin i , and $q_i = (1 - p_i)$. The use of Poisson statistics makes computation of the uncertainty simpler. They are used when p_i is small, since Poisson statistics are the large N /small p_i limit of binomial statistics (Young, 1962). The uncertainty from a strict binomial calculation is a factor of $\sqrt{q_i}$ smaller than a Poisson estimate. This factor is no less than about 80% for any of the bins in any comparisons carried out here. The use of Poisson statistics will slightly overestimate the uncertainty and underestimate the chi-square statistic in the comparisons of this study. This slightly understates the difference between distributions. However, all conclusions remain the same, regardless of whether Poisson or binomial statistics are used to estimate the uncertainty of the data points, for all solar wind or magnetic index associations with Pc1/2 occurrence.